High Efficiency Nanowire-Based Phosphor-Free White and Deep Ultraviolet Light Sources

Mehrdad Djavid

Department of Electrical and Computer Engineering
Faculty of Engineering
McGill University
Montreal

February 2016

A thesis submitted to McGill University in partial fulfilment of the requirements of the degree of Doctor of Philosophy

Table of Contents

List of figures IV

List of acronyms XIV

Abstract XV

Abrégé XVII

Acknowledgment XIX

Contribution of authors XX

1 Introduction 1

1.1 Recent developments and challenges of GaN based LEDs 2

1.1.1 Defects and dislocations 3

1.1.2 Polarization field 4

1.1.3 Auger recombination 5

1.1.4 Electron overflow 7

1.2 Ultraviolet LEDs 9

1.2.1 Lattice mismatch 9

1.2.2 Inefficient *p*-doping 10

1.3 GaN based nanowire LEDs 11

1.3.1 Nanowire UV LEDs 13

1.4 Light extraction efficiency 14

1.4.1 Light extraction efficiency of deep UV LEDs 16

1.5 Dissertation overview 17

2 Theoretical methods 22

2.1 Introduction 22

2.2 Lumerical FDTD software package 23

2.3 ABF model 26

2.4 Crosslight APSYS software package 30

2.5 Conclusion 32

3 Different approaches for electron blocking layers 33

3.1 Introduction 33

3.2 Conventional electron blocking layer 33
3.3 Distributed electron blocking layer 46
3.4 Conclusion 55
4 Tunnel injection InGaN/GaN dot-in-a-wire white-light emitting diodes 57
4.1 Introduction 57
4.2 Simulation results and discussions 58
4.3 Experimental details and discussions 61
4.4 Conclusion 64
5 Improvement of light extraction efficiency in GaN-based LEDs using GaN nanotubes 65
5.1 Introduction 65
5.2 Simulation model and definitions 66
5.3 Results and discussion 69
5.3.1 Effect of the single nanotube geometry on light extraction efficiency 69
5.3.2 Effect of the position of source on light extraction efficiency 71
5.3.3 Effect of nanotube arrays on light extraction efficiency 73
5.4 Conclusion 74
6 Deep UV light propagation in nanowire arrays 76
6.1 Introduction 76
6.2 Periodic nanowire UV LEDs 79
6.3 Random nanowire UV LEDs 81
6.4 Photonic band edge nanowire UV LEDs/lasers 83
6.5 Biperiodic nanowire UV LEDs 84
6.6 Conclusion 86
7 Achieving high efficiency deep ultraviolet LEDs by using nanowire structures 87
7.1 Introduction 87
7.2 Simulation model and definitions 88
7.3 Results and discussion 90
7.3.1 Optimizing the spacing and diameter of nanowires 90
7.3.2 Effect of the diameter of nanowires on the light extraction efficiency 91
7.3.3 Effect of the spacing of nanowires on the light extraction efficiency 92

7.3.4 Effect of the p-GaN layer thickness on the light extraction efficiency.....93
7.3.5 Effect of the device size on the light extraction efficiency.......................94
7.3.6 Effect of the random variation in the nanowire diameter and spacing on the light extraction efficiency...95
7.4 Conclusion...96
8 Summary and future Work...98
8.1 Summary of the present work...98
8.2 Future work...101
8.2.1 High efficiency UV LEDs...101
8.2.2 High performance nanowire UV lasers..105
8.2.3 Two-dimensional semiconductor lasers...106
List of publications...110
References...115

List of figures

Figure 1-1. The efficiency droop shows the efficiency reaches it maximum at a lower current density and then the efficiency decreases as the current increases. 3

Figure 1-2. The conduction and valence band edges of a single QW including the effects of polarization. The electron and the hole wave functions shown in the figure are shifted to the right and left respectively. 5

Figure 1-3. In the Auger process, an electron and a hole are recombined and the excess energy released from this process is transferred to another electron. 6

Figure 1-4. The electron overflow mechanism in the LED structure which shows overflowing some electrons with sufficient energy out of the active region without recombining with holes. 8

Figure 1-5. The activation energy of Mg acceptor of in AlGaN as a function of Al composition which increases from ~170 meV to ~530 meV with increasing Al composition from 0 to 1 [53]...11

Figure 2-1. The 3D schematic of the hexagonal array of nanowires with the spacing (center to center) ~ 194 nm and diameter of the nanowires ~ 119 nm................25

Figure 2-2. (a) The two-dimensional layer by layer schematic of the nanowire-based UV LED structure. Each nanowire consists of 10 nm p-GaN, 100 nm p-AlGaN, 60 nm AlGaN multiple quantum well active region, and 400 nm n-AlGaN, and (b) the simulated mode profile of LED plotted in the log scale, base 10. 26

Figure 2-3. Different carrier recombination processes in LEDs including Shockley-Read-Hall recombination, radiative recombination, and Auger recombination. 27

Figure 2-4. (a) Schematic illustration of InGaN/GaN dot-in-a-wire LEDs. (b) Variations of the relative EQE related to the emission from the quantum dot active region measured at 80, 200, and 300 K. The simulated IQE based on the ABF model is also shown for comparison. 29

Figure 2-5. (a) Schematic illustration of InGaN/GaN dot-in-a-wire LEDs. (b) Calculated band diagram of the InGaN/GaN LED including quantum dots wave functions. Dashed lines represent quasi-Fermi levels. 32

Figure 3-1. (a) Schematic illustration of InGaN/GaN dot-in-a-wire LEDs grown on Si(111) substrates. (b) Illustration of the three LED designs. From left to right: InGaN/GaN dot-in-a-wire LEDs with the incorporation of an InGaN test well (LED I), an AlGaN electron blocking layer and an InGaN test well (LED II), and an AlGaN electron blocking layer (LED III) between the quantum dot active region and the p-GaN section. 35

Figure 3-2. (a) Room-temperature photoluminescence spectra of the three LED device heterostructures. The emission peak at ~ 430 nm is due to the presence of the InGaN test well, which can be clearly measured for LEDs I and II. (b) A 45° tilted scanning electron microscopy image of the InGaN/GaN dot-in-a-wire LED heterostructure grown on Si(111) substrates. 36

Figure 3-3. Bright field TEM image of InGaN/GaN dot-in-a-wire LED II. 37

Figure 3-4. (a) Normalized electroluminescence spectra of LED I under various injection currents. The peak at ~ 550 nm is related to the emission from the quantum dot active region, while the peak at ~ 430 nm is related to the emission from the InGaN/GaN test quantum well. (b) Variations of the relative EQE with injection current for the emission from the quantum dot active region and the test well of LED I measured at room temperature. 38

Figure 3-5. (a) Normalized electroluminescence spectra of LED I measured at 300K (solid line) and 80K (dashed line) under an injection current density of ~ 450A/cm^2. (b) Variations of the relative EQE related to the emission from the quantum dot active region measured at 80, 200, and 300 K. The simulated IQE based on the ABF model is also shown for comparison. The dotted blue line is the calculated IQE versus injection currents in the absence of any 3rd or higher order carrier loss mechanisms. 39

Figure 3-6. (a) Simulated electron current density across the InGaN/GaN quantum dot active region using the APSYS simulation package with (red curve) and without (black curve) the incorporation of an AlGaN EBL. (b) The electron density distribution across the near surface GaN region of the nanowire LEDs with (red curve) and without (black curve) the incorporation of an AlGaN electron blocking layer. 42

Figure 3-7. Normalized electroluminescence spectra of LED II measured under an injection current density of ~ 1,222 A/cm^2 at 80, 200, and 300 K. Emission peak from the InGaN test well is not observed, suggesting the drastically reduced, or the absence of electron overflow in the LED devices with the incorporation of an AlGaN electron blocking layer. 43

Figure 3-8. Variations of the measured relative external quantum efficiencies of LED III with injection current at 80 K, 200 K, and 300 K. The simulated IQE using the ABF model shows a good agreement with experimental results. 44

Figure 3-9. (a) – (d) Illustration of the epitaxial growth of catalyst-free InGaN/AlGaN dot-in-a-wire core-shell LED heterostructures on Si substrate. (a) GaN:Si segment was first grown on Si(111) substrate. (b) 3 nm InGaN dot was grown on GaN:Si. (c) The formation of AlGaN barrier and shell. (d) The formation of a thick AlGaN shell surrounding the InGaN quantum dot active region after the growth of multiple, vertically aligned InGaN/AlGaN dots. (e) Schematic illustration of the energy band diagram of the InGaN/AlGaN dot-in-a-wire core-shell LED active region, showing the three-dimensional carrier confinement. (f) A 45° tilted SEM image of a typical InGaN/AlGaN dot-in-a-wire core-shell LED heterostructure grown on Si substrate. 47

Figure 3-10. (a, b) STEM-HAADF images of the InGaN/AlGaN dot-in-a-wire core-shell heterostructures showing the InGaN dots, AlGaN barriers, and the Al-rich core-shell by atomic-number contrast. (c) Higher magnification atomic-resolution HAADF image of the selected region (boxed in red dashed line) in (b) showing the AlGaN core-shell and barriers in detail. 48

Figure 3-11. Photoluminescence spectra showing significantly enhanced emission for the InGaN/AlGaN dot-in-a-wire core-shell LED structure, compared to the InGaN/GaN nanowire sample without AlGaN shell measured using a 405 nm laser at room-temperature...49

Figure 3-12. (a) Current vs. voltage characteristics of an InGaN/AlGaN dot-in-a-wire core-shell white LED on Si. (b) Electroluminescence spectra of the core-shell LED measured under different injection currents. (c) CIE diagram showing the stable white light emission for injection current from 50 mA to 500 mA, with the x and y values in the ranges of ~ 0.35 – 0.36 and 0.37 – 0.38, respectively. (d) Output power vs. injection current of the InGaN/AlGaN dot-in-a-wire core-shell LEDs measured under 1% duty cycle. Variations of the output power vs. current for the InGaN/GaN axial nanowire LED without AlGaN shell are also shown for comparison (blue triangle). 51

Figure 3-13. Schematics of (a) the InGaN/GaN LED heterostructure, (b) the InGaN/GaN LED with an equivalent AlGaN EBL, and (c) the InGaN/AlGaN LED heterostructure. 52

Figure 3-14. Simulated hole concentration (a) and electron concentration (b) in the active regions of the InGaN/AlGaN (dashed blue), the InGaN/GaN with an equivalent EBL (dotted red), and the InGaN/GaN LED heterostructures (black). (c) Simulated output power vs. injection current for the three LED structures. In this simulation, the effect of nonradiative surface recombination was not considered, which can lead to dramatically reduced power for conventional InGaN/GaN axial nanowire LEDs. 53

Figure 3-15. (a) Simulated electron current density for the InGaN/AlGaN LED (blue), the InGaN/GaN LED with an equivalent EBL (red), and the InGaN/GaN LED (black). (b) Simulated radiative recombination coefficients of the InGaN/AlGaN LED (dotted blue), the InGaN/GaN LED with an EBL (dotted red), and the InGaN/GaN LED (solid black) at an injection current of 1000 A/cm2. 54

Figure 4-1. InGaN/GaN dot-in-a-wire tunnel injection LED heterostructures. (a) Schematic illustration and (b) energy band diagram under a forward bias of 3.1 V. 59

Figure 4-2. (a) Simulated electron current density across the InGaN/GaN quantum dot active region (dashed arrow in Figure 1(a)) at an injection current of 1000 A/cm^2 with (red curve) and without (black curve) the incorporation of InGaN injector wells. (b) Electron current density across the near-surface of InGaN/GaN quantum dot active region (solid arrow in Figure 1(a)) at an injection current of 1000 A/cm^2 with (red curve) and without (black curve) the incorporation of InGaN injector wells. (c) The electron density distribution along the axial direction of the nanowires at an injection current of 1000 A/cm^2 with (red curve) and without (black curve) the incorporation of InGaN injector wells. 60

Figure 4-3. (a) Room-temperature photoluminescence spectrum and (b) a 45^{o} tilted scanning electron microscopy image of the InGaN/GaN dot-in-a-wire heterostructures grown on Si(111) substrate. 62

Figure 4-4. (a) Current-voltage characteristics of the fabricated dot-in-wire LED device on Si(111). (b) Electroluminescence spectra of the device measured under various injection currents. (c) The electroluminescence spectrum of the LED under 700 mA injection current at 5 K (d) Variations of the relative external quantum efficiency of the tunnel injection dot-in-a-wire LED with current. 63

Figure 4-5. The 1931 Commission International de l'Eclairage chromaticity diagram. The devices exhibit relatively stable emission with x and y in the ranges of 0.341-0.347 and 0.383-0.386, respectively. 64

Figure 5-1. Schematic of the integrated GaN LED and nanotube structure. The nanotube shown here has 1.5 turns and θ is $45°$. C_1 and C_2 denote the integration paths for calculating the light extraction efficiency. 67

Figure 5-2. Comparison between the light extraction efficiency of a GaN thin film LED (a) without and (b) with a nanotube for light emission at 526 nm. The nanotube used here has 1.25 turns and the wall thickness is 20 nm. 69

Figure 5-3. Light extraction efficiency of (a) TE waves and (b) TM waves vs. the number of turns and rotation angle θ of the nanotube. The wall thickness is 20 nm. The p-GaN layer thickness is $d_1 = 120\,\mathrm{nm}$ 70

Figure 5-4. Dependence of the light extraction efficiency of TE waves and TM waves on the wall thickness. The p-GaN layer thickness is $d_1 = 120\,\mathrm{nm}$. The nanotube parameters are $N = 1.25,\ \theta = 0°$ 71

Figure 5-5. Dependence of the light extraction efficiency of TE waves on (a) the depth of the active region and (b) the horizontal position of the point source. Nanotube parameters used are $N = 1.6,\ \theta = -75°,\ t = 20\,\mathrm{nm}$. In (a), the light source is positioned right under the nanotube..72

Figure 5-6. (a) Schematic illustration of the integrated nanotube arrays with an LED structure. (b) Comparison between the light extraction efficiency of TE waves for a single nanotube and that for multiple nanotubes for L=1220 nm. Nanotube parameters include $N = 1.6,\ \theta = -75°,\ t = 20nm$ 73

Figure 6-1. The two-dimensional layer by layer schematic of the nanowire-based UV LED structure. Each nanowire consists of 10 nm p-GaN, 100 nm p-AlGaN, 60 nm AlGaN multiple quantum well active region, and 400 nm n-AlGaN............78

Figure 6-2. (a) The 3D schematic of the hexagonal periodic array of nanowires, and (b) the simulated mode profiles with the optimized spacing and diameter which shows the high light extraction efficiency...80

Figure 6-3. (a) The 3D schematic of the random array of nanowires, and (b) its simulated mode profiles with the random spacing and diameter which shows the strongly localized light inside some spaces between nanowires. 82

Figure 6-4. (a) Calculated photonic band structure of a 2D hexagonal array of nanowires, (b) the electric field profile of the band edge mode calculated by 3D FDTD which corresponds to slow light mode at λ = 280 nm. 84

Figure 6-5. (a) The 3D schematic of the rectangular biperiodic array of nanowires, and (b) the simulated mode profiles with two different lattice constant which shows the light mostly emits in longitudinal direction. 85

Figure 7-1. (a) The two-dimensional layer by layer schematic of the nanowire-based UV LED structure. Each nanowire consists of 10 nm p-GaN, 100 nm p-AlGaN, 60 nm AlGaN multiple quantum well active region, and 400 nm n-AlGaN. (b) The 3D schematic of the hexagonal array of nanowires. 88

Figure 7-2. (a) Calculated photonic band structure of a 2D hexagonal array of nanowires with spacing and diameter of 194 nm and 119 nm. The flat photonic band is highlighted by red color. (b) The simulated mode profiles with the optimized spacing and diameter. 90

Figure 7-3. Variations of the light extraction efficiency vs. nanowire diameter.............92

Figure 7-4. Variations of the light extraction efficiency vs. nanowire spacing. 93

Figure 7-5. Dependence of the light extraction efficiency on the thickness of p-GaN thickness which shows the periodic dependence of light extraction efficiency on the thickness. 94

Figure 7-6. Simulated light extraction efficiency for devices with side lengths varying from 2.5 μm to 15 μm. Each device has a square dimension. In this simulation, the nanowire diameter and spacing were kept constant at 119 and 194 nm, respectively. 95

Figure 7-7. (a) The light extraction efficiency for ten different structures with random nanowire spacing, random nanowire diameter, and fully random structure. (b) Simulated mode profile for the fully random structure. 96

Figure 8-1. (a) The schematic of light propagation of TM polarized light in conventional c-plane AlN LEDs. (b) A schematic of the AlN nanowire LEDs with the inset showing the layer-by-layer structure. The arrows indicate the light scattering process. (c) The screen shot of light propagation of AlN nanowire LEDs with average diameter of 30 and spacing of 25 (d) The simulated light output contour plots of AlN nanowire LEDs from top. 103

Figure 8-2. Schematic of the (a) random and (b) periodic nanowire UV laser on Si. The front and end mirrors are defined using multiple SiOx/air distributed Bragg reflectors. 105

Figure 8-3. The simulated mode profiles of the periodic nanowire lasers on Si with multiple SiOx/air distributed Bragg reflectors. 106

Figure 8-4. Cavity configuration and FDTD simulation. a) Schematic configuration of the coupled microsphere/microdisk optical cavity with the incorporation of 2D MoS2. b) Representative top-view SEM image of the coupled microsphere/microdisk cavity. Electric field distribution c) on the x-z plane passing through the microsphere/microdisk contact point, d) inside the microdisk on the x-y plane, and e) on the y-z plane passing through the contact point...107

Figure 8-5. FDTD simulation of a microsphere sitting at the middle of microdisk. a) Schematic configuration of the microsphere and microdisk. Electric distribution b) inside the microdisk (on the x-y plane) and c) inside the microsphere and microdisk (on the y-z plane)...109

List of acronyms

CIE	The 1931 Commission International de L'eclairage Chromaticity Diagrams
EBL	Electron Blocking Layer
EL	Electroluminescence
HAADF	High Angle Annular Dark Field
IQE	Internal Quantum Efficiency
LED	Light Emitting Diode
MBE	Molecular Beam Epitaxy
MQW	Multi-Quantum Well
NW	Nanowire
PL	Photoluminescence
QCSE	Quantum Confined Stark Effect
QD	Quantum Dot
QW	Quantum Well
RF	Radio Frequency
SAE	Selective Area Epitaxy
SEM	Scanning Electron Microscopy
SRH	Shockley-Read-Hall
SSL	Solid State Lighting
STEM	Scanning Tunneling Electron Microscope
TEM	Transmission Electron Microscopy
UV	Utraviolet

Abstract

We have developed several methods to enhance the external quantum efficiency of GaN light emitting diodes (LEDs). As electron leakage out of the device active region is primarily responsible for internal efficiency degradation in such devices, we have demonstrated that electron overflow in nanowire LEDs can be effectively prevented with the incorporation of a p-doped AlGaN electron blocking layer (EBL), leading to the achievement of phosphor-free white LEDs that can exhibit virtually zero efficiency droop. We further report on the demonstration of a new type of axial nanowire LED heterostructures, with the use of self-organized InGaN/AlGaN dot-in-a-wire core-shell nanowire arrays. The p-doped AlGaN barrier layers as distributed EBLs is found to be more effective in reducing electron overflow, compared to the conventional AlGaN EBL. In the second approach, we have proposed and demonstrated InGaN/GaN dot-in-a-wire tunnel injection white light emitting diodes on Si, wherein electrons and holes are injected into the quantum dot active region through two separate InGaN injector wells. Significantly reduced electron overflow is realized without the use of any Al-containing EBL.

On the other hand, extracting the generated photons out of the GaN LEDs is difficult. Most of the photons are reflected at the GaN/air interface due to the total internal reflection, and consequently are trapped and absorbed inside the LED. We have shown that the light extraction efficiency of GaN LEDs can be significantly enhanced by integrating with nanotube arrays. The light extraction involves two successive steps, including the coupling from the light source to the tube and the subsequent emission from the tube to the air. We have further enhanced the light extraction efficiency of

deep UV LEDs using periodic array of nanowires. The emission of the guided modes could be inhibited and redirected into radiated modes utilizing nanowire structures. We have shown that an unprecedentedly high light extraction efficiency of ~72% can, in principle, be achieved.

Abrégé

Nous avons étudié plusieurs méthodes pour améliorer le rendement quantique externe des diodes électroluminescentes (DEL) GaN. Comme les fuites d'électrons sortantes de la région active du dispositif sont la principale responsable de la dégradation d'efficacité interne de ces dispositifs, nous avons proposé et démontré les diodes électroluminescentes de lumière blanche d'injection de tunnel point-en-fil sur Silicium, dans lesquels les électrons et les trous sont injectés dans la région active des points quantiques à travers deux puits injecteurs InGaN séparés. Le débordement d'électrons est réduit d'une façon importante sans utiliser aucune couche de blocage d'électrons (CBE) contenant de l'Al. Dans la seconde approche, nous avons démontré que le débordement d'électrons dans les DELs à nanofils peut être efficacement empêché en intégrant une CBE AlGaN dopée de type P, conduisant à la réalisation des DELs blanches sans phosphore qui peuvent présenter, pour la première fois dans le monde, pratiquement zéro d'affaissement d'efficacité. De plus, nous rapportons sur la démonstration d'un nouveau type des hétéro-structures DELs nanofils axiales qui utilisent des réseaux nanofils core-shells point-en-fils auto-organisés InGaN / AlGaN. Les couches barrières AlGaN dopées de type P sont plus efficaces, comme les CBEs distribuées, pour réduire le débordement d'électrons par rapport aux CBEs AlGaN classiques.

D'autre part, l'extraction des photons générés hors des DELs GaN est difficile. La plupart des photons sont réfléchis à l'interface GaN / air en raison de la réflexion interne totale, et par conséquent sont piégés et absorbé à l'intérieur de la DEL. Nous avons montré que l'efficacité d'extraction de lumière des DELs GaN peut être

considérablement améliorée par l'intégration des réseaux de nanotubes. L'extraction de la lumière se fait en deux étapes successives, y compris le couplage de la source lumineuse au tube et l'émission subséquente à partir du tube à l'air. Nous avons encore améliorée l'efficacité d'extraction de lumière des DELs UV profondes en utilisant des réseaux périodiques de nanofils. L'émission des modes guidés a été inhibée et redirigée vers les modes rayonnés en appliquant des structures nanofils. Nous avons montré qu'une efficacité d'extraction de lumière sans précédente de ~ 72% peut être atteinte.

Acknowledgment

First of all, I would express a deep sense of gratitude to my parents and sisters for their love and support throughout my life. Special thanks are due to my wife who always strengthened my spirit by standing by me in all situations.

It gives me immense pleasure to thank my supervisor, Prof. Zetian Mi, for his great guidance and constant support during my PhD program. I would also like to thank my committee members, Dr. Peyman Servati and Dr. Lawrence Chen for their valuable suggestions and assessments.

Furthermore, I would like to thank all of my colleagues at McGill University including Dr. Saeed Fathololoumi, Dr. Mohammad H. T. Dastjerdi, Dr. Pablo Bianucci, Dr. Hieu P Nguyen, Dr. Songrui Zhao, Dr. Shaofei Zhang, Dr. Shamsul Arafin, Dr. Yong-Ho Ra, Dr. Ashfiqua Connie, Xianhe Liu, and Sharif Md. Sadaf. A special thanks to Dr. Afshin Moin for translating the abstract in French.

Finally, I would like to thank Natural Sciences and Engineering Research Council of Canada and U.S. Army Research Office for their financial support of this research.

Contribution of authors

This thesis includes a collection of manuscripts written by the candidate, and candidate's colleagues. The results presented in the manuscripts are the collaboration of many coauthors. The designing and optimization of the nanowire LEDs is conducted by the candidate, Dr. Hieu Pham Trung, Dr. Songrui Zhao, and Prof. Zetian Mi. The simulation model used in the manuscripts includes ABF model, APSYS software model and Lumerical FDTD simulations were proposed and developed by the candidate. The molecular beam epitaxial growth and fabrication of the dot-in-wire light emitting diode heterostructures were performed by Dr. Hieu Pham Trung Nguyen, and Dr. Songrui Zhao. The TEM imaging and SEM imaging are carried out by Dr. Hieu Pham Trung Nguyen. Electroluminescence and Photoluminescence measurements were performed by Dr. Hieu Pham Trung Nguyen.

1 Introduction

Nowadays, white light emitting diodes (LEDs) offer a new and revolutionary light source, also called solid state lighting, in the electric lighting market that has a long list of potential benefits including extremely low power consumption, color tunability, no radiated heat, and no UV radiation. The white LED lighting paves the way on the household lighting market, and in the commercial sectors such as offices, factories and other businesses.

White light sources render a combination of the basic colors: red, green, and blue. The most common approach for light rendering is the color conversion utilizing phosphor [1], in which the combination of downconversion of the blue emission into green/red light with the blue emission of an LED leads to the appearance of white color. The white LED lighting is poised to compete successfully with conventional lighting sources such as incandescent, fluorescent and halogen lighting due to its ability to offer high light quality and lower cost. However, the phosphor converted white light sources have several disadvantages including low efficiency, difficulty in color tunability, and short lifetime.

Today, more than 20% of global electricity produced in the world is consumed in general illumination applications [2]. This state has received criticism as it contributes to pollution and environmental harm due to high energy consumption. Therefore, developing lighting technology with significantly improved efficiency has become essential and urgent for our modern society. The incandescent lighting technology first developed in the 19th century, which is still widely used today, includes one of the most inefficient energy conversion processes. Among the new lighting technologies, LED lighting has been identified as the best lighting technology on the market, which can, in principle, be 20 times more efficient than incandescent lighting and 5 times more efficient than florescent lighting [2]. Recent studies over the 20-year analysis period have shown that, with a rapid market penetration of LED lighting, the energy savings from 2010 to 2030 are estimated to be approximately $250 billion worldwide [2]. The above mentioned characteristics of LED lighting have an immense potential to contribute to the field of general lighting, medical instruments, environmental sustainability, and human health.

1.1 Recent developments and challenges of GaN based LEDs

One of the great challenges for the emerging solid state lighting technology is the development of all semiconductor-based white LEDs, consisting of monolithically integrated blue, green, and red devices, that can exhibit ultrahigh efficiency, long term reliability, and tunable color emission. The GaN based semiconductors are of great importance for visible and UV applications such as LCD backlight [3-5], traffic lights [6], automotive lighting [7, 8], biomedical diagnostics [9-11], disinfection [12-14], and water purification [15, 16]. The performance of LEDs is defined by their external quantum efficiency, which is a product of carrier injection efficiency, internal quantum efficiency and light extraction efficiency. The performance of such devices using conventional GaN based planar heterostructures, however, has been severely limited by their low internal efficiency and low extraction efficiency. The low internal efficiency in the GaN based LEDs has been explained by the presence of polarization fields, Auger recombination [17, 18], poor hole transport, defects/dislocations, and electron leakage and overflow [19-21].

The internal efficiency in the GaN based LEDs decreases as current increases - the so-called efficiency droop. The efficiency droop is the gradual decrease of internal quantum efficiency as the injection current density increases (shown in Figure 1.1). The efficiency droop is one of the most significant challenges faced by high power GaN LEDs. It is caused by several mechanisms such as the presence of defects, polarization field, poor hole transport, Auger recombination, and electron overflow which are described in the following sections.

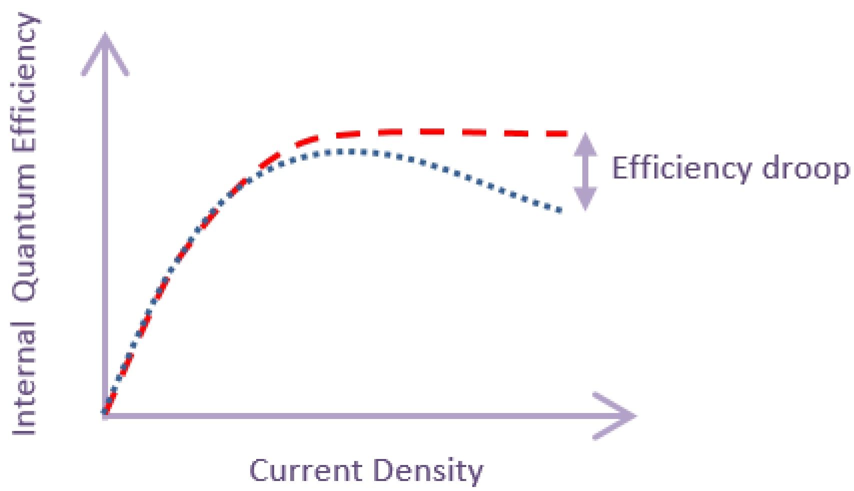

Figure 1-1. The efficiency droop shows the efficiency reaches it maximum at a lower current density and then the efficiency decreases as the current increases.

1.1.1 Defects and dislocations

The defect states in the bandgap act as Shockley–Read–Hall (SRH) non-radiative recombination centers, which result in severe degradation in the performance of GaN LEDs. The origin of defect states can be related to the presence of dislocations, which are commonly caused by large lattice mismatches between the nitride based materials and the substrates such as sapphire, SiC and Si. The dislocations are generated in the layers grown epitaxially on the substrate due to the lattice mismatch, as the thicknesses of layers are above a critical thickness. The dislocations result in defect states in the bandgap and consequently severe degradation in the performance of the GaN LEDs [22-24]. Therefore, it is crucial to reduce the lattice mismatch of LEDs and minimize the performance degradation in the optical and electrical performance of these devices. The defect density is higher in the planar GaN LEDs due to the lattice mismatch of epitaxial layer with respect to substrates.

1.1.2 Polarization field

Sapphire, SiC and Si are among the most commonly used substrates for nitride based LEDs. These materials have different lattice constants which result in large lattice mismatches. The polarization field caused by the large lattice mismatch plays an important role in degrading the performance of nitride based LEDs. The polarization field, including the spontaneous and strained-induced piezoelectric polarization, spatially separates the electron and hole within the quantum wells. This is known as Quantum-confined Stark effect (QCSE) [25, 26]. The spatial separation of carriers decreases the radiative recombination and greatly degrades the performance of LEDs.

Figure 1.2 shows the conduction and valence band edges of a single QW including the effects of polarization. The electron and hole wave functions shown in the figure are shifted to the right and left respectively. Compared to the symmetric wave function without polarization field, the asymmetric wave function of electron and hole reduces the overlap of confined electrons and holes and consequently results in a low radiative recombination rate.

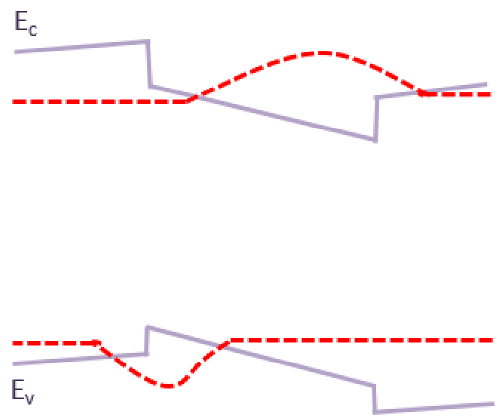

Figure 1-2. The conduction and valence band edges of a single QW including the effects of polarization. The electron and the hole wave functions shown in the figure are shifted to the right and left respectively.

1.1.3 Auger recombination

At high injection current, the Auger recombination, which refers to the three-carrier nonradiative recombination process, is mostly responsible for performance degradation of GaN based LEDs [17, 18, 27]. In this process, a third carrier gets the excess energy released by the recombination of an electron-hole pair. The third carrier, which can be an electron or a hole with high kinetic energy, is then excited to a higher energy state, which leads to a large efficiency droop observed in GaN LEDs. The third carrier then gradually relaxes to the band edge by thermally releasing the excess energy. Since the Auger recombination involves three carriers and is proportional to the third power of carrier concentration, it becomes more dominant at high current densities, or highly doped materials [28, 29]. The Auger process is depicted in Figure 1.3 which shows that the energy released from recombination of an electron and a hole is transferred to another electron. This excited electron is then pushed to the higher energy state in the conduction band.

The Auger recombination rate is typically higher for narrow bandgap materials compared to wide bandgap materials such as GaN [30]. Özgür *et al.* showed that wide bandgap materials such as GaN, have ~50 times smaller Auger recombination rate rather than narrow bandgap materials such as GaAs [30]. Shen *et al.* measured the Auger recombination coefficient for InGaN/GaN quantum well LEDs in the range of ~ 10^{-30} - 10^{-31} cm^6 s^{-1} [31].

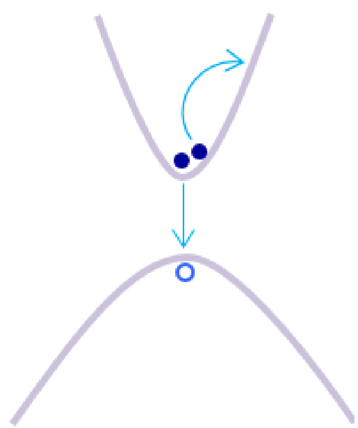

Figure 1-3. In the Auger process, an electron and a hole are recombined and the excess energy released from this process is transferred to another electron.

Recent studies showed that the Auger recombination processes can be either direct or indirect [32]. While the direct Auger recombination is weak in the nitride based devices, the indirect Auger recombination assisted by phonon and alloy scattering was suggested as the dominant factor causing the large Auger coefficient, which affects the efficiency of nitride based devices at high currents [32]. Iveland *et al.* further concluded that Auger recombination can explain the observed efficiency droop in InGaN/GaN quantum well LEDs [33].

On the other hand, Guo *et al.* reported the Auger recombination coefficient in InGaN nanowires with a much smaller value 10^{-33} cm^6 s^{-1} [34]. Such a small Auger coefficient was also measured by Nguyen *et al.* based on the temperature dependent emission characteristics of dot-in-wire white LEDs [29]. Their studies strongly suggest that Auger recombination plays a very small, or negligible role on the performance of nanowire LEDs.

1.1.4 Electron overflow

The performance of GaN LEDs is adversely affected by the poor hole injection caused by the heavy effective mass, and poor mobility of holes [35]. While the electron distribution is rather uniform across the entire active region, the injected holes largely reside in the small region close to the *p*-GaN region. The highly nonuniform distribution of carriers results in a significantly enhanced electron overflow, and efficiency droop at high injection levels. The presence of the polarization field could tilt the band-edge and effectively diminish the barrier height for electrons, which enhances the electron overflow, and thus degrades the LED performance. The overflowed electrons can recombine with the holes in the *p*-GaN region, reduce the radiative recombination rate, and thus degrade the LED performance. The non-uniform carrier distribution in the active region of the GaN LEDs is another important mechanism which limits the performance of GaN LEDs. The poor hole mobility results in non-uniform carrier distribution in the active region of the GaN LEDs. The non-uniform carrier distribution in active region of the GaN LEDs reduces the radiative recombination rate and promotes electron overflow.

Figure 1.4 shows the electron overflow mechanism in the LED structure. The electrons and holes injected into the device can recombine in the active region. However, some electrons having sufficient energy can surmount the barrier and flow out of the active region without recombining with holes. The electron overflow has been reduced by implementing an Electron Blocking Layer (EBL) in the p-side of the LED.

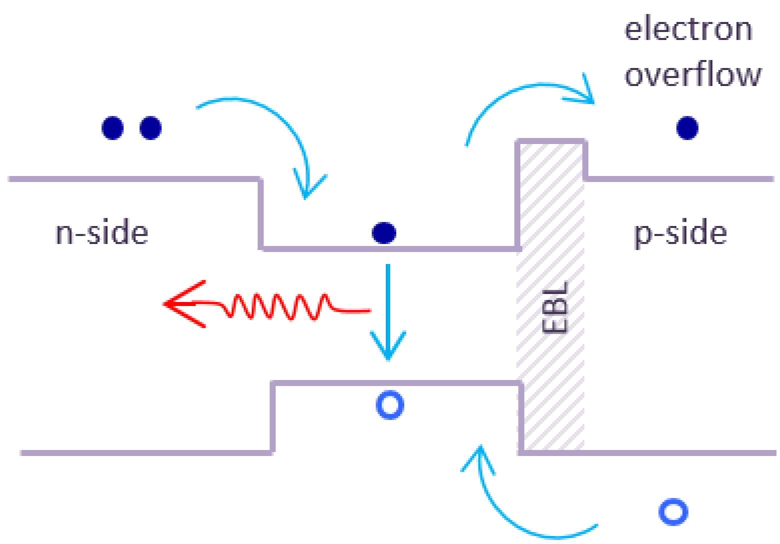

Figure 1-4. The electron overflow mechanism in the LED structure which shows overflowing some electrons with sufficient energy out of the active region without recombining with holes.

A wide bandgap AlGaN layer can be typically inserted between the active region and the p-side in the GaN LEDs to prevent the electrons from overflowing out of the active region. However, the EBL could reduce the hole injection efficiency depending on the band offset. Nguyen *et al.* showed that electron overflow could be largely suppressed with the use of a *p*-doped AlGaN electron blocking layer in nanowire structures [36].

1.2 Ultraviolet LEDs

These days, as the demand for various applications of ultraviolet (UV) light such as sterilization, disinfection, water and air purification, and biological sensors increases, the previously used UV sources such as mercury and xenon lamps are found to be unsatisfactory as they are bulky, expensive, and have a short lifetime. It has become increasingly important to investigate a new advanced technology as a source of UV emission for these applications. The UV LEDs are the tunable, long life, and environmentally friendly alternatives to traditional UV sources.

One promising candidate for such light sources is aluminum nitride (AlN), which has a direct bandgap energy of ~ 6.2 eV (~ 200 nm in wavelength) at room temperature. Progress in this field, however, has been limited by the difficulty in realizing electrically injected AlN LEDs, and to date, there are only a few reports on AlN LEDs [37-39].

The challenges for UV LEDs include the presence of large dislocation densities and the resultant low internal quantum efficiencies (<10 %), large device turn on voltages due to poor p-type doping, and TM polarization of emitted light which makes the light extraction from conventional *c*-plane AlN LEDs extremely challenging [38, 40-43]. The device performance is severely limited by several mechanisms such as the presence of large lattice mismatch for AlGaN materials, inefficient p-doping, and light emission with TM polarization which are described in the following sections.

1.2.1 Lattice mismatch

Since the GaN based LEDs are generally grown on SiC, sapphire, or Si substrate, the lattice mismatch occurs due to different lattice constants between the GaN materials and the substrate. The lattice mismatch is even larger for the AlGaN than for the GaN based LEDs and it can lead to large dislocations and cracking. Moreover, the lattice mismatch between AlGaN and the substrate induces extremely high dislocation densities in AlGaN epilayers [44-46], leading to poor material quality, and thus a low material internal quantum efficiency (IQE). For wavelengths in the range of 250–300 nm, the IQE can exceed 50% [44, 47, 48]. However, the IQE drops very fast to less than 10% when approaching the wavelengths of 210 nm [47].

Nishida *et al.* demonstrated a UV LED on AlN substrates to reduce dislocations in the active region [49]. The UV LEDs on AlN substrate have a lower density of defects compared to UV LEDs on sapphire. Although the AlN substrates reduce the defect density, they have a high absorption coefficient in the UV range, high cost, and limited availability. Later, Wang *et al.* studied the properties of GaN grown on AlN/sapphire templates and showed the dislocation reduction in GaN [50]. By replacing the AlN substrates with the AlN/sapphire template, the substrate absorption and defect density are reduced while internal quantum efficiency is improved [51].

1.2.2 Inefficient *p*-doping

Generally, p-type doping into Al-rich AlGaN UV LEDs is inefficient, largely due to the large dopant ionization energy in AlGaN. Mg is the most commonly used acceptor for GaN based materials. The Mg ionization energy increases with the increase in the material band gap. Since Mg ionization energy is higher for AlN, ~500 meV compared to GaN ~250 meV, efficient *p*-doping for AlGaN materials is very hard to reach [52]. Consequently, the inefficient *p*-doping leads to a decrease in the conductivity of the AlGaN based devices.

Figure 1.5 shows the activation energy of Mg acceptor of AlGaN as a function of Al composition [53]. The activation energy of Mg acceptor increases from ~170 meV to ~530 meV with increasing the Al composition in AlGaN from 0 to 1.

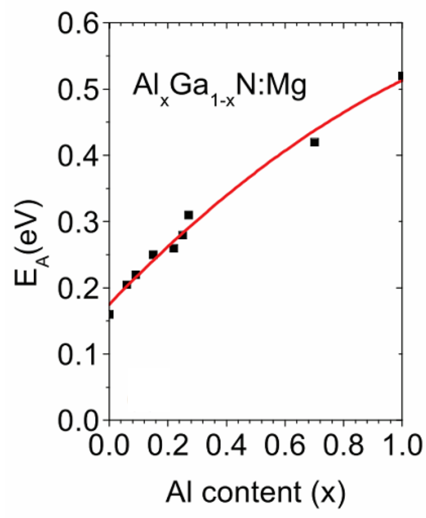

Figure 1-5. The activation energy of Mg acceptor of in AlGaN as a function of Al composition which increases from ~170 meV to ~530 meV with increasing Al composition from 0 to 1 [53].

Compared to the relatively mature GaN-based blue LEDs, the UV LEDs generally exhibit a very high turn on voltage. Sun *et al.* reported AlGaN based deep UV LEDs with emission wavelengths of 245-247 nm, which exhibit turn on voltage ~8 V [54]. This is largely due to the large Mg activation energy and the extremely low Mg doping efficiency at room temperature. The first demonstrated thin film AlN LEDs have a turn on voltage of more than 20 V [55], significantly larger than the bandgap of AlN (~6 eV).

1.3 GaN based nanowire LEDs

As described in previous sections, the GaN-based planar heterostructures have been severely limited by their low efficiency and their efficiency droop. Recently, significant progress has been made in nanowire LEDs, with the active regions consisting of well/disk-in-a-wire, core-shell, and dot-in-a-wire nanoscale heterostructures [56-60]. Nanowire LEDs are emerging as prospective candidates for GaN based devices. In nanowire devices, mechanisms that may contribute to efficiency degradation of GaN devices, such as dislocations, polarization fields, as well as the associated Quantum Confined Stark Effect (QCSE), can be greatly minimized [61-64].

Nanowire LEDs can be grown spontaneously using molecular beam epitaxy (MBE) on low cost, large area Si [65, 66]. Kikuchi *et al.* reported such nanowire LEDs with the embedded InGaN/GaN multiple quantum disk in 2004 [67]. Selective area growth is another method to achieve nanowire LEDs with well-defined position and size [68, 69]. The emission characteristics of nanowire LEDs grown by the selective area method can be controlled by the position and size of holes arrays on pre-patterned substrates.

Nanowire LEDs offer an efficient light emission across nearly the entire visible spectral range [66, 70, 71]. The different *In* compositions in InGaN/GaN active regions lead to the different color emissions. White light LEDs can be achieved by mixing multiple color emissions from a single nanowire. Such white light LEDs were reported by Lin *et al.* [71].

Compared to the performance of conventional planar heterostructures, however, the performance of such nanoscale LEDs is more susceptible to electron leakage out of the device active region due to large densities of defects along the nanowire. The resulting carrier loss and nonradiative carrier recombination severely limit the maximum quantum efficiency achievable at high injection currents. The electron overflow has been mitigated by utilizing the *p*-modulation doped nanowire LEDs [61], or the high bandgap AlGaN EBL inserted next to the *p*-GaN side of nanowire LEDs [72].

The nanowire structure, having high surface-to-volume ratio, offers more area for the photons to escape. This results in a higher light extraction which will be described later. Although the large surface-to-volume ratio of nanowires is advantageous for high light extraction efficiency, it also causes a high density of surface states. The defect states are introduced in the forbidden band gap of the semiconductor due to the termination of the crystal structure periodicity at the surface. The performance of a nanowire is limited by the surface states, which can reduce the carrier injection efficiency by capturing carriers from the active region [73]. With the use of self-organized InGaN/AlGaN dot-in-a-wire core-shell nanowire arrays we can significantly improve carrier injection efficiency. In this structure, an AlGaN shell can be spontaneously formed on the sidewall of the nanowire during growth of the AlGaN barrier of the quantum dot active region, which can lead to drastically reduced nonradiative surface recombination.

1.3.1 Nanowire UV LEDs

Another significant advantage of nanowire LEDs is the emission spectra tuning, by incorporating the materials with different compositions in the active region, to reach wide frequency ranges from UV to infrared. To address the challenges related to UV LEDs, besides further improving the planar AlN technology, various approaches with low dimensional structures have been explored, such as photonic crystals [74] and nanowires [75-81].

The nanowire structures can be an alternative solution for the UV LED applications, as they offer effective strain relaxation and fewer dislocations. Because of the efficient strain relaxation to the nanowire large area side walls, the nanowires can be essentially defect free, and thus they can provide a much higher material internal quantum efficiency compared to thin films. Recently, with the improved MBE growth of AlGaN nanowires on Si, high quality AlGaN nanowires were demonstrated [82], and the AlN nanowire LEDs with high internal quantum efficiency and excellent electrical performance were realized [39].

1.4 Light extraction efficiency

Generally, the output power of LEDs is defined by the external quantum efficiency (EQE) of the device, which is determined by light extraction efficiency (LEE) together with the IQE, described previously. To date, however, the device performance is severely limited by the EQE. In the case of planar LEDs, the light extraction is significantly reduced by the total internal reflection, due to the refractive index contrast between the semiconductor material and the air. Recently, various techniques have been developed to increase the light extraction efficiency, including chip shaping [83], surface roughness [84-86], patterned sapphire substrate [85, 87], photonic crystal structures [88, 89], graded refractive index material [90], and surface plasmon resonance [91]. The basic principle behind these approaches is to increase the escape cone by expanding the escape surface, or to enable multiple photon entry into the escape cone by surface roughening [92-94].

The nanowire structure, having high surface-to-volume ratio, offers more area for the photons to escape, resulting in a reduction in the total internal reflection. The light extraction efficiency can be enhanced by guiding the photons towards the nanowire surface. By careful design of the nanowires, considering several design parameters such as the nanowire diameter and spacing between nanowires, ~70% light extraction efficiency is achievable.

The light extraction efficiency of a GaN LED can also be significantly enhanced by integrating the GaN LED with nanotube arrays as an alternative approach. Optical microcavities are structures wherein light can be confined at microscopic scales. Semiconductor materials are suitable for microcavities for a number of reasons. One of the major reasons is that the high refractive index of semiconductors allows for the design of compact microcavities with strong optical confinement. The designs of semiconductor optical microcavities include microdisks [95], microrings [96], micropillars [97], and photonic crystals [98]. Another recent addition to the design of microcavities is the rolled-up tubes [99]. These tube cavities are formed by the self-rolling of strained nano-membranes as they are released from the host substrates. They can be manufactured in various material systems that allow for the creation and subsequently selective release of strained membranes. Rolled-up tube cavities offer an unprecedented control over the confined optical modes [100, 101] and the emission characteristics [102, 103]. These properties, in conjunction with the possibility of transferring them onto foreign substrates [104], set them apart from the previously mentioned microcavities. In this regard, rolled-up semiconductor tubes have emerged as promising candidates to enhance light extraction efficiency. In GaN LEDs, extracting the generated photons out of the device is difficult. Most of the photons are reflected at the GaN/air interface due to the total internal reflection, and consequently are trapped and absorbed inside the LED. The use of rolled-up nanotubes [105-107] significantly enhances the light extraction efficiency of GaN based LEDs. The light extraction involves two successive steps: the coupling from the light source to the tube and the subsequent emission from the tube to the air.

1.4.1 Light extraction efficiency of deep UV LEDs

The light extraction efficiency is one of the main limiting factors of the external quantum efficiency of deep UV LEDs, which remains significantly lower than that of visible LEDs. The low light extraction efficiency of the UV LEDs is attributed to total internal reflection, due to the high refractive index of the semiconductors compared to that of the air, and the optical polarization property of high composition AlGaN quantum wells (QWs).

The valence band profile of GaN and AlN present different band orders. Although Transverse Electric (TE) emission, perpendicular to the c-axis ($E \perp c$), is dominant in GaN based visible LEDs, the portion of Transverse Magnetic (TM) emission, parallel to the c-axis ($E \parallel c$), in AlGaN based UV LEDs increases significantly with the higher Al composition [108, 109], due to the different band structures of the AlN and GaN at the Γ-point of the Brillouin zone [110]. For the ternary compound $Al_xGa_{1-x}N$, the polarization of the emitted light changes from TE to TM with increasing Al composition. TM emission becomes dominant for AlGaN LEDs operating at ~ 280 nm, or shorter wavelengths, which largely prevents the light extraction from the top surfaces. As the light with TM polarization propagates mainly in the horizontal direction, the light can only propagate in-plane and cannot escape from the large area top surface. This unique light polarization in AlGaN LEDs, therefore, causes the light extraction efficiency to be ~ 10%, or less in the deep UV wavelength range [111-113].

Our LED research has been reported on LabTalk-Nanotechnology on June 28th 2012. They mentioned that "Compared with conventional planar LED heterostructures, the use of nanowires offers several extraordinary advantages, including drastically reduced dislocation densities and polarization fields, enhanced light output efficiency due to the large surface-to-volume ratios and compatibility with low cost, large-area silicon substrates. However, the quantum efficiency of currently reported nanowire LEDs generally exhibits a very slow rise with injection current. To find out more, researchers at McGill University in Canada have examined the emission characteristics in detail and attempted to identify the fundamental carrier loss mechanisms."

1.5 Dissertation overview

In this context, the optical and electrical characteristics of nanowire-based light sources for photonic integrated circuits have been intensely studied. We have investigated several methods to enhance the external quantum efficiency of GaN based nanowire LEDs. We have demonstrated that electron overflow in nanowire LEDs can be effectively prevented with the incorporation of a p-doped AlGaN EBL, leading to the achievement of phosphor-free white light emitting diodes that can exhibit virtually zero efficiency droop. We have further reported on the demonstration of a new type of axial nanowire LED heterostructures, with the use of self-organized InGaN/AlGaN dot-in-a-wire core-shell nanowire arrays. We have proposed InGaN/GaN dot-in-a-wire tunnel injection white light emitting diodes, wherein electrons and holes are injected into the quantum dot active region through two separate InGaN injector wells. Moreover, we have shown that the light extraction efficiency of GaN LEDs can be significantly enhanced by integrating with nanotube arrays. The light extraction involves two successive steps, including the coupling from the light source to the tube and the subsequent emission from the tube to the air. We have enhanced the light extraction efficiency of deep UV LEDs using periodic array of nanowires. The emission of the guided modes could be inhibited and redirected into radiated modes utilizing nanowire structures. We have shown that an unprecedentedly high light extraction efficiency of ~72% can be achieved.

Chapter 2 presents an overview of the theoretical methods utilized for the simulation of GaN based LEDs. We have utilized the finite difference time domain to determine the light extraction efficiency and simulate the mode profile of nanowire-based GaN LEDs. We have investigated the contribution of different processes inside the LED structures including Shockley-Read-Hall recombination, radiative recombination, and Auger recombination using the ABF model. We have further presented the APSYS to study the unique characteristics of nanowire LEDs including energy band diagram, wave functions, carrier distributions, and electron overflow and recombination rate, etc.

Several p-doped AlGaN EBLs such as conventional and distributed EBLs will be presented in Chapter 3 to achieve phosphor-free white LEDs that can exhibit virtually zero efficiency droop at high injection currents. We have investigated the impact of electron overflow on the performance of nanowire LEDs operating in the entire visible spectral range. We have demonstrated that, with the incorporation of a p-doped AlGaN electron blocking layer between the active region and the p-GaN section, electron overflow can be effectively prevented. Moreover, we have developed a new type of LED heterostructures, with the use of self-organized InGaN/AlGaN dot-in-a-wire core-shell nanowire arrays that can significantly reduce the electron overflow. The AlGaN barrier layers can function as distributed EBLs, which is found to be much more effective in reducing electron overflow, one of the primary causes of efficiency droop, compared to the conventional AlGaN EBL.

In Chapter 4, we have performed a detailed investigation of tunnel injection phosphor-free nanowire white LEDs, wherein injected electrons are first thermalized in an InGaN injector well and can be subsequently injected to the electronically coupled quantum dot active region by tunneling. It is shown that electron overflow can be significantly reduced without using any Al-containing EBL. An additional InGaN hole injector well is incorporated between the quantum dot active region and p-GaN, which can further enhance the hole injection efficiency and harvest electrons escaped through the near-surface region of nanowires. By combining the green and red emission from the quantum dot active region with the blue emission from the InGaN hole injector, we have demonstrated highly stable, phosphor-free white light emission.

In Chapter 5, we have numerically investigated the light extraction efficiency of GaN-based visible LEDs with the presence of rolled-up tube structures using the finite element method based solver Comsol Multiphysics. The effects of nanotube feature on the light extraction efficiency, including the wall thickness, the number of turns, the positions of notches and active region, and the array configuration are studied in detail. It is observed that the light extraction efficiency can be enhanced by nearly fourfold with the use of optimally designed GaN nanotubes. Such monolithically integrated nanotube/LED structure provides a flexible, low cost approach to significantly enhance the light extraction efficiency of the emerging micron- and sub-micron LED arrays.

The different regimes of light extraction in deep UV LEDs using nanowire arrays is analyzed in chapter 6. Finite difference time domain simulations show that the use of nanowire arrays leads to an increase in the light extraction efficiency of ultraviolet LEDs by ~7 times compared to conventional UV LEDs. The light extraction efficiency enhancement is attributed to the decrease in total internal reflection due to refractive index contrast between semiconductor and air. The effects of nanowires topology on the light extraction efficiency are also investigated and the directional UV LEDs are achieved by employing biperiodic arrays of nanowires. We have further investigated nanowire ultraviolet LEDs which support the slow light modes. The slow light UV LEDs with extremely low group velocities are predicted to give a strong gain enhancement which could be applicable for UV edge emitting lasers.

In chapter 7, we utilize the side emission properties of periodic nanowires to realize significantly enhanced extraction efficiency of UV LEDs. Due to the extremely large surface-to-volume ratios, light escapes from the nanowire structure and the total internal reflection inside the nanowire is considerably reduced. A nanowire structure can be utilized to inhibit the emission of the guided modes and redirect trapped light into radiated modes. We have investigated the light extraction efficiency of UV LEDs using three-dimensional (3D) finite difference time domain method. We have studied the dependence of light extraction efficiency on nanowire structural parameters such as the nanowire size and density and the p-GaN thickness, which play an important role on the light extraction efficiency. We have further investigated the effect of device sizes, as well as the random variation in the nanowire diameter and spacing on the light extraction efficiency. It is observed that an unprecedentedly large light extraction efficiency of up to 72% can be achieved.

Finally, summary of this context and a guideline to future works are discussed in Chapter 8.

2 Theoretical methods

2.1 Introduction

The optical and electrical properties of GaN LEDs, including the output power, the electron and hole distributions, and electric mode profile are numerically calculated using different simulation tools and models. We have successfully applied Finite Difference Time Domain (FDTD) to optimize the design of nanowire LEDs. We have calculated the Poynting vectors utilizing FDTD to determine the light extraction efficiency of GaN LEDs. We have further simulated the mode profile of nanowire-based GaN LEDs using the FDTD simulation.

We have comprehensively investigated the dependence of the internal quantum efficiency of nanowire LEDs on the current density using the ABF model. Through these studies, we have identified the significance and impact of various recombination processes including Shockley-Read-Hall recombination, radiative recombination, and Auger recombination on the device performance. The simulation results are further correlated with experimental measurements.

Further studies on the unique characteristics of nanowire LEDs were performed by simulating the energy band diagram and carrier distribution in the device active region using the advanced LED device simulation software APSYS. Utilizing APSYS, critical parameters related to the device performance can be calculated, including energy band diagram, wave functions, carrier distributions, electron overflow and recombination rate, etc.

2.2 Lumerical FDTD software package

There are different methods for the analysis of optical devices, such as the Finite Element Method, the Beam Propagation Method and the FDTD method [114]. The FDTD is an accurate method and the most popular method for studying electromagnetic problems such as optical cavities and light emitting diodes. The essence of the FDTD method consists in solving a time and space discretized version of Maxwell's equations. The time dependent Maxwell's equations for a linear isotropic material in a source free region can be written in the following form:

$$\frac{\partial H}{\partial t} = -\frac{1}{\mu(r)} \nabla \times E \tag{1}$$

$$\frac{\partial E}{\partial t} = \frac{1}{\varepsilon(r)} \nabla \times H \tag{2}$$

In these equations $\varepsilon(r)$ is permittivity and $\mu(r)$ is permeability of the material both of which are position dependent. In two dimensions, the fields can be decoupled into two transversely polarized modes, the TM and TE modes. These equations are discretized in the space and time domain using the principles of Yee algorithm [115].

Equations 1 and 2 can be discretized to stepping formulas in time and two dimensional mesh within the x–y coordinate system for the E-polarization, Where the index n denotes the discrete time step, indices i and j denote the discretized grid point in the x–y planes respectively. Equations 3, 4, and 5 show the discretized formulas for the 2D E-polarization.

$$H_x\Big|_{i,j+\frac{1}{2}}^{n+\frac{1}{2}} = H_x\Big|_{i,j+\frac{1}{2}}^{n-\frac{1}{2}} - \frac{\Delta t}{\mu_0}\left[\frac{E_z\big|_{i,j+1}^{n} - E_z\big|_{i,j}^{n}}{\Delta y}\right] \tag{3}$$

$$H_y\Big|_{i+\frac{1}{2},j}^{n+\frac{1}{2}} = H_y\Big|_{i+\frac{1}{2},j}^{n-\frac{1}{2}} - \frac{\Delta t}{\mu_0}\left[\frac{E_z\big|_{i+1,j}^{n} - E_z\big|_{i,j}^{n}}{\Delta x}\right] \tag{4}$$

$$E_z\Big|_{i,j}^{n+1} = E_z\Big|_{i,j}^{n} + \frac{\Delta t}{\varepsilon_{i,j}}\left[\left(\frac{H_y\big|_{i+\frac{1}{2},j}^{n+\frac{1}{2}} - H_y\big|_{i-\frac{1}{2},j}^{n+\frac{1}{2}}}{\Delta x}\right) - \left(\frac{H_x\big|_{i,j+\frac{1}{2}}^{n+\frac{1}{2}} - H_x\big|_{i,j-\frac{1}{2}}^{n+\frac{1}{2}}}{\Delta y}\right)\right] \tag{5}$$

The FDTD cell size (if $\Delta x = \Delta y$) and the time step (Δt) should comply with the well-known “Courant Condition”:

$$\Delta t \le \frac{\Delta x}{\sqrt{m} \cdot c} \tag{6}$$

where c is the speed of light in free space and m is the dimension of the simulation (m=2 throughout this context). Berenger’s perfectly matched layers (PML) are located around the whole structure as absorbing boundary condition and acts as free space [116]. An adequately broadband and modulated Gaussian pulse is launched into the active region, and then we placed some detectors which measure the time varying electric and magnetic field. Using the Fast Fourier Transform (FFT) of the fields calculated by FDTD, the Poynting vector over the detectors is integrated and power transmission spectra are computed.

Recently the FDTD has been successfully applied in different electromagnetic applications such as the optical filters [117-119] and the LED designs [88, 120, 121]. Figures 2.1 shows the 3D schematic of a nanowire LEDs used for FDTD simulation.

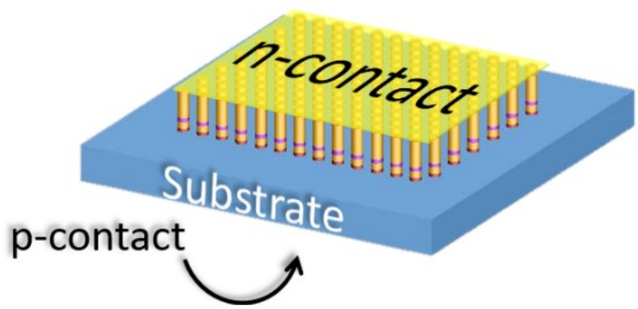

Figure 2-1. The 3D schematic of the hexagonal array of nanowires with the spacing (center to center) ~ 194 nm and diameter of the nanowires ~ 119 nm.

Schematically shown in Figure 2.2 is the simplified two-dimensional (2D) layer by layer structure of a nanowire LED. The LED structure consists of a hexagonal array of nanowires. The spacing (center to center) and diameter of the nanowires are 194 and 119 nm respectively. Each nanowire consists of 10 nm p-GaN, 100 nm p-AlGaN, 60 nm AlGaN multiple quantum well active region, and 400 nm n-AlGaN. The underlying substrate is assumed to be a reflective layer. It is assumed the whole structure with a top surface area of 2.5×2.5 μm^2 is enclosed with PMLs to absorb outgoing waves without causing any reflection [122]. Several refractive index models are supported by the material database in Lumerical FDTD including *sampled data model* obtained by experimental material data, *dielectric model* which is used to create a material with a constant real index at all frequencies, and *(n,k) material model* which is used to create a material with a specific value of *n* and *k* at a single frequency. In our simulation, we use *(n,k) material model* to have materials with different refractive indexes at different frequencies. A single dipole source with Gaussian shape spectrum and TM mode (parallel to the nanowire axis) is positioned in the middle of the AlGaN MQW active region. The wavelength used for the simulation is 280 nm. The Poynting vectors used to determine the light extraction efficiency of UV LEDs are calculated on the path shown as dotted red line. The light extraction efficiency from the device side surfaces is defined as the ratio of emitted power out from the side surfaces of the LED to the total emitted power of the device active region. Figures 2.2 shows the simulated mode profile of nanowire-based UV LED using the FDTD simulation. The figure actually shows the sum of the amplitude squares for all electric field components, i.e. $|E_x|^2+|E_y|^2+|E_z|^2$. To clearly show the electric mode profile we used the log scale, base 10.

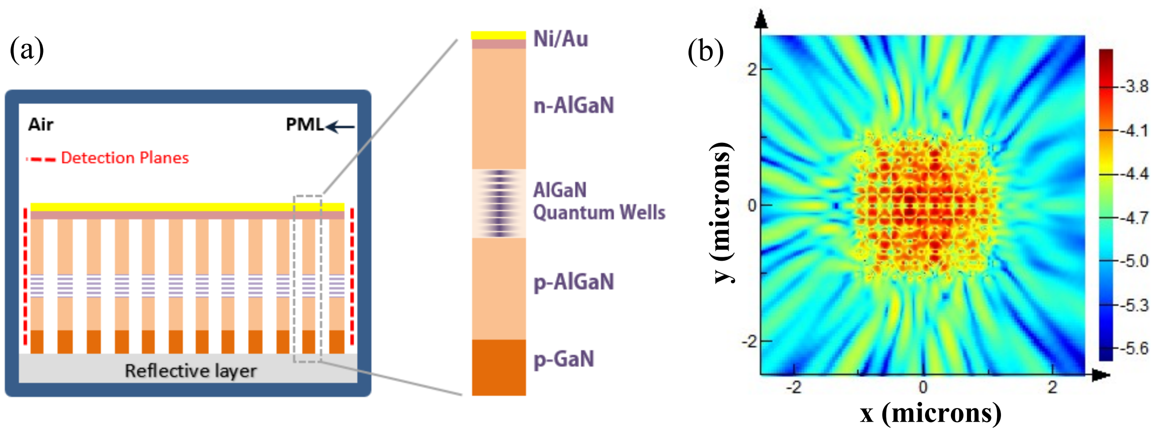

Figure 2-2. (a) The two-dimensional layer by layer schematic of the nanowire-based UV LED structure. Each nanowire consists of 10 nm p-GaN, 100 nm p-AlGaN, 60 nm AlGaN multiple quantum well active region, and 400 nm n-AlGaN, and (b) the simulated mode profile of LED plotted in the log scale, base 10.

2.3 ABF model

Generally, the electrically injected electrons and holes in LED devices could recombine radiatively to generate the photons or non-radiatively known as Shockley-Read-Hall recombination, and Auger recombination illustrated in Figure 2.3. There is a competition between the radiative and nonradiative recombination processes.

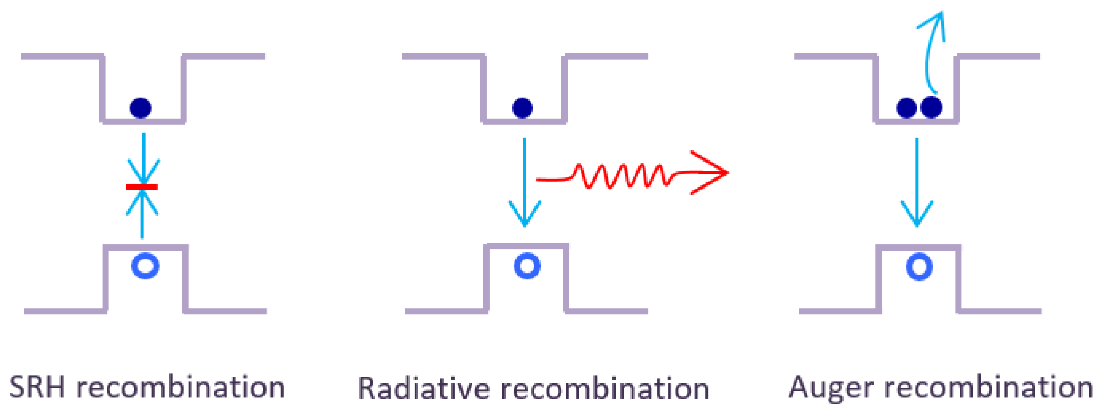

Figure 2-3. Different carrier recombination processes in LEDs including Shockley-Read-Hall recombination, radiative recombination, and Auger recombination.

The internal quantum efficiency (η) of LEDs can be well simulated by using the following model which is known as the ABF model [19, 123-126]:

$$\eta_i = \frac{BN^2}{AN+BN^2+f(N)} \tag{7}$$

where N is the carrier density in the device active region, and A and B are the Shockley-Read-Hall nonradiative recombination and radiative recombination coefficients, respectively [127, 128]. $f(N)$ represents for any other higher order effects, including Auger recombination and carrier leakage outside of the device active region, which are generally described by $CN^3 + DN^4$. The carrier density (N) is related to the injection current density (J) by:

$$J = qW_{QD}[AN + BN^2 + f(N)] \tag{8}$$

where W_{QD} represents the total thickness of the quantum dot active region. In this model, carriers are assumed to be uniformly distributed in the active region, and the contribution of all materials in the active region is equal in the radiative recombination.

The ABF model is a highly effective approach to analyze experimental results and to gain the critical information of the LED performance [129, 130]. Recent studies have shown this relatively simple model was successfully applied to nanowire LEDs [29, 34, 131]. The insightful information of LED operation could be obtained from the derived values of *A*, *B* and *C*.

The *A* value is directly related to Shockley-Read-Hall nonradiative recombination with the unit of s^{-1}. Commonly reported values of *A* for conventional planar LEDs are in the range of ~ 10^7 s^{-1}. From the ABF model, the *A* is associated with the first order of carrier density. The contribution of *A* in the ABF model decreases with increasing carrier density compared to other factors with the higher order of carrier density. This agrees with the physical principle in which the nonradiative recombination caused by defects will be saturated under high carrier densities. Due to the enhanced surface recombination in nanowire LEDs, their IQEs exhibit slow rising trend which can lead to large values of *A* [29, 34, 36, 65].

The *B* value with the unit of cm^3s^{-1} is associated with radiative recombination due to the spontaneous emission in the active region. From the ABF model, the *B* is associated with the second order of carrier density which determine the maximum value of IQE. In nanowire LEDs, the *B* value can be greatly enhanced due to the reduced polarization effect and quantum confinement stark effect.

The *C* value is responsible for efficiency droop that commonly observed in GaN LEDs [36]. The large values of *C* in GaN LEDs are basically caused by enhanced Auger recombination and electron overflow. The presence of electron overflow or any other high order carrier loss mechanisms can lead to efficiency droop under high injection currents and has been commonly measured for previously reported nanowire LEDs [34, 132, 133].

We modeled the IQE of a typical dot-in-a-wire GaN LED using the ABF model as an example. The dot-in-a-wire GaN LED with the incorporation of a p-doped InGaN/GaN test quantum well between the device active region and p-GaN layer is shown in Figure 2.4(a). Illustrated in Figure 2.4(b), the measured relative external quantum efficiency at various temperatures can be well simulated using this model. The derived values of (A, B, C) are ~ (2.6×10^{8} s^{-1}, 6.0×10^{-10} $cm^{3}s^{-1}$, 1.0×10^{-28} $cm^{6}s^{-1}$), (6×10^{8} s^{-1}, 4×10^{-10} $cm^{3}s^{-1}$, 6×10^{-29} $cm^{6}s^{-1}$), and (7.0×10^{8} s^{-1}, 3×10^{-10} $cm^{3}s^{-1}$, 4.5×10^{-29} $cm^{6}s^{-1}$) at 80 K, 200 K, and 300 K, respectively.

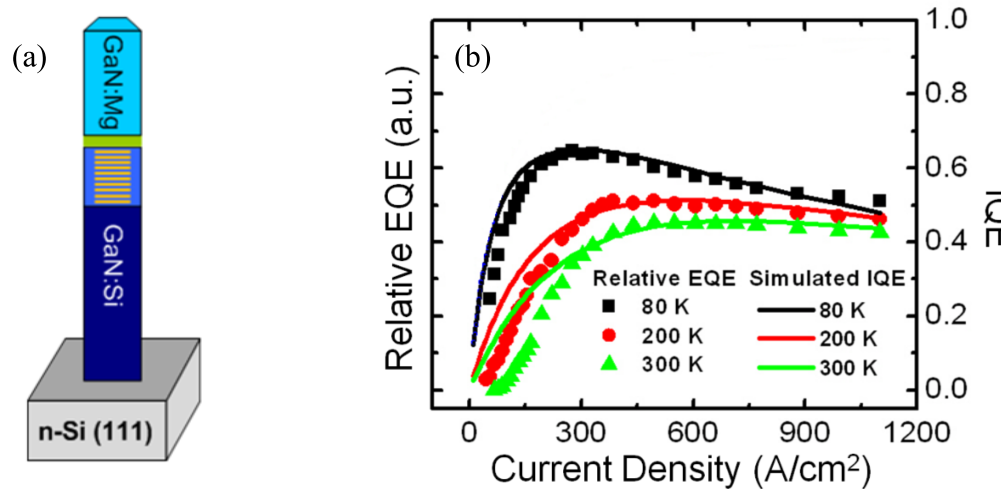

Figure 2-4. (a) Schematic illustration of InGaN/GaN dot-in-a-wire LEDs. (b) Variations of the relative EQE related to the emission from the quantum dot active region measured at 80, 200, and 300 K. The simulated IQE based on the ABF model is also shown for comparison.

The simulated Shockley-Read-Hall recombination coefficient (A ~ 1×10^{9} s^{-1}) at 300 K in the present nanowire LEDs is significantly larger than the values commonly employed in InGaN/GaN quantum well blue-emitting LEDs [134-136] and can be partly explained by the significantly enhanced nonradiative surface recombination, due to the very large surface-to-volume ratios of nanowires. The commonly observed surface band bending in GaN nanowires [137], as well as the inefficient carrier capture by quantum dots due to hot carrier effect [138, 139], may also contribute considerably to the nonradiative carrier recombination on nanowire surfaces. As a consequence, emission characteristics of nanowire LEDs are predominantly determined by surface-related nonradiative carrier recombination under relatively low carrier injection conditions. The continuous decrease in the quantum efficiency under high injection currents, efficiency droop, suggests the presence of electron overflow or any other high order carrier loss mechanisms.

2.4 Crosslight APSYS software package

Further study on the unique characteristics of nanowire LEDs is performed by simulating the band diagram and carrier distribution in the device active region using the advanced LED device simulation software APSYS (Crosslight Software). Advanced physical models are offered to generate meaningful results for the GaN based LEDs [129, 140, 141]. It can solve self-consistently with hydrodynamic equations, quantum mechanical wave equation, and Poisson's equation, etc. Physical parameters (mobility, bandgap, carrier life time, etc.) can also be modified accordingly for the simulation. Simulations are controlled by several input files in APSYS which represent the device structure and the parameters. Commonly accepted parameters are used in the simulation, including Shockley-Read-Hall life time (100 ns) [141] and Auger recombination coefficient ($1\times10^{-33}cm^6s^{-1}$) [34]. With given structural designs and conditions, critical parameters related to the device performance can be calculated, including energy band diagram, wave functions, carrier distributions, leakage current and recombination rate, etc.

APSYS contains several models to simulate the spontaneous and strain-induced polarization field for GaN based LEDs. The first one leads to automatically defined interface charges at heterojunction interfaces which their intensity may vary from one structure to another depending on various materials used. In the case of nanowire structures, due to the effective strain relaxation, polarization field should be much smaller than that in planar structures. The reduction of the polarization field can affect the interface charges at heterojunction interfaces.

The self-consistent model in the software was applied to iterate between the Poisson/drift-diffusion equations and the Schrodinger solver, and to find a self-consistent solution. Since the electrical field could be different for each QW in a MQW active region due to the interface charges, the independent-MQW model was utilized to apply the Schrodinger solver for each QW separately.

The second model to simulate the spontaneous and strain-induced polarization field for GaN based materials is the interface model. In the interface model, the semiconductor interface states and the physical models used by the simulation software was specified manually.

Shown in Figure 2.5 are the typical dot-in-a-wire GaN LED and its calculated band structures using APSYS. The simulated structures consist of active regions with ten $In_{0.25}Ga_{0.75}N$ quantum dots separated by 3 nm GaN barriers. Figure 2.5 (b) shows the energy band diagrams of GaN LED at 1000A/cm^2. The quasi Fermi level for holes (dashed line near the valance band) is gradually shifted away from the valance band near the *n*-region due to the low hole transport and poor injection efficiency which is the direct reflection of the large hole effective mass and small mobility.

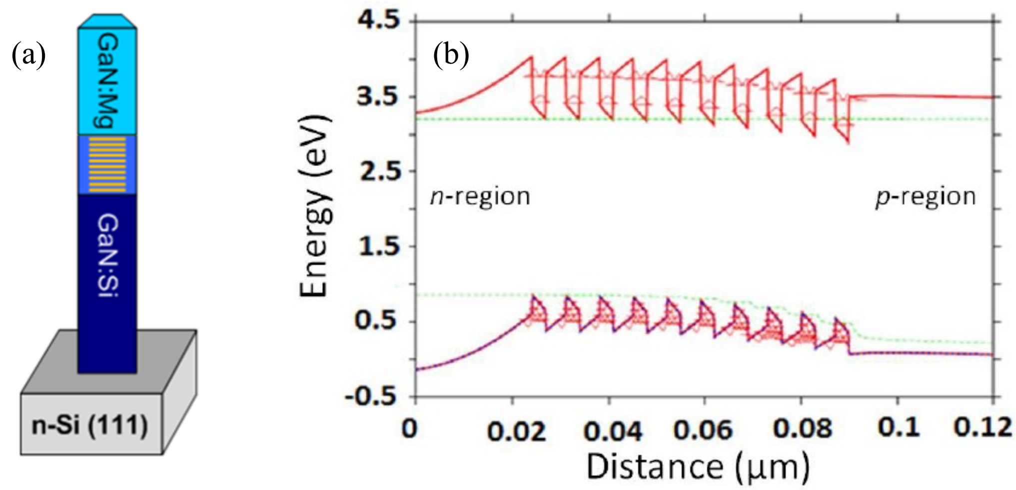

Figure 2-5. (a) Schematic illustration of InGaN/GaN dot-in-a-wire LEDs. (b) Calculated band diagram of the InGaN/GaN LED including quantum dots wave functions. Dashed lines represent quasi-Fermi levels.

2.5 Conclusion

In summary, we introduced the different simulation tools and models used in our studies. We utilized the FDTD to determine the light extraction efficiency and simulate the mode profile of nanowire based GaN LEDs. We investigated the contribution of different processes inside the LED structures including Shockley-Read-Hall recombination, radiative recombination, and Auger recombination using ABF model. We further presented the APSYS to study the unique characteristics of nanowire LEDs including energy band diagram, wave functions, carrier distributions, and electron overflow and recombination rate, etc.

3 Different approaches for electron blocking layers

3.1 Introduction

One of the grand challenges for future solid state lighting is the development of all semiconductor-based white LEDs, consisting of monolithically integrated blue, green and red devices, that can exhibit ultrahigh-efficiency, long-term reliability, and tunable color emission. The achievement of such devices using conventional GaN-based planar heterostructures, however, has been severely limited by their low efficiency and efficiency droop. In this regard, significant progress has been made in nanowire white LEDs, with the active regions consisting of well/disk-in-a-wire [142, 143], core/shell [144], ternary nanowire [65, 145], and dot-in-a-wire nanoscale heterostructures [133, 146]. In such nanowire devices, mechanisms that may contribute to efficiency degradation, including dislocations, polarization fields, as well as the associated QCSE [129, 147-149] can be greatly minimized [146, 150, 151]. Compared to conventional planar heterostructures, however, the performance of such nanoscale LEDs is more susceptible to electron leakage out of the device active region, due to the presence of large densities of states/defects along the nanowire surface. Several p-doped AlGaN EBLs such as conventional and distributed EBLs will be proposed in this chapter to achieve phosphor-free white LEDs that can exhibit virtually zero efficiency droop at high injection currents.

3.2 Conventional electron blocking layer

In this section, we have investigated the impact of electron overflow on the performance of nanowire LEDs operating in the entire visible spectral range. Intrinsic white-light emission is achieved by incorporating self-organized InGaN quantum dots, with controlled compositions and sizes, in defect-free GaN nanowires on a single chip. The role of electron overflow on the performance limit of such nanoscale LEDs has been elucidated by characterizing, both experimentally and theoretically, the current-dependent electroluminescence emission of an InGaN/GaN test quantum well embedded between the quantum dot active region and the p-GaN, wherein electrons escaping the quantum dot active region can be correlated with the optical emission from the test well. It is measured that electron overflow is present even under relatively low injection conditions, which, in conjunction with the nonradiative carrier recombination related to the surface states/defects, largely determines the unique emission characteristics of nanowire LEDs. Moreover, we have demonstrated that, with the incorporation of a p-doped AlGaN electron blocking layer between the active region and the p-GaN section, electron overflow can be effectively prevented. The resulting white LEDs can exhibit virtually no efficiency droop, thereby providing a highly promising approach for future high-power, all semiconductor-based solid state lighting.

In this experiment, vertically aligned InGaN/GaN dot-in-a-wire heterostructures were grown on Si(111) substrates by radio-frequency plasma-assisted molecular beam epitaxy under nitrogen rich condition. The device active region contains 10 vertically coupled InGaN/GaN quantum dots. Each InGaN quantum dot has a height of ~ 3 nm and is capped by ~ 3nm GaN layer. Figure 3.1(a) shows the schematic of a typical dot-in-a-wire LED device.

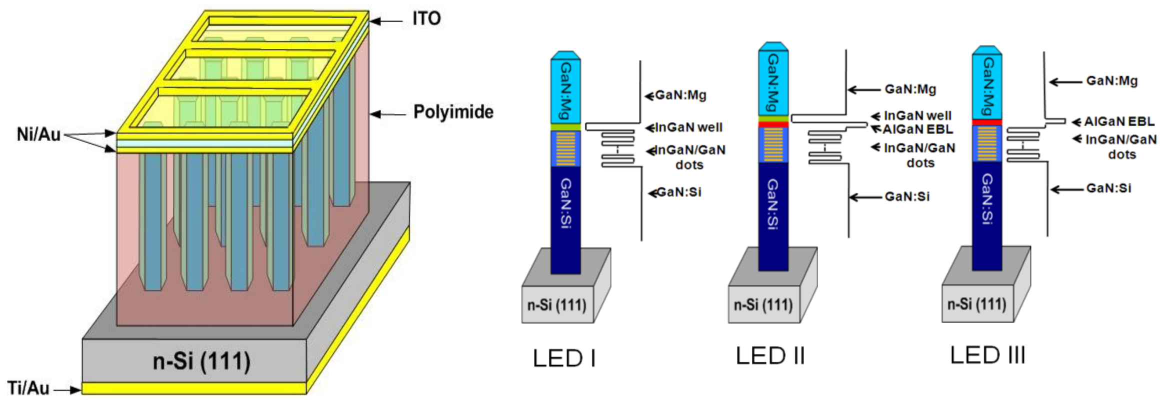

(a) (b)

Figure 3-1. (a) Schematic illustration of InGaN/GaN dot-in-a-wire LEDs grown on Si(111) substrates. (b) Illustration of the three LED designs. From left to right: InGaN/GaN dot-in-a-wire LEDs with the incorporation of an InGaN test well (LED I), an AlGaN electron blocking layer and an InGaN test well (LED II), and an AlGaN electron blocking layer (LED III) between the quantum dot active region and the p-GaN section.

To investigate the electron overflow phenomena, an InGaN/GaN dot-in-a-wire LED heterostructure, with the incorporation of a p-doped InGaN/GaN test quantum well between the device active region and p-GaN section is grown (LED I shown in Figure 3.1(b)). In this design, electrons leaking out of the quantum dots can recombine with holes in the test well, which has smaller *In* compositions than that of the InGaN/GaN quantum dots. The resulting optical emission can therefore be used to evaluate electron overflow in nanowire LEDs. Additionally, we have designed nanoscale LEDs (LED II) with the incorporation of a p-doped AlGaN electron blocking layer between the LED active region and the InGaN test quantum well, in order to study its effect in preventing the electron overflow [152, 153]. Finally, a 3rd LED device that consists of a p-doped AlGaN electron blocking layer, but without the InGaN test well is also investigated. The three nanowire LED designs are schematically shown in Figure 3.1(b). The flat energy band diagrams along the nanowire axial dimension are also shown in the insets.

Illustrated in Figure 3.2(a) are the photoluminescence spectra of such nanowire LEDs measured at room temperature. The peak at ~ 550 nm is related to the emission from the quantum dot active region, while the peak at ~ 430 nm is due to the presence of an InGaN test well, which can be measured for the 1st and 2nd nanowire LEDs. The dot-in-a-wire LEDs exhibit excellent structural properties. Shown in Figure 3.2(b) is a 45° tilted scanning electron microscopy image of the devices grown on Si(111) substrates. The wire diameters and densities are in the ranges of 40 to 100 nm and ~ 1×10^{10} cm^{-2}, respectively. The nanowires are vertically aligned to the substrate and exhibit a high degree of size uniformity.

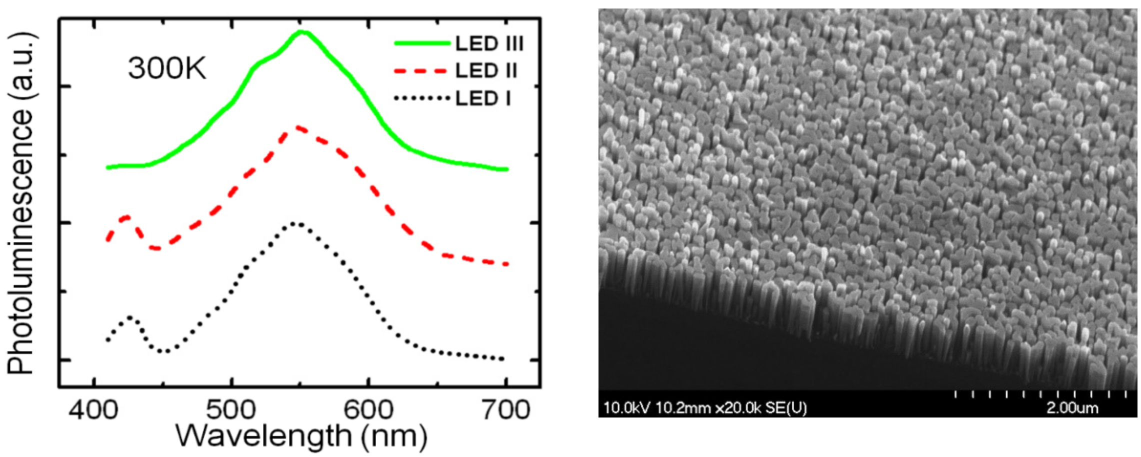

(a) (b)

Figure 3-2. (a) Room-temperature photoluminescence spectra of the three LED device heterostructures. The emission peak at ~ 430 nm is due to the presence of the InGaN test well, which can be clearly measured for LEDs I and II. (b) A 45° tilted scanning electron microscopy image of the InGaN/GaN dot-in-a-wire LED heterostructure grown on Si(111) substrates.

A CM200 microscope with acceleration voltage of 200 kV was used to obtain bright field transmission electron microscopy (TEM) images. The TEM images for LED II are shown in Figure 3.3, wherein the 10 InGaN/GaN quantum dots, the AlGaN electron-blocking layer as well as the InGaN quantum well are identified. There are no extended defects, such as misfit dislocations and stacking faults observed in the view of the current images. InGaN/GaN quantum dots are positioned in the center of the nanowires, due to the strain-induced self-organization.

Emission characteristics of the InGaN/GaN dot-in-a-wire LEDs were studied. Electroluminescence was measured under pulsed biasing condition at various temperatures. Junction heating is minimized by using a low (~ 0.1%) duty cycle.

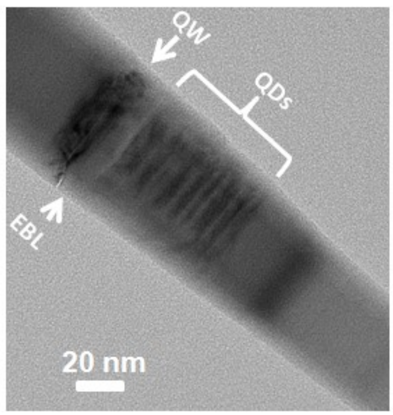

Figure 3-3. Bright field TEM image of InGaN/GaN dot-in-a-wire LED II.

Figure 3.4(a) shows the normalized electroluminescence spectra of LED I under various injection currents, which incorporates an InGaN test well between the device active region and the p-GaN. The peak at ~ 550 nm is related to the emission from the quantum dot active region, which agrees well with the photoluminescence measurements shown in Figure 3.2(a). However, with increasing current, it is seen that the emission at ~ 430 nm becomes progressively stronger, which is attributed to the carrier recombination in the InGaN/GaN test well. This observation confirms that injected electrons can escape from the quantum dot active region and subsequently recombine with holes in the InGaN test well. Shown in Figure 3.4(b) is the derived relative external quantum efficiency (in arbitrary units) related to the electroluminescence emission from the quantum dot active region as well as that from the test well measured at room temperature. It is seen that, for the emission from the test well, the quantum efficiency continuously increases with current, which can be explained by the increased electron overflow and therefore enhanced emission from the test well region with increasing current. For the emission of the quantum dot active region, the relative external quantum efficiency reaches its peak value at ~ 300-400 A/cm^2 and shows a continuous drop (~ 6%) with further increasing current up to 1,100 A/cm^2, which can be explained by the enhanced electron overflow at high injection conditions. It may also be noticed that electron overflow is appreciable below such injection levels, evidenced by the presence of emission peak from the test well at an injection current of ~ 300 A/cm^2.

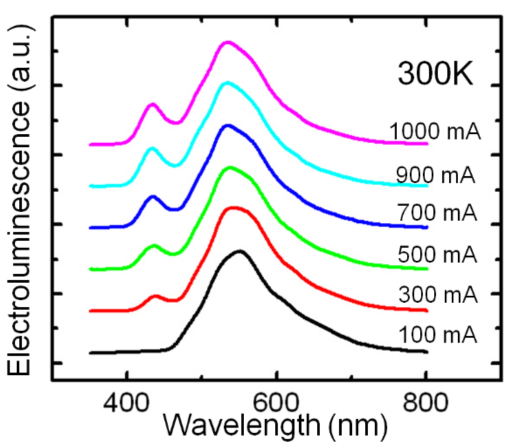

(a)

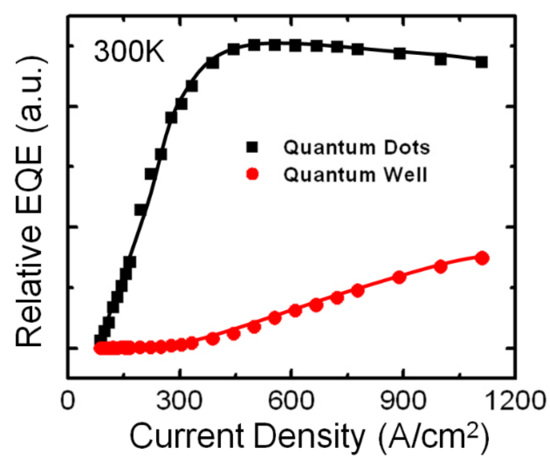

(b)

Figure 3-4. (a) Normalized electroluminescence spectra of LED I under various injection currents. The peak at ~ 550 nm is related to the emission from the quantum dot active region, while the peak at ~ 430 nm is related to the emission from the InGaN/GaN test quantum well. (b) Variations of the relative EQE with injection current for the emission from the quantum dot active region and the test well of LED I measured at room temperature.

It is further measured that electron overflow is relatively enhanced with decreasing temperature. Shown in Figure 3.5(a), the emission intensity from the test well becomes comparable to that from the quantum dots when measured under an injection current of ~ 450 A/cm^2 at low temperatures (80K), while its intensity is only ~ 10% of that from the dots when measured at the same injection current at room temperature. Illustrated in Figure 3.5(b), the estimated efficiency drop is ~ 6%, 10%, and 21% for measurements performed under an injection current of ~ 1,100 A/cm^2 at 300 K, 200 K, and 80 K, respectively.

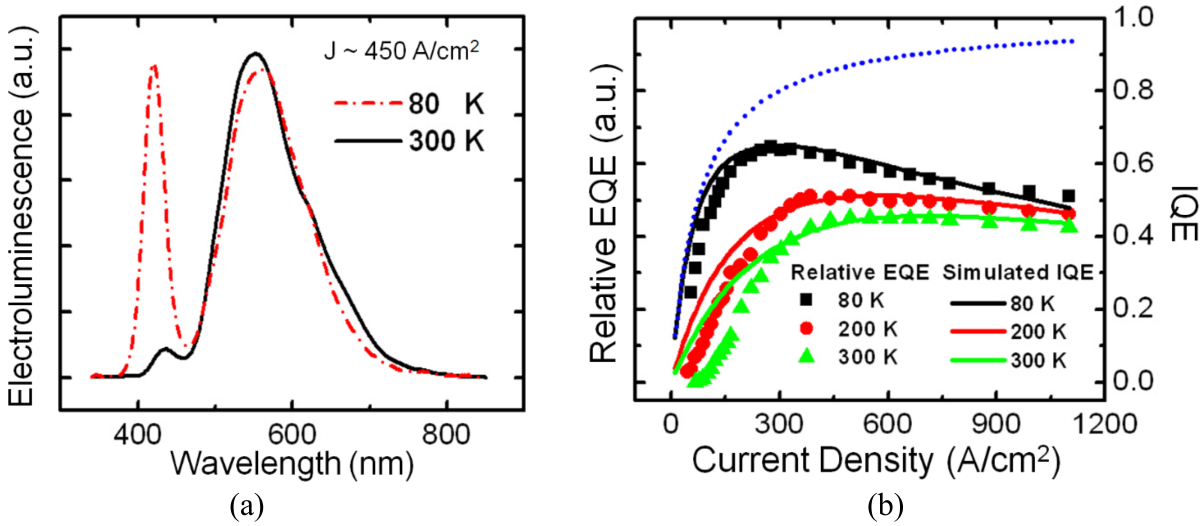

Figure 3-5. (a) Normalized electroluminescence spectra of LED I measured at 300K (solid line) and 80K (dashed line) under an injection current density of ~ 450A/cm^2. (b) Variations of the relative EQE related to the emission from the quantum dot active region measured at 80, 200, and 300 K. The simulated IQE based on the ABF model is also shown for comparison. The dotted blue line is the calculated IQE versus injection currents in the absence of any 3rd or higher order carrier loss mechanisms.

The increased electron overflow at low temperatures is consistent with recent theoretical studies [141]. At low temperatures, the hole concentration in the p-GaN region is drastically reduced, due to the large activation energy for Mg dopant, thereby leading to reduced hole injection efficiency and further enhanced electron overflow. It is also observed that, with decreasing temperature, the peak quantum efficiency shifts to lower current densities, shown in Figure 3.5(b), due to the reduced Shockley-Read-Hall recombination as well as enhanced bimolecular radiative recombination rate.

These phenomena can be well simulated by using the following model for the internal quantum efficiency,

$$\eta_i = \frac{BN^2}{AN+BN^2+f(N)} \tag{1}$$

where *N* is the carrier density in the device active region, and *A* and *B* are the Shockley-Read-Hall nonradiative recombination and radiative recombination coefficients, respectively [127, 154]. $f(N)$ represents for any other higher order effects, including Auger recombination and carrier leakage outside of the device active region, which are generally described by $CN^3 + DN^4$. The carrier density (*N*) is related to the injection current density (*J*) by:

$$J = qW_{QD}[AN + BN^2 + f(N)] \tag{2}$$

where W_{QD} represents the total thickness (~ 25-30 nm) of the quantum dot active region. The commonly reported surface recombination velocity on GaN surfaces is in the range of ~ 10^3 to 10^4 cm/s [155, 156]. In the present context, the average radius of GaN-nanowires is ~ 100 nm. Therefore, the *A* coefficient, due to carrier surface recombination, is estimated to be in the range of ~ 10^8 to 10^9 s^{-1}, which is considered as initial value in ABF model. Illustrated in Figure 3.5(b), the measured relative external quantum efficiency at various temperatures can be well simulated using this model. The derived (A, B, C) values are shown in Table I.

Table I: The derived (A, B, C) values at 80 K, 200 K, and 300 K

Temperature	A (s^{-1})	B (cm^3s^{-1})	C (cm^6s^{-1})
80K	2.6×10^{8}	6.0×10^{-10}	1.0×10^{-28}
200K	6.0×10^{8}	4.0×10^{-10}	6.0×10^{-29}
300K	7.0×10^{8}	3.0×10^{-10}	4.5×10^{-29}

Additionally, it may be noticed that the quantum efficiency of nanowire LEDs generally reaches its peak value at significantly higher current densities (> 200 A/cm^2), compared to that (< 20 A/cm^2) of conventional InGaN/GaN quantum well blue LEDs [34, 133, 157-159]. This observation is consistent with the simulated Shockley-Read-Hall recombination coefficient (A ~ 7×10^{8} s^{-1}) at 300 K in the present nanowire LEDs, which is significantly larger than the values commonly employed in InGaN/GaN quantum well blue-emitting LEDs [134-136] and can be partly explained by the significantly enhanced nonradiative surface recombination, due to the very large surface-to-volume ratios of nanowires. As a consequence, emission characteristics of nanowire LEDs are predominantly determined by surface-related nonradiative carrier recombination under relatively low carrier injection conditions. In the absence of any 3^{rd} or higher order carrier loss mechanisms, it is further expected that the quantum efficiency should display a small, continuous increase under high injection conditions, illustrated as the dotted blue line in Figure 3.5(b). To date, however, such phenomena have not been observed in nanowire LEDs, suggesting the presence of electron overflow or any other high order carrier loss mechanisms, which can lead to either a nearly constant quantum efficiency or efficiency droop under high injection currents and has been commonly measured for previously reported nanowire LEDs [34, 132, 133] .

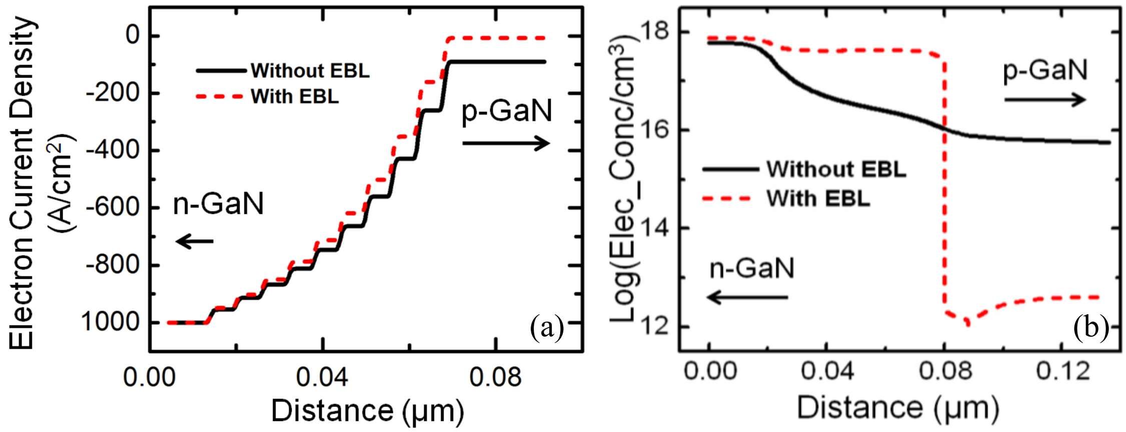

Figure 3-6. (a) Simulated electron current density across the InGaN/GaN quantum dot active region using the APSYS simulation package with (red curve) and without (black curve) the incorporation of an AlGaN EBL. (b) The electron density distribution across the near surface GaN region of the nanowire LEDs with (red curve) and without (black curve) the incorporation of an AlGaN electron blocking layer.

Further study on the electron overflow is performed by simulating the band-diagram and carrier distribution in the device active region using the advanced LED device simulation software APSYS. The simulated LED active region consists of ten vertically coupled InGaN quantum dots, separated by ~ 3 nm GaN barrier layers. With an average *In* composition of ~ 20% in the dots, ~ 10% of the injected current density can leak into the p-GaN region under an injection current density of ~ 1,000 A/cm^2, illustrated as the black curve in Figure 3.6(a).

However, much more severe electron overflow is expected, due to the highly nonuniform *In* distribution along the lateral dimension of the wires. More importantly, the current path associated with the near-surface GaN region, presented by the black curve in the Figure 3.6(b), can contribute significantly to electron overflow in InGaN/GaN dot-in-a-wire LEDs as well. Simulations were also performed on LED III, wherein a p-doped AlGaN electron blocking layer is incorporated between the quantum dot active region and p-GaN. It can be seen that the electron overflow, through either the quantum dot active region or the near-surface GaN, can be largely eliminated, illustrated as the red curves in Figure 3.6(a) and (b) [152, 153], for Al compositions in the range of ~ 10% to 20%. The use of higher Al composition, however, may significantly reduce the hole injection efficiency.

Experimentally, the effectiveness of utilizing an AlGaN electron blocking layer in preventing electron overflow in nanowire LEDs is demonstrated by examining the electroluminescence spectra of LED II, wherein an 8 nm $Al_{0.15}Ga_{0.85}N$ electron blocking layer is incorporated between the quantum dot active region and the InGaN test well. The measurements were performed up to very high injection conditions (~ 1,222 A/cm^2) at 80 K, 200 K, and 300 K, illustrated in Figure 3.7.

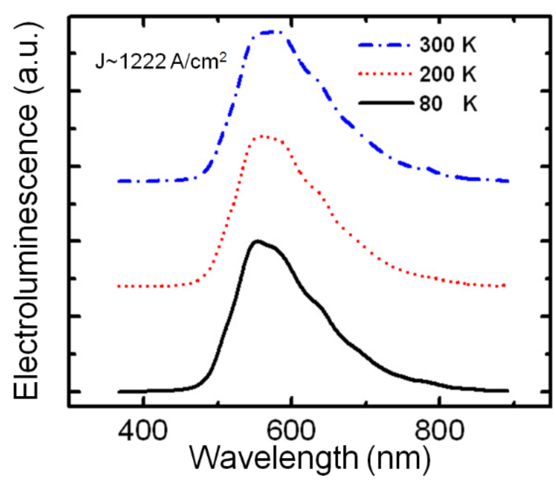

Figure 3-7. Normalized electroluminescence spectra of LED II measured under an injection current density of ~ 1,222 A/cm^2 at 80, 200, and 300 K. Emission peak from the InGaN test well is not observed, suggesting the drastically reduced, or the absence of electron overflow in the LED devices with the incorporation of an AlGaN electron blocking layer.

Compared to the photoluminescence results shown in Figure 3.1(c), however, only emission from the quantum dot active region (λ_{peak} ~ 550 nm) can be observed under electrical injection, and any emission from the test well (~ 430 nm) is absent for measurements performed at various injection conditions and temperatures, which confirms the drastically reduced, or eliminated electron overflow by the AlGaN electron blocking layer.

The performance characteristics of LED III, which consists of ten vertically aligned InGaN/GaN quantum dots and an AlGaN electron blocking layer are subsequently investigated. Variations of the relative external quantum efficiency with injection current are measured at 80 K, 200 K, and 300 K, depicted in Figure 3.8.

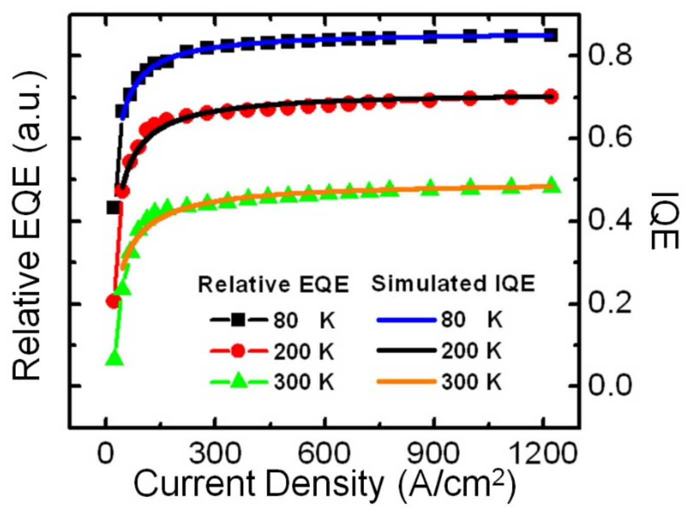

Figure 3-8. Variations of the measured relative external quantum efficiencies of LED III with injection current at 80 K, 200 K, and 300 K. The simulated IQE using the ABF model shows a good agreement with experimental results.

It is observed that the quantum efficiency first shows a drastic increase with increasing current, which is directly related to the saturation of surface defects with increasing carrier density. A very interesting phenomenon, however, is that the quantum efficiency shows a small, continuous increase upto very high injection currents (~ 1,222 A/cm^2), which has not been measured in previously reported nanowire LEDs [34, 133]. Such unique characteristics can be well modeled using the ABF model, described by Eqn. (1), for the LED internal quantum efficiency. Shown in Figure 3.8, the calculated internal quantum efficiencies (solid curves) are in excellent agreement with the experimental results. The derived (A, B, C) values are shown in Table II.

Table II: The derived (A, B, C) values at 80 K, 200 K, and 300 K

Temperature	A (s^{-1})	B (cm^3s^{-1})	C (cm^6s^{-1})
80K	7.2×10^{7}	6.8×10^{-10}	1.0×10^{-34}
200K	8.9×10^{7}	5.6×10^{-10}	2.0×10^{-34}
300K	9.6×10^{7}	3.9×10^{-10}	3.0×10^{-34}

While the values for A and B are reasonably close to those calculated for LED I, the smaller values for C confirms the drastic reduction of electron overflow by the AlGaN electron blocking layer. It is seen that the derived *C* coefficient (~ 10^{-34} $cm^{-6}s^{-1}$) is nearly four orders of magnitude smaller than the commonly reported values in InGaN quantum well heterostructures [158, 160, 161], thereby suggesting that Auger recombination plays an essentially negligible role on the performance of the InGaN/GaN dot-in-a-wire LEDs.

3.3 Distributed electron blocking layer

In this section, we have developed a new type of LED heterostructures, with the use of self-organized InGaN/AlGaN dot-in-a-wire core-shell nanowire arrays that can significantly reduce electron overflow. In this process, during growth of the AlGaN barrier of the quantum dot active region, an AlGaN shell is also spontaneously formed on the sidewall of the nanowire, which can lead to drastically reduced nonradiative surface recombination. The AlGaN barrier layers can function as distributed EBLs, which is found to be much more effective in reducing electron overflow, one of the primary causes of efficiency droop, compared to the conventional AlGaN EBL. Moreover, the hole injection and transport process can be significantly enhanced in such InGaN/AlGaN quantum dot superlattice structures. The device exhibits strong white light emission, due to compositional variations of the dots. An output power of more than 5 mW is measured for an InGaN/AlGaN dot-in-a-wire LED device.

Catalyst-free InGaN/AlGaN dot-in-a-wire core-shell nanowire LED heterostructures were grown on Si substrates by radio-frequency plasma-assisted MBE. The self-organized formation process of the dot-in-a-wire core-shell heterostructures is schematically illustrated in Figures 3.9(a)-(d). GaN:Si nanowires, with a height of 0.4 µm, were first grown directly on Si substrate. Shown in Figure 3.9(b), the InGaN dot, with a height of ~ 3 nm is formed at the center of the nanowire. Due to the strain-induced self-organization, the dot diameter is smaller than the nanowire dimension. The subsequently grown AlGaN barrier layer can cover the entire growth front, including the top and sidewalls of the InGaN dot, illustrated in Figure 3.9(c), thereby leading to the spontaneous formation of a large bandgap shell structure. The repeated growth of multiple, vertically aligned InGaN/AlGaN quantum dots, shown in Figure 3.9(d), enable the formation of a relatively thick, uniform AlGaN shell surrounding the device active region. The barrier of each quantum dot is also modulation doped *p*-type using Mg to enhance hole transport [133, 162]. White light emission with well controlled properties can be achieved by varying the In compositions of the dots. Finally, a 0.2 μm GaN:Mg section was grown on top, shown in Figure 3.9(d).

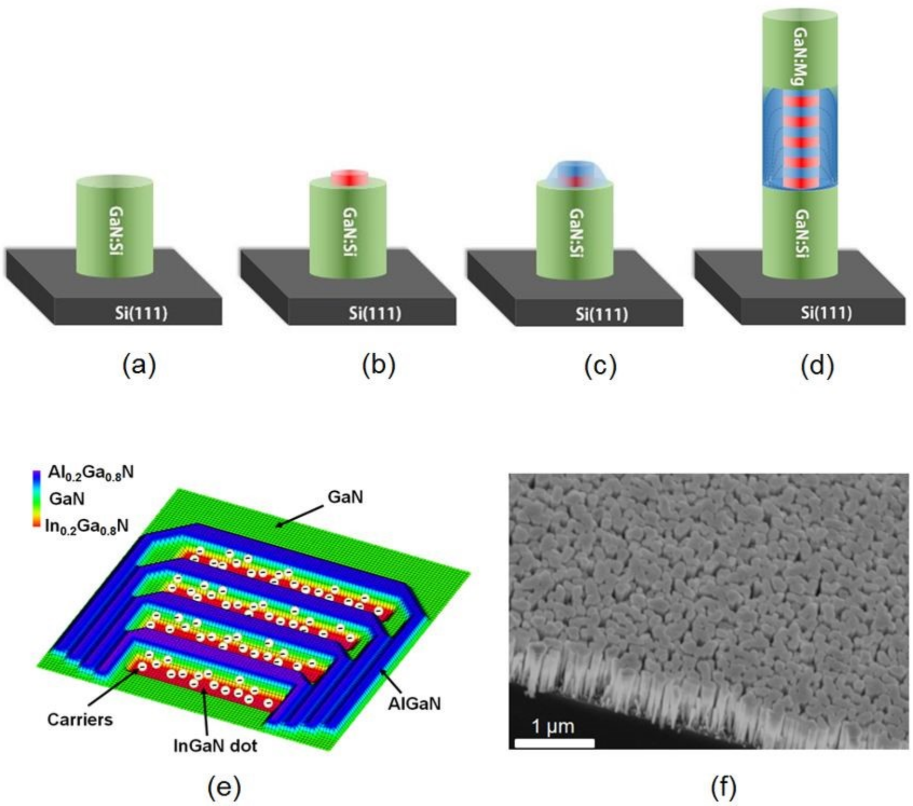

Figure 3-9. (a) – (d) Illustration of the epitaxial growth of catalyst-free InGaN/AlGaN dot-in-a-wire core-shell LED heterostructures on Si substrate. (a) GaN:Si segment was first grown on Si(111) substrate. (b) 3 nm InGaN dot was grown on GaN:Si. (c) The formation of AlGaN barrier and shell. (d) The formation of a thick AlGaN shell surrounding the InGaN quantum dot active region after the growth of multiple, vertically aligned InGaN/AlGaN dots. (e) Schematic illustration of the energy band diagram of the InGaN/AlGaN dot-in-a-wire core-shell LED active region, showing the three-dimensional carrier confinement. (f) A 45° tilted SEM image of a typical InGaN/AlGaN dot-in-a-wire core-shell LED heterostructure grown on Si substrate.

Figure 3.9(e) shows the energy band diagram of the InGaN/AlGaN dot-in-a-wire core-shell LED active region, which exhibits superior three-dimensional carrier confinement, due to the multiple AlGaN shell and barrier layers. Figure 3.9(f) is a 45 degree-tilted scanning electron microscopy (SEM) image for an InGaN/AlGaN dot-in-a-wire core-shell heterostructure grown on Si (111) substrate. It is seen that the vertically aligned nanowire arrays exhibit a high degree of size uniformity. Previous studies have shown that the majority of nanowires grown on Si by MBE are N-polar [163, 164].

High-angle annular dark-field (HAADF) atomic-number contrast imaging of single nanowires is shown in Figures 3.10(a) and (b), presenting clearly the ten InGaN/AlGaN quantum dots in the GaN nanowire. A detailed view of the active region in Figure 3.10(b) show that the ten InGaN dots (bright contrast) are centrally confined and capped by the AlGaN barriers (dark contrast), each of which form an Al-rich core-shell at the nanowire sidewall.

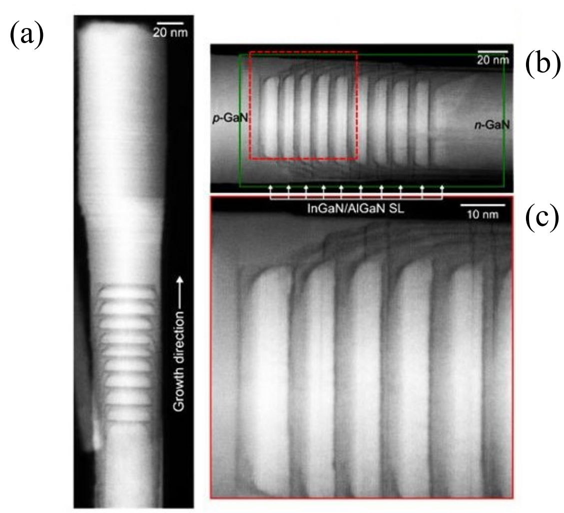

Figure 3-10. (a, b) STEM-HAADF images of the InGaN/AlGaN dot-in-a-wire core-shell heterostructures showing the InGaN dots, AlGaN barriers, and the Al-rich core-shell by atomic-number contrast. (c) Higher magnification atomic-resolution HAADF image of the selected region (boxed in red dashed line) in (b) showing the AlGaN core-shell and barriers in detail.

A higher magnification HAADF image of the core-shell (Figure 3.10(c)) also shows the continuity of the core-shell from the AlGaN barriers, suggesting their formation during the growth of the AlGaN barriers from the strong lateral diffusion of Al-rich AlGaN. The overall high crystalline quality of the dot-in-a-wire core-shell heterostructures is demonstrated in the atomic-resolution images of Figures 3.10(b) and (c).

Photoluminescence spectra of nanowire LED structures were measured using a 405 nm laser as the excitation source at room-temperature. The PL emission was spectrally resolved by a high-resolution spectrometer, and detected by a photomultiplier tube. Figure 3.11 shows the PL spectra of an InGaN/AlGaN core-shell nanowire LED (solid black) and an InGaN/GaN dot-in-a-wire structure with otherwise identical conditions (dotted red).

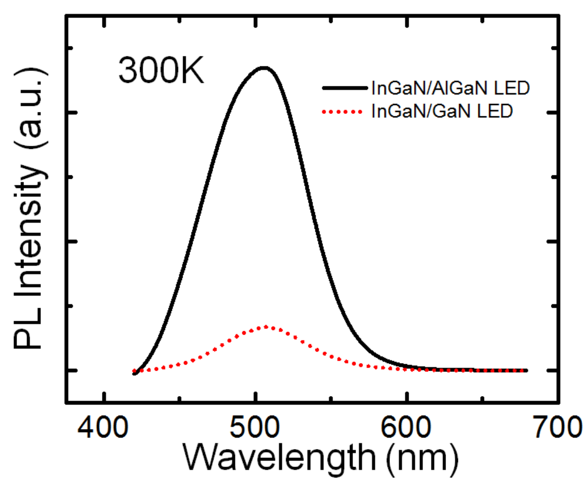

Figure 3-11. Photoluminescence spectra showing significantly enhanced emission for the InGaN/AlGaN dot-in-a-wire core-shell LED structure, compared to the InGaN/GaN nanowire sample without AlGaN shell measured using a 405 nm laser at room-temperature.

It is seen that the core-shell LED structure exhibits significantly enhanced PL intensity for emission from InGaN quantum dots, which is a factor of ~ 7 times higher than that of InGaN/GaN nanowire LED without using any AlGaN shell. The enhancement in PL intensity is directly correlated with the increase of Al composition in the AlGaN barrier layers. This is explained by the drastically reduced nonradiative surface recombination, due to the presence of large bandgap AlGaN shell, that leads to much more efficient carrier injection and radiative recombination in the quantum dot active region [165].

The performance of InGaN/AlGaN core-shell LED devices with an areal size of 1 × 1 mm^2 is then described. To minimize junction heating effect, the devices were measured under pulsed biasing conditions (~ 1% duty cycle). The InGaN/AlGaN LEDs exhibit excellent current-voltage characteristic with low resistance, shown in Figure 3.12(a). The output spectra under various injection currents are shown in Figure 3.12(b). It is seen that the spectra are highly stable and nearly independent of injection currents. The stable emission characteristics with increasing current are further illustrated in the CIE diagram in Figure 3.12(c). The derived *x* and *y* values are in the ranges of ~0.35–0.36 and 0.37–0.38, respectively. The devices exhibit nearly neutral white light emission, with correlated color temperature of ~ 4,450 K. The stable emission is attributed to the large inhomogeneous broadening of the dots and the enhanced hole transport in the *p*-type modulation doped InGaN/AlGaN quantum dot superlattices.

Illustrated in Figure 3.12(d), the output power increases monotonically with current. An output power of ~ 5.2 mW was measured for the core-shell LED at an injection current of ~ 600 mA at 10°C. Such output powers are more than two orders of magnitude higher than conventional InGaN/GaN axial nanowire LEDs without AlGaN shell and also much higher than the previously reported InGaN/GaN/AlGaN nanowire

LEDs [59]. The greatly improved output power is attributed to the increased carrier injection efficiency into the device active region, due to the effective carrier confinement offered by the shell structure and the drastically reduced surface recombination [165].

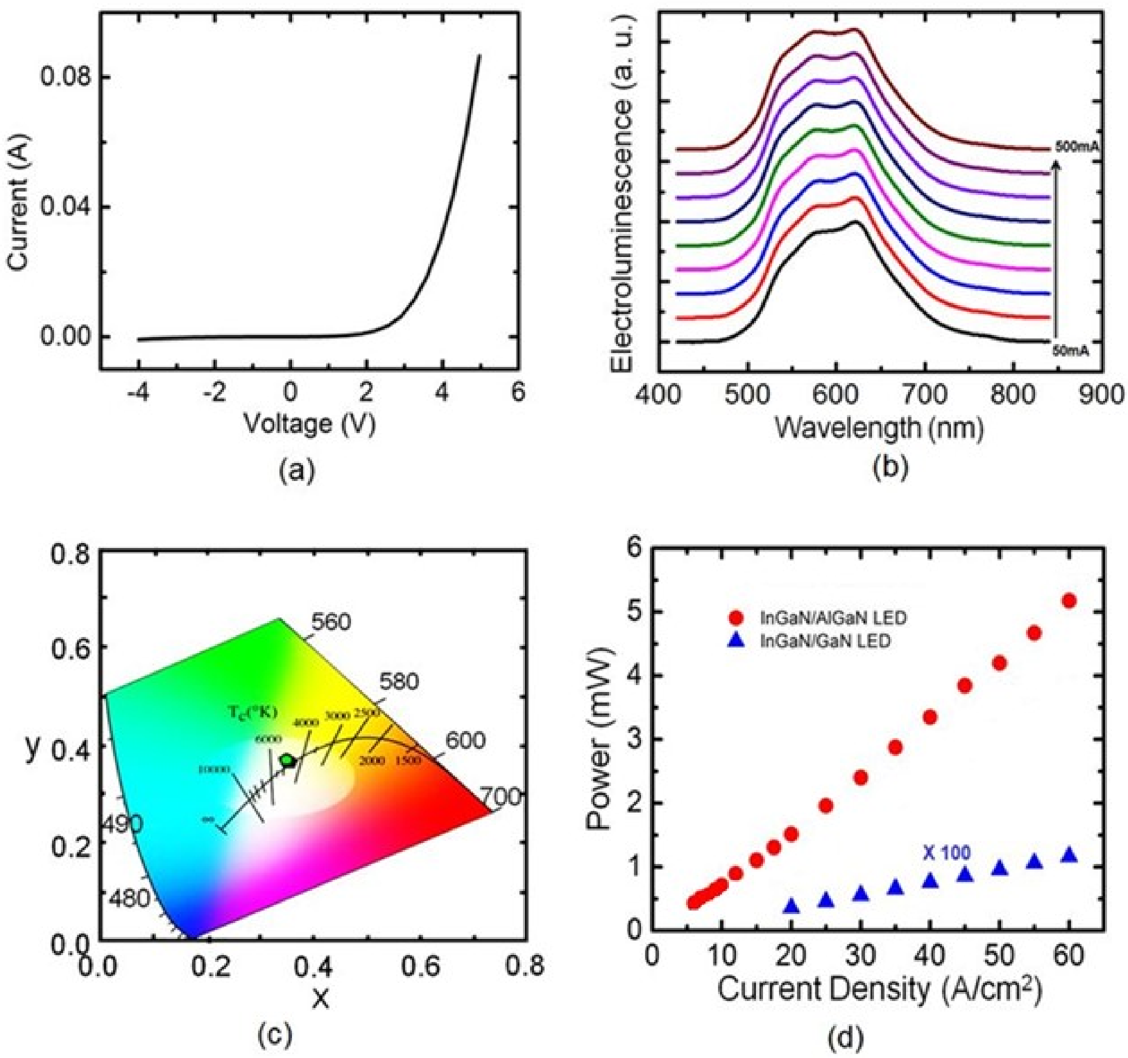

Figure 3-12. (a) Current vs. voltage characteristics of an InGaN/AlGaN dot-in-a-wire core-shell white LED on Si. (b) Electroluminescence spectra of the core-shell LED measured under different injection currents. (c) CIE diagram showing the stable white light emission for injection current from 50 mA to 500 mA, with the *x* and *y* values in the ranges of ~ 0.35 – 0.36 and 0.37 – 0.38, respectively. (d) Output power vs. injection current of the InGaN/AlGaN dot-in-a-wire core-shell LEDs measured under 1% duty cycle. Variations of the output power vs. current for the InGaN/GaN axial nanowire LED without AlGaN shell are also shown for comparison (blue triangle).

The optical and electrical properties of InGaN/AlGaN LEDs, including the output power and the electron and hole distributions are numerically calculated using the APSYS simulation software and compared to those of InGaN/GaN LED structures with and without the presence of an equivalent EBL. Schematics of the simulated structures are shown in Figure 3.13.

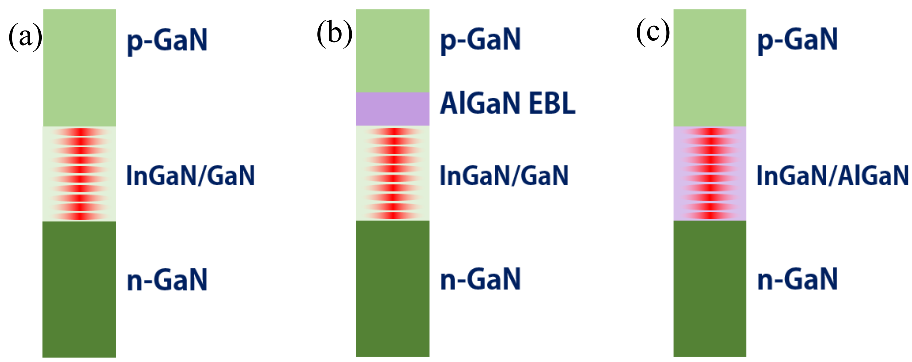

Figure 3-13. Schematics of (a) the InGaN/GaN LED heterostructure, (b) the InGaN/GaN LED with an equivalent AlGaN EBL, and (c) the InGaN/AlGaN LED heterostructure.

The APSYS is based on 2D finite element analysis of electrical and optical properties of semiconductor devices solving the Poisson's equation, carrier transport equation, and photon rate equation. Shown in Figure 3.13, the device active region consists of InGaN (3 nm)/(Al)GaN (3 nm) superlattice structures. An average In composition of 20% is used. For the core-shell structure, the Al composition in the AlGaN barrier layer is ~ 20%, shown in Figure 3.13(c). An equivalent AlGaN EBL (thickness ~ 30 nm) is also incorporated in the InGaN/GaN LED structure, illustrated in Figure 3.13(b).

The use of AlGaN EBL has been previously proposed and implemented to overcome the leakage of electrons outside of the LED active region [166-169]. However, in order to form a relatively thick AlGaN shell surrounding the device active region, a relatively thick (~ 30 nm) AlGaN EBL is required for the nanowire LEDs, which adversely affects the hole transport and injection into the active region, leading to highly nonuniform carrier distribution [129, 168, 170, 171]. We show that such an issue can be largely addressed by using distributed AlGaN EBL, i.e. InGaN/AlGaN superlattice structures. The presence of multiple AlGaN barrier layers in the device active region can lead to significantly reduced electron leakage.

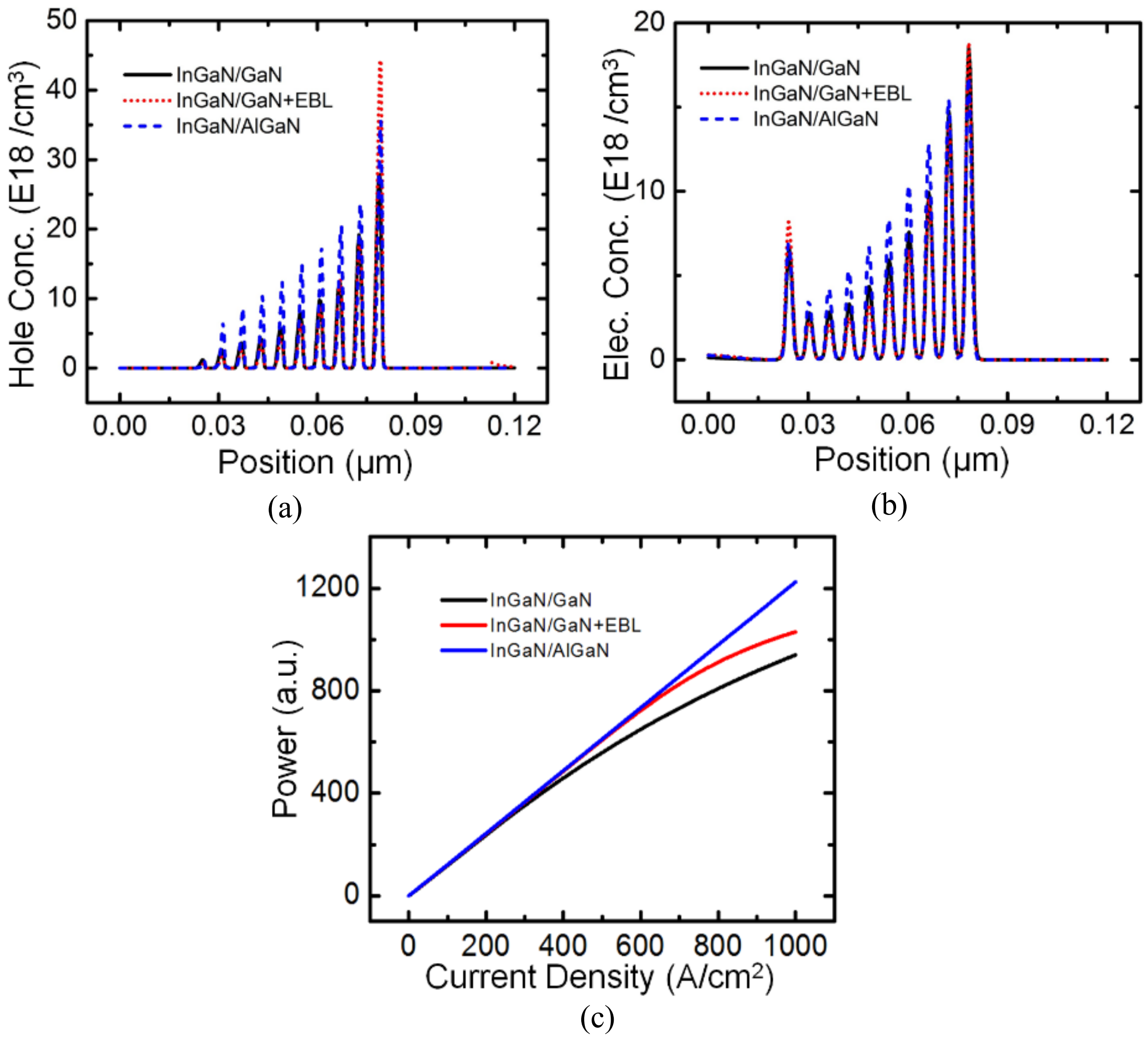

Figure 3-14. Simulated hole concentration (a) and electron concentration (b) in the active regions of the InGaN/AlGaN (dashed blue), the InGaN/GaN with an equivalent EBL (dotted red), and the InGaN/GaN LED heterostructures (black). (c) Simulated output power vs. injection current for the three LED structures. In this simulation, the effect of nonradiative surface recombination was not considered, which can lead to dramatically reduced power for conventional InGaN/GaN axial nanowire LEDs.

Moreover, illustrated in Figures 3.14, detailed simulation shows that the InGaN/AlGaN LEDs can exhibit more uniform electron and hole concentrations and significantly enhanced power, compared to InGaN/GaN LEDs. The improvement in efficiency droop is also evident in Figure 3.14(c).

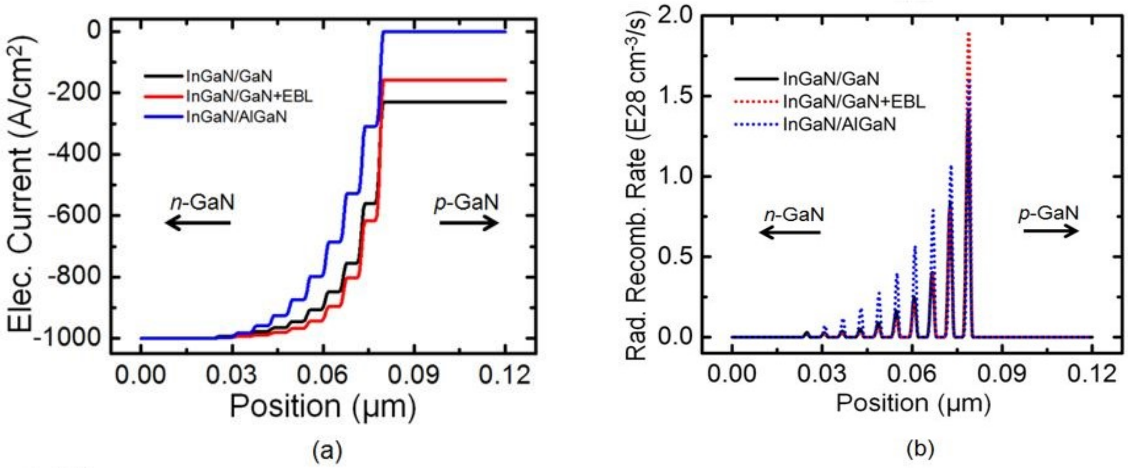

Figure 3-15. (a) Simulated electron current density for the InGaN/AlGaN LED (blue), the InGaN/GaN LED with an equivalent EBL (red), and the InGaN/GaN LED (black). (b) Simulated radiative recombination coefficients of the InGaN/AlGaN LED (dotted blue), the InGaN/GaN LED with an EBL (dotted red), and the InGaN/GaN LED (solid black) at an injection current of 1000 A/cm2.

Illustrated in Figure 3.15(a), electron overflow is near-completely suppressed with the use of InGaN/AlGaN superlattices, which is significantly better than InGaN/GaN LEDs. For comparison, in the conventional EBL design, the use of a relatively thick AlGaN EBL layer adversely affects hole transport from *p*-GaN to the active region [168, 171], which leads to non-negligible electron leakage, shown in Figure 3.15(a). Our studies further confirm that the distributed AlGaN EBL is comparable to, or better than conventional EBL with optimum designs in reducing electron overflow. Moreover, it is evident from Figure 3.15(a) that, in InGaN/AlGaN dot-in-a-wire core-shell LEDs, the *p*-AlGaN distributed EBLs can serve as multiple barriers and enable tunnel injection of electrons, thereby leading to significantly reduced hot carrier effect and more uniform carrier distribution across the device active region [172].

The improved performance by using distributed *p*-AlGaN EBLs is also directly related to the enhanced hole injection and transport process in the device active region. Illustrated in Figure 3.15(b), detailed simulation further shows that the InGaN/AlGaN LEDs can exhibit enhanced and more uniform radiative recombination, compared to InGaN/GaN LEDs, which leads to significantly enhanced output power and reduced efficiency droop.

3.4 Conclusion

In summary, through extensive theoretical and experimental studies, we have demonstrated unambiguously that the maximum achievable quantum efficiency of GaN-based nanowire LEDs is ultimately limited by electron leakage and overflow. Detailed temperature-dependent studies further confirm that efficiency droop in nanowire LEDs becomes more severe at lower temperatures, which is directly correlated with the relatively enhanced electron overflow with decreasing temperature. We have further achieved an effective control of electron overflow in phosphor-free InGaN/GaN dot-in-a-wire white LEDs by incorporating a p-doped AlGaN electron blocking layer between the quantum dot active region and the p-GaN. The resulting nanowire LEDs exhibit the white-light emission with virtually zero efficiency droop at high injection currents. We have further shown that self-organized InGaN/AlGaN dot-in-a-wire core-shell structures can overcome some of the critical challenges of previously reported axial nanowire LEDs, including large surface recombination and poor carrier dynamics, leading to significantly reduced carrier leakage and enhanced output power. Moreover, the *p*-AlGaN barrier layers can function as distributed EBLs, which is found to be highly effective in reducing electron overflow and enhancing hole transport. The dot-in-a-wire core-shell heterostructures can also emit light across the entire visible spectral range. Such unique nanowire heterostructures, with controllable carrier dynamics, will significantly advance the development of a broad range of nanowire photonic devices, including lasers, solar cells, and photodetectors.

4 Tunnel injection InGaN/GaN dot-in-a-wire white-light emitting diodes

4.1 Introduction

The performance of GaN-based quantum well LEDs has been severely limited by carrier leakage and electron overflow [36, 173], which leads to efficiency droop at high injection current [140, 174-178]. For the emerging nanowire LEDs, carrier leakage from the device active region may be much more severe, due to the extremely large surface-to-volume ratios and the presence of surface states/defects [29]. To effectively reduce electron overflow, a p-doped AlGaN EBL has been commonly incorporated between the device active region and p-GaN layer [36, 179-181]. Several p-doped AlGaN EBLs such as conventional and distributed EBLs have been studied in the previous chapter to achieve white LEDs with virtually zero efficiency droop at high injection currents. However, due to the strain-induced polarization field, a triangular potential well is formed in the valence band, which adversely affects the hole injection [182] and transport process and severely limits its uniform distribution in the device active region. The resulting non-uniform carrier distribution can further enhance Auger recombination [17, 18] and carrier leakage at high injection currents. Alternatively, electron overflow can be mitigated by suppressing hot-carrier effect in LEDs using thin InGaN barrier [176] and InGaN stair-case electron injector [174, 175]. More recently, reduced efficiency droop and current leakage has been measured by tunneling injection of holes into the LED active region [183-185] and by employing a p-InGaN hole reservoir layer [186]. An important consideration in these approaches, however, is the control of strain in the device active region in order to minimize the generation of extensive dislocations [187], which limits the incorporation of these special techniques in GaN-based LEDs operating in the green and red wavelength range.

Compared to quantum well LEDs, InGaN/GaN nanowire devices can exhibit significantly reduced strain distribution, and the emission wavelength can be readily tuned across nearly the entire visible wavelength range [65, 188, 189]. In this chapter, we have performed a detailed investigation of tunnel injection phosphor-free nanowire white LEDs, wherein injected electrons are first thermalized in an InGaN injector well and can be subsequently injected to the electronically coupled quantum dot active region by tunneling [190]. It is shown that electron overflow can be significantly reduced without using any Al-containing electron blocking layer. An additional InGaN hole injector well is incorporated between the quantum dot active region and p-GaN, which can further enhance the hole injection efficiency and harvest electrons escaped through the near-surface region of nanowires. By combining the green and red emission from the quantum dot active region with the blue emission from the InGaN hole injector, we have demonstrated highly stable, phosphor-free white light emission.

4.2 Simulation results and discussions

The InGaN/GaN dot-in-a-wire tunnel injection LED heterostructure is schematically shown in Figure 4.1(a). The device active region consists of ten vertically aligned InGaN quantum dots. Each quantum dot has a height of ~3 nm and is capped by a ~3 nm GaN barrier layer. Indium compositions of the dots are varied to achieve broadband emission in the green and red wavelength range. Previous studies suggested that the indium compositions of the dots were significantly reduced toward the near-surface region of the nanowires [66], illustrated in Figure 4.1(a). A 15nm $In_{0.13}Ga_{0.87}N$ well is grown on the n-GaN and is separated from the quantum dot active region by a ~3 nm GaN tunnel barrier. Illustrated in Figure 4.1(b), injected electrons are first thermalized in the relatively thick InGaN well and can be subsequently tunneled into the quantum dot active region. An additional p-doped InGaN hole injector well is incorporated between the quantum dot active region and p-GaN layer. The injector wells can extend through the entire nanowire lateral dimension, due to the relatively large thickness, which can reduce electron leakage through the near-surface region of the nanowires.

(a)

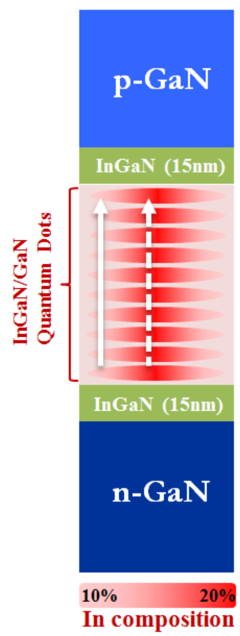

(b)

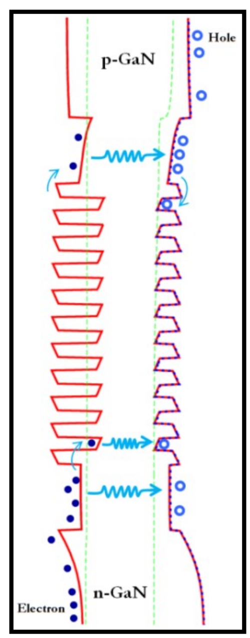

Figure 4-1. InGaN/GaN dot-in-a-wire tunnel injection LED heterostructures. (a) Schematic illustration and (b) energy band diagram under a forward bias of 3.1 V.

Studies on the electron overflow were first performed by simulating the band-diagram and carrier distribution in the device active region using the advanced LED device simulation software APSYS. Shown in Figure 4.2(a), electron overflow can be observed through the center region of the dot-in-wire structures, with an average indium composition of ~20% (dashed white arrow in Figure 4.1(a)). In axial nanowire LED structures, carrier leakage through the near-surface region may dominate, due to the large surface-to-volume ratios and the reduced indium incorporation in this region. As an example, much more severe electron overflow is observed, shown in Figure 4.2(b), in regions where the indium compositions of the quantum dot active region are comparatively low (~10% for this simulation, indicated by the solid white arrow in Figure 4.1(a)).

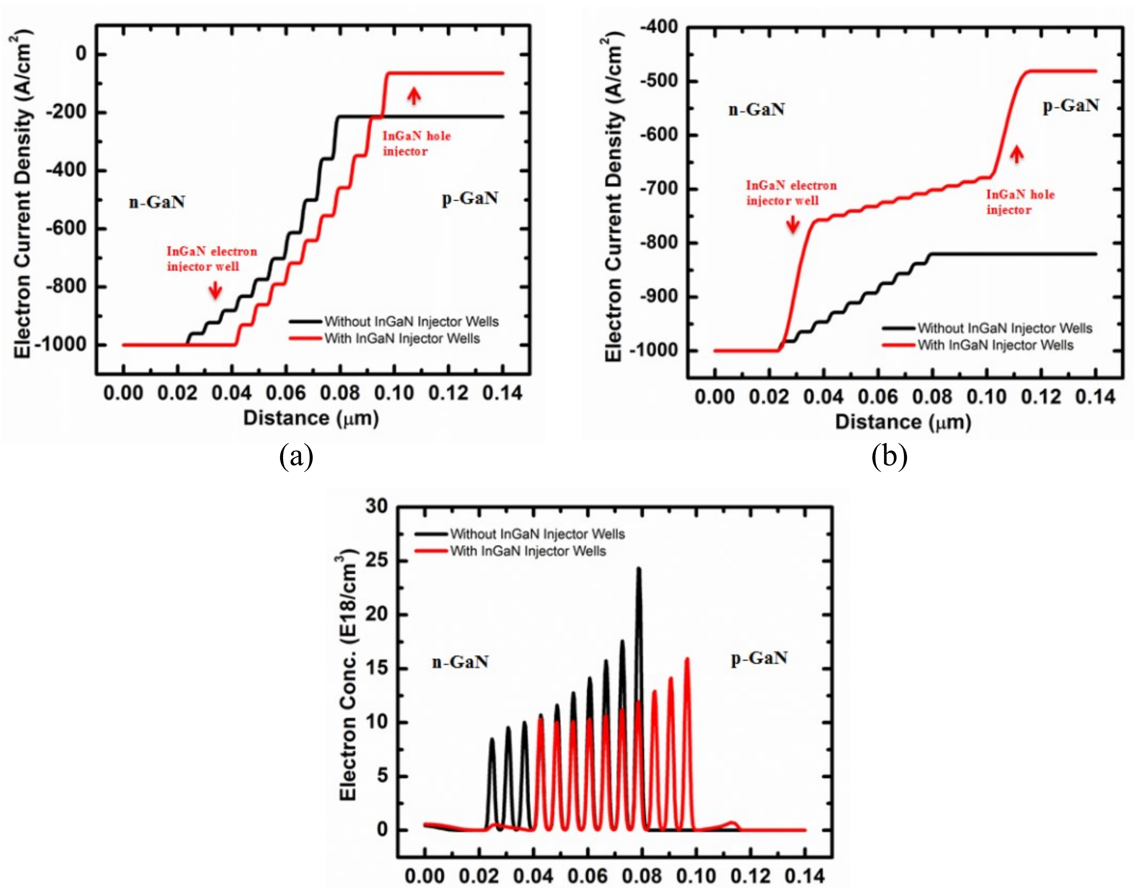

(a) (b)

(c)

Figure 4-2. (a) Simulated electron current density across the InGaN/GaN quantum dot active region (dashed arrow in Figure 1(a)) at an injection current of 1000 A/cm^2 with (red curve) and without (black curve) the incorporation of InGaN injector wells. (b) Electron current density across the near-surface of InGaN/GaN quantum dot active region (solid arrow in Figure 1(a)) at an injection current of 1000 A/cm^2 with (red curve) and without (black curve) the incorporation of InGaN injector wells. (c) The electron density distribution along the axial direction of the nanowires at an injection current of 1000 A/cm^2 with (red curve) and without (black curve) the incorporation of InGaN injector wells.

However, with the incorporation of $In_{0.13}Ga_{0.87}N$ injector wells, it is seen that electron overflow is significantly reduced in both the center and near-surface regions of the nanowires, shown in Figs. 4.2(a) and (b). The electron distribution along the axial direction of the nanowires at an injection current of 1000 A/cm^2 is shown in Figure 4.2(c). It is seen that the electron exhibit relatively uniform distribution with the presence of InGaN injector wells. Compared to the commonly used AlGaN electron blocking layer, the incorporation of a suitable InGaN quantum well between n-GaN and the active region does not adversely affect the hole injection process. It is further expected that the hole injector can harvest electrons escaped through the near-surface region, generate useful light emission, and reduce electron leakage into the p-GaN layer.

4.3 Experimental details and discussions

The nanowire LED heterostructures were grown directly on Si substrate using a Veeco Gen II radio frequency plasma-assisted molecular beam epitaxial system under nitrogen-rich conditions. A 45^{o} tilted scanning electron microscopy image of the dot-in-a-wire heterostructures on Si(111) is shown in the Figure 4.3(b). The wire diameters and densities are ~ 100 nm and ~ 1×10^{10} cm^{-2}, respectively. The nanowires are vertically aligned to the substrate and exhibit relatively uniform height. Strong photoluminescence intensity is measured at room-temperature. Shown in Figure 4.3(a), the peak emission wavelength at 430 nm corresponds to the emission from the injector wells, and the broad emission peak in the green and red wavelength range is directly related to the emission from the quantum dot active region.

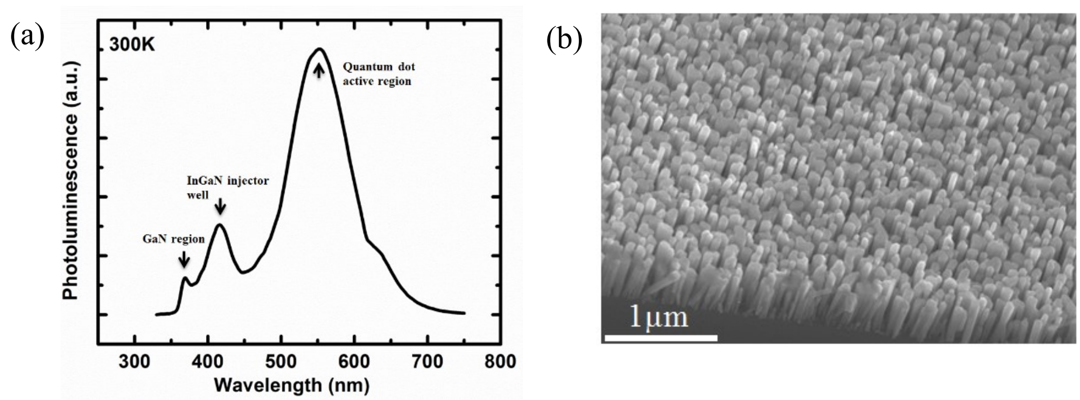

Figure 4-3. (a) Room-temperature photoluminescence spectrum and (b) a 45° tilted scanning electron microscopy image of the InGaN/GaN dot-in-a-wire heterostructures grown on Si(111) substrate.

The current-voltage characteristics for a device with an-areal size of 500×500 μm^2 are shown in Figure 4.4(a). Figure 4.4(b) shows the normalized electroluminescence spectra of the fabricated LED device under various injection currents. It is seen that strong emission from both the InGaN injector and quantum dot active region can be measured. Detailed studies further confirm the emission at ~ 430 nm is from the injector well positioned between the active region and p-GaN, due to the recombination between overflown electrons and injected holes. It is also of interest in noticing that the emission from the injector well is significantly stronger than that of the dots when measured at 5 K, shown in the Figure 4.4(c). This is a direct reflection of the enhanced electron overflow, due to the highly inefficient hole injection and transport process with decreasing temperature [191, 192]. The relative EQE for the overall emission of the device is shown in Figure 4.4(d). The relative EQE stays nearly constant at high injection current, shown in Figure 4.4(d), suggesting negligible electron overflow with the presence of electron and hole injectors, which agrees well with the simulation results shown in Figs. 4.2(a) and (b).

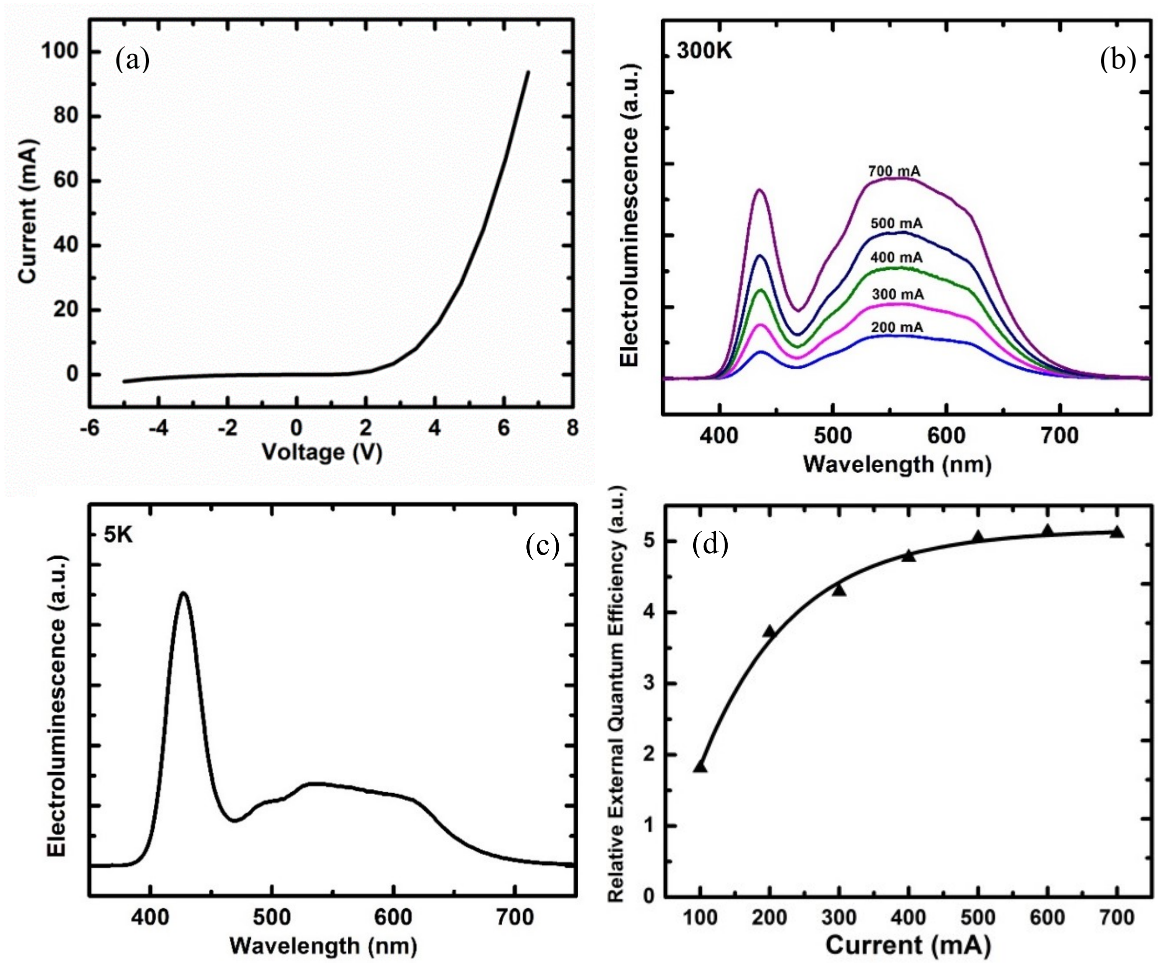

Figure 4-4. (a) Current-voltage characteristics of the fabricated dot-in-wire LED device on Si(111). (b) Electroluminescence spectra of the device measured under various injection currents. (c) The electroluminescence spectrum of the LED under 700 mA injection current at 5 K (d) Variations of the relative external quantum efficiency of the tunnel injection dot-in-a-wire LED with current.

The peak wavelengths of both the injector wells and quantum dot active region are nearly invariant with injection current, which is attributed to the reduced quantum-confined Stark effect [193]. The highly stable emission from the quantum dot active region is also directly related to the large inhomogeneous broadening of the dots. As such, the resulting phosphor-free nanowire white LEDs exhibit highly stable emission characteristics.

Illustrated in Figure 4.5 are variations of the light emission on the Commission International de l'Eclairage (CIE) chromaticity diagram with current varying from 100 to 700 mA. It is seen that the CIE chromaticity coordinates are nearly constant ($x \approx$ 0.341 – 0.347, and $y \approx$ 0.383 to 0.386). The device shows neutral white light emission, with a correlated color temperature (CCT) of ~ 4,700 K.

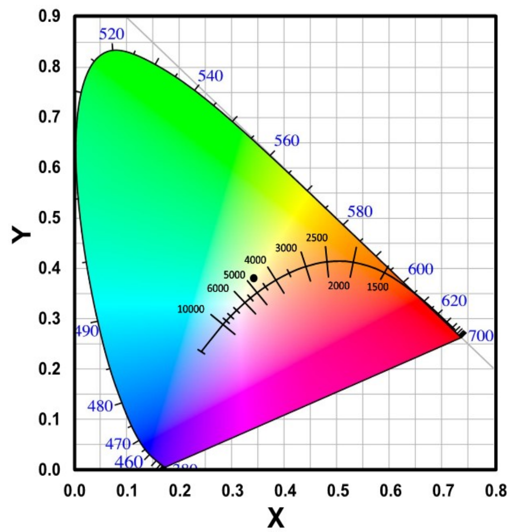

Figure 4-5. The 1931 Commission International de l'Eclairage chromaticity diagram. The devices exhibit relatively stable emission with x and y in the ranges of 0.341-0.347 and 0.383-0.386, respectively.

4.4 Conclusion

In summary, we have developed a new approach, with the use of tunnel injection, to control electron overflow and carrier leakage in GaN-based nanowire LEDs without using any Al-containing electron blocking layer. Electron and hole injector wells are separately incorporated in the device active region to reduce electron overflow and enhance hole injection. It is further observed that the hole injector can effectively harvest electrons escaped through the near-surface region of the nanowires, leading to a highly stable, neutral white light emission.

5 Improvement of light extraction efficiency in GaN-based LEDs using GaN nanotubes

5.1 Introduction

Light emitting diodes are attractive for various applications such as LCD backlight [3-5], projection displays, automotive lighting [7, 8], and traffic lights [6], in addition to general lighting applications. To date, LEDs with emission wavelengths in the near infrared to near ultraviolet regions could be realized using InGaN QWs or nanowires with different indium compositions [66, 194]. Several approaches have been studied in the previous chapters to enhance the internal quantum efficiency of GaN LEDs. However, extracting the generated photons out of the GaN LEDs is difficult. Most of the photons are reflected at the GaN/air interface due to the total internal reflection, and consequently are trapped and absorbed inside the LEDs. Recently, various techniques have been developed to increase the light extraction efficiency, including chip shaping [83], surface roughness [84-86], patterned sapphire substrate [85, 87], photonic crystal structures [88, 89], graded refractive index material [90], and surface plasmon resonance [91]. In this chapter, we have studied the use of rolled-up nanotubes [105-107] to significantly enhance the light extraction efficiency of GaN based LEDs. Recent studies have shown that rolled-up micron- and nanoscale tubular optical cavities can be realized using GaAs, InP, SiGe, SiO_x, and GaN based materials by standard photolithography and etching process [106, 107, 195-200]. Moreover, such flexible nanophotonic structures can be readily fabricated or transferred on virtually any substrates [197, 201, 202]. While previous studies have largely focused on the light confinement in such ring-like optical resonators [203, 204], it is of immense interest to explore the coupling between the leaky modes of a tube cavity and the guided modes of an LED structure. The coupling efficiency may be significantly enhanced through variations in the design of the tube structure, including the diameter and wall thickness, thereby dramatically enhancing the light extraction efficiency of GaN LEDs.

In this chapter, we have numerically investigated the light extraction efficiency of GaN-based visible LEDs with the presence of rolled-up tube structures using the finite element method (FEM) [205] based solver Comsol Multiphysics [206]. The effects of nanotube features on the light extraction efficiency, including the wall thickness, the number of turns, the positions of notches and active region, and the array configuration are studied in detail. It is observed that the light extraction efficiency can be enhanced by nearly fourfold with the use of optimally designed GaN nanotubes. Such monolithically integrated nanotube/LED structure provides a flexible, low cost approach to significantly enhance the light extraction efficiency of the emerging micron- and sub-micron LED arrays.

5.2 Simulation model and definitions

Schematically shown in Figure 5.1 is a typical GaN-based LED structure with a nanotube placed on top. The LED structure consists of a 120 nm p-GaN, 50 nm InGaN/GaN multiple quantum well (MQW) active region, and 630 nm n-GaN. The underlying substrate is assumed to be Si (~ 400 nm).

The derived results can also be readily applied for LEDs grown on sapphire or other substrates. The nanotube, with a radius of 500 nm, is assumed to be GaN. In practice, such nanotubes can be readily fabricated using AlGaN, SiO_x, or various polymer materials [199, 207, 208]. The wavelength used for the simulation is 526 nm. The refractive indices of Si, GaN and InGaN are approximated to be 4.6, 2.42, and 2.6, respectively [209-211].

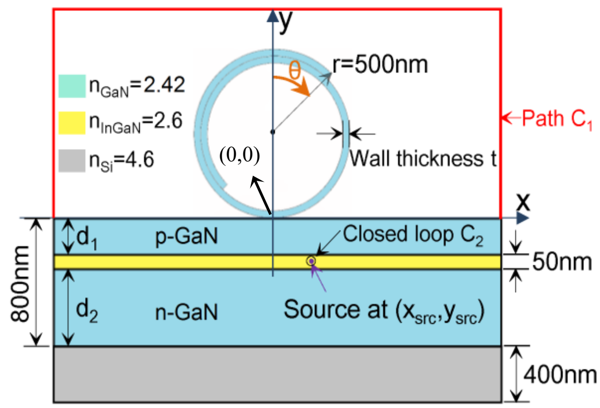

Figure 5-1. Schematic of the integrated GaN LED and nanotube structure. The nanotube shown here has 1.5 turns and θ is $45°$. C_1 and C_2 denote the integration paths for calculating the light extraction efficiency.

Simulations for different parameters and configurations were performed. The width of the simulated region is adjusted according to the number of nanotubes to ensure accuracy. Shown in Figure 5.1, $x = 0$ is defined as the middle of the simulation region in the horizontal direction. $y = 0$ is defined as the interface between the LED and the air. In this study, the number of turns of the nanotube (N) was varied from 1 to 2. The angle between the y-axis and the nanotube's outer notch in the clockwise direction is defined as θ. It is assumed that the whole structure is enclosed with perfectly matched layers to absorb outgoing waves without causing any reflection. Light extraction efficiency is then calculated as,

$$\eta = \frac{\int_{C_1} S_n dl}{\oint_{C_2} S_n dl} \qquad (1)$$

where C_1 is the boundary of the air region colored red, C_2 is a closed path surrounding the light source shown in Figure 5.1, and S_n is the component of the Poynting vector normal to the integration path.

Since the wall thickness of the nanotubes is much smaller than the emission wavelength, the ray tracing method [212] used in the traditional calculation of light extraction efficiency is no longer accurate. We have therefore utilized the FEM method to numerically analyze the LED efficiency with/without the presence of nanotubes. In this study, two-dimensional simulation was performed to provide a conceptual understanding of the light extraction physics. Given the non-coherent LED light emission, we have focused primarily on the extraction from a single light source positioned in the middle of the InGaN layer. In this simulation, TE wave is defined as the electric field parallel to the nanotube axis, whereas TM wave is defined as the magnetic field parallel to the tube axis.

Snapshot of the time-domain simulation without (Figure 5.2(a)) and with (Figure 5.2(b)) the single nanotube is depicted in Figure 5.2, which shows the electrical field pattern (λ = 526 nm). Significantly enhanced light extraction can be clearly observed with the presence of a nanotube. As the wall thickness of the nanotubes is well below the wavelength of the optical modes, it has lower effective refractive index. The light distribution coupled to the nanotube feels refractive index of the air rather than that of the GaN, the nanotube matches the refractive index between bulk GaN and air. Therefore, the light extraction in LEDs could be enhanced by coupling guided modes in bulk structure into the leaky modes. In other words, the photons trapped inside the bulk LED are coupled to GaN nanotube and emit through the GaN nanotube.

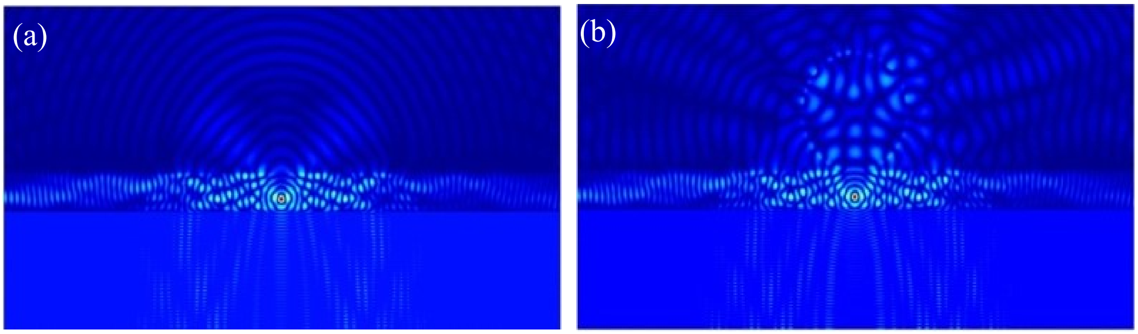

Figure 5-2. Comparison between the light extraction efficiency of a GaN thin film LED (a) without and (b) with a nanotube for light emission at 526 nm. The nanotube used here has 1.25 turns and the wall thickness is 20 nm.

5.3 Results and discussion

5.3.1 Effect of the single nanotube geometry on light extraction efficiency

We have first studied the dependence of the light extraction efficiency on the number of turns (N) and the rotation angle (θ). Shown in Figure 5.3, there is clearly a region across which the light extraction increases to a higher level. The region is denoted in both figures, which actually corresponds to the thicker part of the nanotube being landed on the LED surface, thereby leading to enhanced light extraction. However, a major difference between Figures 5.3(a) and (b) is that when N increases and approaches to around two, the extraction efficiency of TE waves decreases drastically while that of TM waves does not change much. This is due to the different propagation properties of TE and TM waves. Light propagation along the azimuthal direction of a tubular cavity is similar to a bent dielectric waveguide; in both cases, the process of light scattering into air depends on the propagation constant.

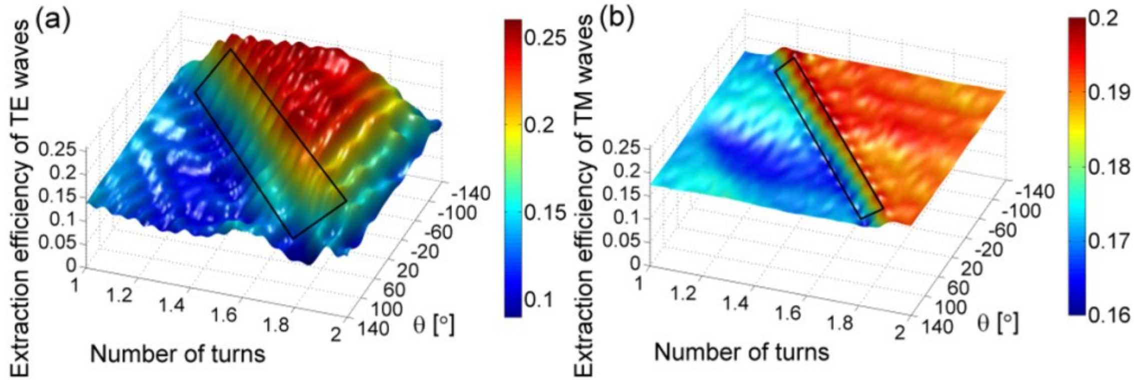

Figure 5-3. Light extraction efficiency of (a) TE waves and (b) TM waves vs. the number of turns and rotation angle θ of the nanotube. The wall thickness is 20 nm. The p-GaN layer thickness is $d_1 = 120\,\text{nm}$.

As the thickness of the guiding layer increases, the propagation constant of TE waves increases rapidly while the propagation constant of TM waves increases very slowly [213]. Therefore, when the outer notch and the inner notch meet forming a two-turn tube, the propagation constant of TE waves has a larger mismatch with air around the tube, leading to much reduced scattering and stronger confinement. However, TM waves, with magnetic field parallel to the tube axis, are not supported by a thin-walled tube structure, due to the strong scattering related to diffraction [214], which explains the relatively constant light extraction with the number of turns.

The light extraction efficiency also depends on the wall thickness (t), shown in Figure 5.4. For TM waves, the light extraction efficiency increases with wall thickness. Since TM waves are not confined in such nanotubes, the light extraction efficiency is largely affected by the coupling between the nanotube and the active region, which explains the enhanced light extraction with wall thickness. The light extraction efficiency of TE waves, however, exhibits a rather complicated behavior. It shows a decreasing trend with increasing wall thickness. This is explained by the increased propagation constant and better confinement of TE waves, which limits light scattering to the air and therefore reduces the light extraction efficiency. Also due to the better optical confinement with increased wall thickness, TE waves may develop destructive or constructive interference around the tube, which further induces oscillations in the light extraction efficiency, shown in Figure 5.4.

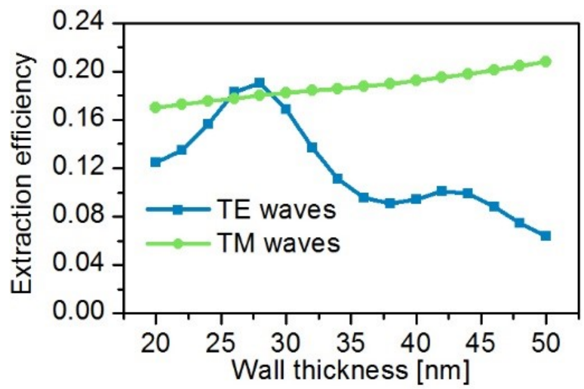

Figure 5-4. Dependence of the light extraction efficiency of TE waves and TM waves on the wall thickness. The p-GaN layer thickness is $d_1 = 120\,\mathrm{nm}$. The nanotube parameters are $N = 1.25,\ \theta = 0°$.

5.3.2 Effect of the position of source on light extraction efficiency

The nanotube parameters used in the following studies include $N = 1.6, \theta = -75°, t = 20\,\mathrm{nm}$. This configuration is chosen because it offers the highest light extraction efficiency, shown in Figure 5.3. The dependence of light extraction efficiency on the depth of InGaN active region, i.e. the thickness of p-GaN layer, is shown in Figure 5.5(a) for TE waves. The light extraction efficiency is clearly enhanced when nanotube is present. For example, for a p-GaN layer thickness of 120 nm, the light extraction efficiency of TE waves is 24.8%, which is nearly four times the efficiency without the tube. It is further observed that the enhancement in the light extraction efficiency becomes smaller with increased p-GaN layer thickness, due to reduced coupling between the nanotube and the light source. The oscillations in the light extraction efficiency is related to the interference effect for waves propagating in the LED structure [215]. Similar trend is also observed for TM waves (not shown).

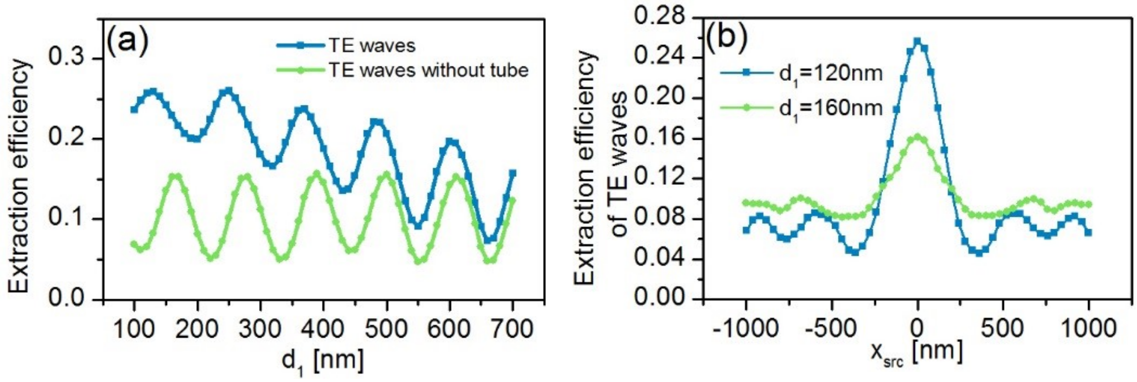

Figure 5-5. Dependence of the light extraction efficiency of TE waves on (a) the depth of the active region and (b) the horizontal position of the point source. Nanotube parameters used are $N = 1.6,\ \theta = -75°,\ t = 20\,\text{nm}$. In (a), the light source is positioned right under the nanotube.

In addition, as the source moves horizontally away from the tube, the light extraction efficiency decreases because of its weaker coupling with the tube and the reflection from the tube surface. Illustrated in Figure 5.5(b) is the calculated light extraction efficiency vs. the lateral distance between the point source and the nanotube for p-GaN thicknesses of 120 nm and 160 nm. When the source is far away enough, the light extraction efficiency approaches to the value without the presence of a tube. This is evident by correlating Figure 5.5(b) with points at $d_1 = 120\,\text{nm}, 160\,\text{nm}$ of the green curve (without tube) in Figure 5.5(a). Similar observations can be made for TM waves (not shown). In short, the light extraction efficiency is generally high for a source that is close to the nanotube for both TE and TM waves.

5.3.3 Effect of nanotube arrays on light extraction efficiency

The afore-described analysis shows that the light extraction efficiency can be enhanced only if the light source is positioned near the nanotube. Therefore, to enhance the light extraction efficiency of a large area device, it is imperative to incorporate densely packed nanotube arrays on the LED surface. To understand the effect of multiple nanotubes, nanotube arrays with different separation distances are simulated. Illustrated in Figure 5.6(a), an array of identical nanotubes are placed on the thin film LED surface, and the source is moved from $x=-L/2$ to $x=L/2$, where L is the distance between the centers of two adjacent tubes. Since nanotubes positioned outside $-3L/2<x<3L/2$ generally have very weak effect on the light extraction of any source located between $x=-L/2$ and $x=L/2$, only four nanotubes are used in the simulation. It may be naturally expected that a small separation distance between adjacent nanotubes may lead to enhanced light extraction. However, some of the light coupled to a nanotube can actually be coupled again to the adjacent tubes and be guided back to the GaN layer instead of being scattered to the air, which will lead to reduced light extraction efficiency.

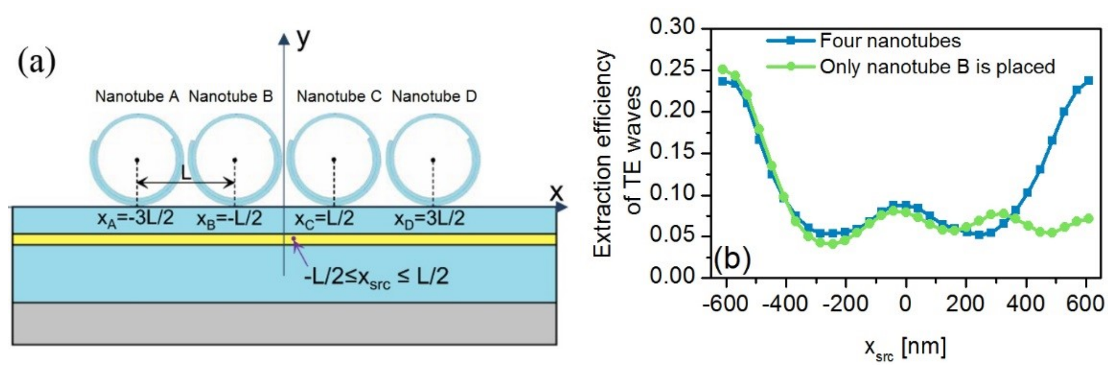

Figure 5-6. (a) Schematic illustration of the integrated nanotube arrays with an LED structure. (b) Comparison between the light extraction efficiency of TE waves for a single nanotube and that for multiple nanotubes for L=1220 nm. Nanotube parameters include $N=1.6, \theta=-75°, t=20nm$.

Through detailed studies, the optimum distance is derived to be $L \sim 1220$ nm for nanotubes with a radius of 500 nm. Shown in Figure 5.6(b), it is seen that, compared to a single nanotube (tube B), the light extraction efficiency with four nanotubes is significantly enhanced for a point source positioned in the region [0, L / 2]. In the region [-L / 2, 0], it is nearly identical to the light extraction efficiency enhanced by a single nanotube. Similar results are also obtained for TM waves (not shown).

5.4 Conclusion

In summary, we have shown that the light extraction efficiency of a GaN LED can be significantly enhanced by integrating with nanotube arrays. The light extraction involves two successive steps, including the coupling from the light source to the tube and the subsequent emission from the tube to the air. For the first step, a relatively large wall thickness in the bottom region of the nanotube is favorable for both TE and TM waves, and a smaller distance between the nanotube and the source offers stronger coupling. For the second step, TE waves and TM waves exhibit different behaviors, since the tube wall thickness has dramatically different effects on their respective propagation properties. In the case of nanotube arrays, the dependence of light extraction efficiency on the source position is similar to that of a single nanotube except that the extraction efficiency is also negatively affected by the light coupling from nanotubes back to the LED structure. There is an optimal separation distance of adjacent nanotubes which balances the need for minimizing this effect and the need for high surface coverage of nanotubes. It is envisioned that the use of nanotubes can offer a flexible, low cost approach for significantly enhancing the light extraction of the emerging micron- and submicron-scale LEDs for display, imaging, sensing, and communication applications.

6 Deep UV light propagation in nanowire arrays

6.1 Introduction

The GaN based semiconductors are of great importance for visible and UV applications such as LCD backlight [3-5], traffic lights [6], automotive lighting [7, 8], biomedical diagnostics [9-11], disinfection [12-14], and water purification [15, 16]. The performance of LEDs is largely determined by the internal quantum efficiency and light extraction efficiency, in addition to the current injection efficiency. Recently, various approaches based on nanowire structures have been pursued in order to enhance the internal quantum efficiency in the visible and UV wavelength ranges [56, 70, 190, 216, 217]. The internal quantum efficiency enhancement is due to the drastically reduced dislocation densities, smaller strain field and the resulting negligible quantum-confined Stark effect [56, 70, 190, 216, 217].

As described in Chapter 1, the low light extraction efficiency caused by the narrow light escape cone is one of the main limitations for achieving high efficiency UV LEDs. The large refractive index difference between semiconductor and air leads to the total internal reflection and consequently the narrow light escape cone. Thus, increasing the light extraction efficiency is crucial to enhance the external quantum efficiency of UV LEDs. Several technologies such as surface roughing [218], patterned substrates [219, 220], rolled-up nanotubes [221] and photonic crystal patterns [222] have been developed to enhance the light extraction efficiency of UV LEDs but with limited success. Recently, nanowire structures have been utilized for realizing high efficiency LEDs in the visible range [56, 70, 190], which can offer large surface emission area.

However, there have been few reports on nanowire-based deep UV LEDs [216, 217]. Moreover, it has remained elusive if the extraction of TM emission can be significantly enhanced in nanowire-based structures.

Since the AlN and GaN show different band structures at the Γ-point of the Brillouin zone [110], the TM emission in AlGaN based UV LEDs becomes more dominant with higher Al compositions [108, 109] for emission wavelengths ~ 280 nm or shorter. The polarization of light emission in AlGaN quantum wells also depends on strain in the active region and alloy compositions in the barrier layers. The TM emission means that the emitted light can only be extracted from side surfaces rather than from the top surface. In this chapter, we only focus the TM polarization and the related light extraction of UV LEDs.

The effect of different topologies of nanowire arrays on the light extraction efficiency of the UV LEDs has been investigated by using FDTD method. The PML boundary conditions are employed all around the UV LEDs in order to avoid unnecessary light reflection at the simulation domain boundaries [122]. The light extraction efficiency is calculated as the ratio of the Poynting vectors collected by some monitors placed around the UV LED to the total emitted power generated in the nanowire active region. To reduce the calculation size, the simulation domain was taken to be 2.5 μm × 2.5 μm, and adaptive mesh was used during the computation. A single TM dipole source with the emission wavelength of 280 nm was positioned in the center of the active region for all simulations. The LED structure used in the simulations consists of a hexagonal, rectangular, or random array of nanowires. Each nanowire consists of 10 nm p-GaN, 100 nm p-AlGaN, 60 nm AlGaN multiple quantum well active region, and 400 nm n-AlGaN which could be grown using the MBE [36, 66, 157]. The underlying substrate is assumed to be a reflective layer. Schematically shown in Figure 6.1 is the two-dimensional (2D) layer structure of a nanowire UV LED. The Poynting vectors used to determine the light extraction efficiency of UV LEDs are calculated on the path shown as dotted red line. Side light extraction efficiency is defined as the ratio of emitted power out from the side surfaces of the LED to the total emitted power of the device active region.

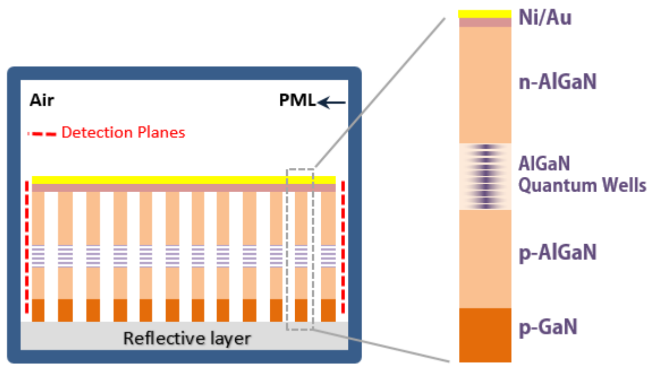

Figure 6-1. The two-dimensional layer by layer schematic of the nanowire-based UV LED structure. Each nanowire consists of 10 nm p-GaN, 100 nm p-AlGaN, 60 nm AlGaN multiple quantum well active region, and 400 nm n-AlGaN.

One of the major benefits of utilizing nanowires is to increase the probability of photons to escape from the nanowire surfaces due to the extremely large surface-to-volume ratios. As described in the following sections, the enhancement of light extraction efficiency of UV LEDs was achieved by employing the nanowire arrays. The light extraction efficiencies of UV LEDs were enhanced by ~7 times by utilizing periodic nanowire arrays compared to that (~10%, or less) of previously reported quantum LEDs in the deep UV wavelength range [111-113]. The simulation results show that the perfectly periodic structures could further improve the light extraction efficiency much more than random structures. The main reason for the lower efficiency of random nanowire structures is attributed to the light multipath scattering among adjacent nanowires which may localize the light inside the nanowires or to the increase of the length of light escaping path.

We have further studied two different nanowire array designs, including photonic band edge nanowire UV LEDs, and biperiodic nanowire UV LEDs. We have investigated nanowire UV LEDs which support the slow light modes. The slow light UV LEDs with extremely low group velocities are obtained at the photonic band edge of the structure band diagram. This kind of LEDs shows strong gain enhancement which will be utilized in the UV edge emitting lasers. The biperiodic UV LEDs proposed with two different periodicities can break the structure symmetry and consequently UV LEDs with directional emission could be achieved. The directional LEDs can be implemented in photonic integrated circuits with high efficiency.

6.2 Periodic nanowire UV LEDs

The periodic array of nanowire LEDs are actually similar to the active photonic crystal structures. Though the photonic crystals are mostly utilized in photonic bandgap regions, which are sets of wavelengths prohibited from propagating through the structure, the periodic array of nanowire LEDs are highly desired to operate in photonic non-bandgaps region which could allow for light propagation through the structure to the surrounding air.

Since the radius of nanowires and the spacing between nanowires known as lattice constant *a* are the key parameters for the periodic array of nanowire LEDs, the selective area growth by plasma-assisted molecular beam epitaxy could be utilized to achieve nanowire arrays with uniform size and position distribution.

The particle swarm optimization (PSO) algorithm [223, 224] which is very popular for different electromagnetic applications such as the filter design [225, 226] was used to optimize the lattice constant and the diameter of nanowires to reach optimum efficiency for the UV LEDs. The lattice constant (labeled as *a* in Figure 6.2) and diameter of the hexagonal periodic nanowires are found to be 194 and 119 nm, respectively, to have a maximum light extraction efficiency ~72%.

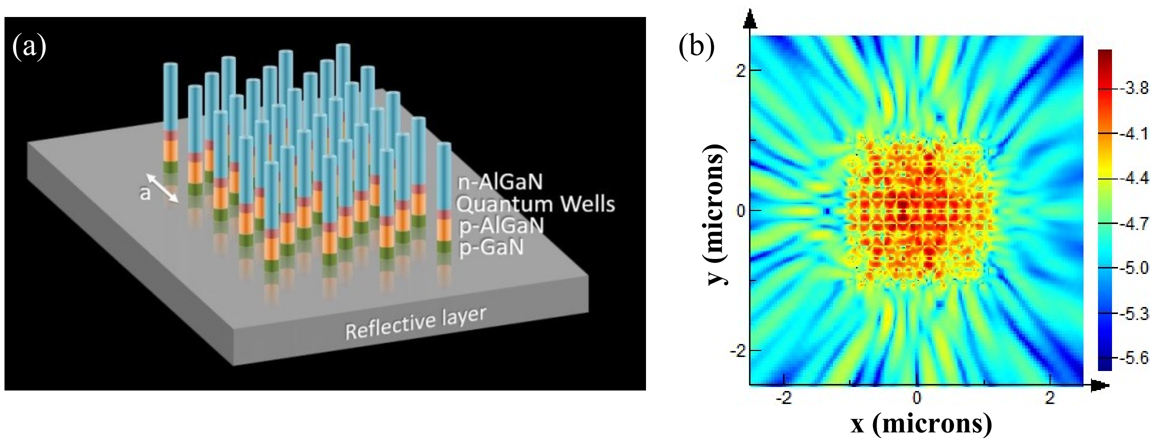

Figure 6-2. (a) The 3D schematic of the hexagonal periodic array of nanowires, and (b) the simulated mode profiles with the optimized spacing and diameter which shows the high light extraction efficiency.

The principle behind the high light extraction efficiency from the periodic array of nanowire LEDs is directly related to the coupling of light modes through the nanowires in the photonic non-bandgap region which could not inhibit the light propagation inside the structure. The simulation results show that the coupled modes formed between nanowires can be easily extracted from the UV LED structure.

The periodic array of nanowire LEDs could increase the probability of photons to escape from the nanowire surfaces and overcome the total internal reflection at the semiconductor and air interface, and therefore improve the efficiency of UV LEDs. Figures 6.2(a) and (b) show the 3D schematic of the hexagonal periodic array of nanowires and its simulated mode profiles with the optimized nanowire spacing and diameter, respectively. The simulated mode profile supports the high light extraction efficiency.

The designed structure is scalable to different wavelength ranges which means scaling the design to a different wavelength does not affect the simulation results and similar properties can be achieved at various wavelengths after the scaling of nanowire diameter and spacing.

6.3 Random nanowire UV LEDs

In order to get a better understanding of the influence of periodic structures in the nanowire UV LED design, the random nanowire UV LED is discussed in this section. Another light extraction scheme is to utilize multiple scattering of light inside random nanowire UV LEDs. In such structures, the multiple scattering of light inside the nanowires takes places due to spatially random and high contrast refractive index nanowires. Structural randomness of the nanowire UV LEDs is introduced by dislocating the nanowires to random positions compared to periodic nanowire UV LEDs. With the increase of nanowires dislocations, the structure deviates from the perfectly periodic structure and becomes a completely random structure.

As previously mentioned, when the structure is a completely ordered periodic nanowire UV LED, it exhibited the band diagram which is typical for photonic crystals.

The random nanowire LED structure is fully uncorrelated due to the strong random deviation, and could not support the typical dispersion characteristics of ordered photonic crystals.

The 3D schematic of the random array of nanowires and the spatial profile of the electric field are shown in Figure 6.3. The randomly shaped electric field is strongly localized inside the structure as shown in Figure 6.3(b), thereby forcing the generated photons to be trapped inside the UV LED structure. Depending on the random nanowire geometries, the pattern of localized modes could be randomly formed inside the structure. Considering the localized modes inside the random nanowire UV LEDs, the light extraction efficiency is drastically decreased (~15%) compared to the periodic nanowire UV LEDs. Multiple scattering between the random nanowires can provide the sufficient gain for lasing. Recently Chang *et al.* reported the observation of random lasing from optically pumped GaN quasicrystal nanorod arrays [227].

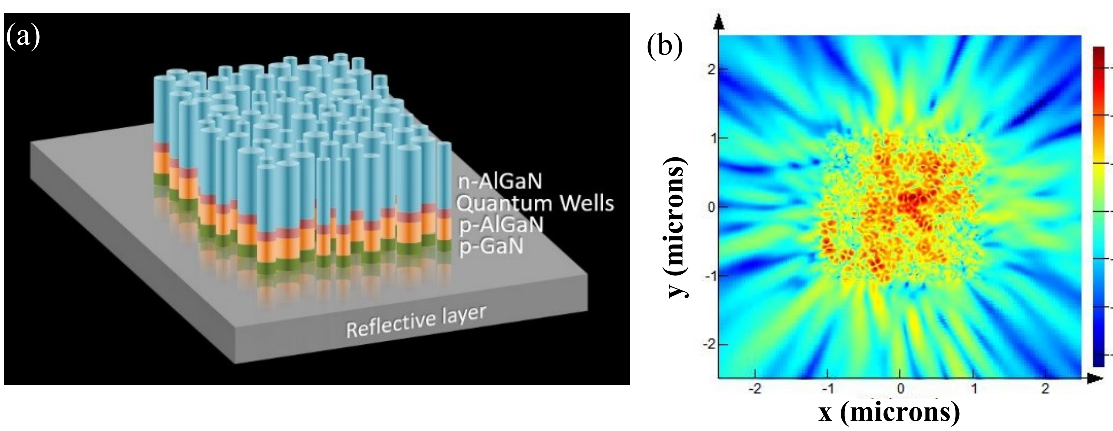

Figure 6-3. (a) The 3D schematic of the random array of nanowires, and (b) its simulated mode profiles with the random spacing and diameter which shows the strongly localized light inside some spaces between nanowires.

6.4 Photonic band edge nanowire UV LEDs/lasers

The photonic band edges are one of the many interesting properties of photonic crystal structures, which is at the boundary of the photonic bandgap and non-bandgaps regions. It is possible to achieve lasing through gain enhancement at the photonic band edge modes. It is particularly interesting because distributed Bragg reflectors (DBRs) are not required anymore for this kind of lasers compared to the conventional edge-emitting lasers. Recently, stimulated emission from the periodic nanowire arrays arranged in a rectangular lattice have been observed [228], where lasing modes are the photonic band edge modes. The light intensity is enhanced at the photonic crystal band edge modes, indicating the function of distributed feedback.

Figure 6.4(a) shows the photonic band structure of a 2D hexagonal array of nanowires for TM polarization, which was calculated by the plane wave expansion method. The flat photonic bands exhibit the low group velocity of light and consequently high gain enhancement. For a nanowire radius of 0.15a, where a is the lattice constant, the normalized frequency of the band-edge mode is 0.5623, which corresponds to λ = 280 nm for a = 157.4 nm. The extremely low group velocity leads to the long interaction time between radiation field and active material and consequently gives a strong gain enhancement. Recent studies show that the photonic crystals could behave as mirrorless resonant cavities for the wavelengths near the photonic band edge modes [229]. The quality factors for the photonic band edge lasers is on the order of $(L/\lambda)^3$ where λ is the vacuum wavelength and $L >> \lambda$ is the length of structure.

Figure 6.4(b) shows the electric field profile of band edge mode which was calculated using the FDTD simulation method. Although a single dipole source is placed at the center nanowire in the simulation field, the electric field of the band edge mode spreads across the entire periodic nanowire structure, which is a characteristic of the band edge modes. Note that the light emission is strongly enhanced in flat higher bands (red curve), because the group velocity is reduced over an extended region of k space.

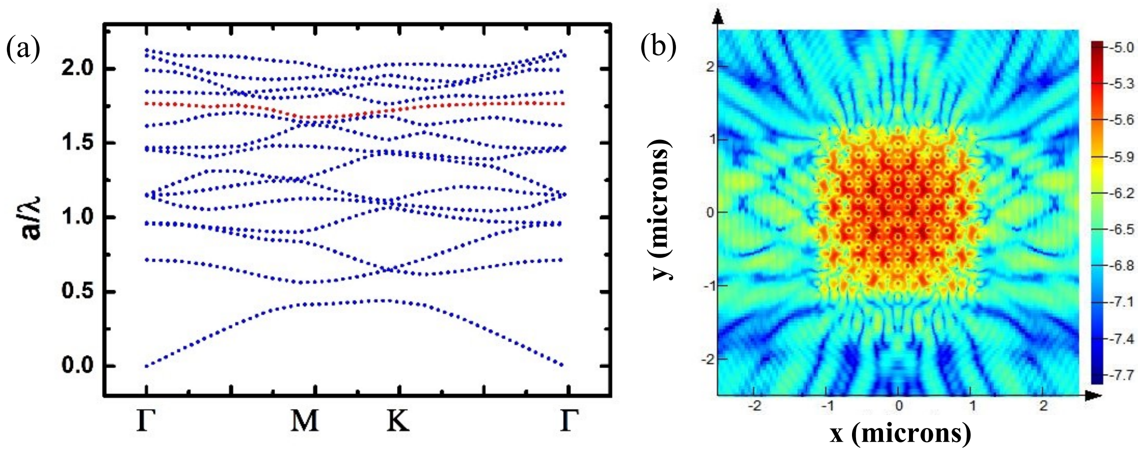

Figure 6-4. (a) Calculated photonic band structure of a 2D hexagonal array of nanowires, (b) the electric field profile of the band edge mode calculated by 3D FDTD which corresponds to slow light mode at λ = 280 nm.

6.5 Biperiodic nanowire UV LEDs

Photonic band edge is utilized for the aforementioned UV LEDs/lasers in which the group velocity of light is slowed down due to the flat curvature of the band. Generally speaking, typical photonic crystal structures can support two different kinds of modes including Bragg guided and effective index guided modes. For Bragg guided modes, light is confined by Bragg reflection arising from a photonic bandgap in the transverse directions. The Bragg guided modes have been typically utilized in photonic crystal surface emitting lasers.

For effective index guided modes, confinement in the transverse direction is due to the weak coupling between the nanowires, while strong coupling in the longitudinal direction could form an efficient waveguide to couple photons to the free space. These structures are directional edge-emitting devices and are well suited for planar photonic integration circuits. Utilizing the SiOx/air distributed Brag reflectors at the both end of the longitudinal direction leads to the UV edge-emitting lasers. The UV laser bar consists of the periodic nanowire arrays, and optical feedback provided by distributed Bragg reflectors in both ends, which are defined by multiple SiO_x/air stacks.

Figure 6.5 (a) shows a schematic of 2.5 μm × 2 μm two dimensional effective index guided UV LED structure. The structure consists of a rectangular array of nanowires with different lattice constants of 250 nm and 203 nm (labeled as *a* and *b* in Figure 6.5(a)) in the transverse and longitudinal directions, respectively. Figure 6.5(b) shows the associated electric fields for the biperiodic UV LED. It is seen that the light mostly emits in the longitudinal direction (~52%) rather than all around the whole LED structure.

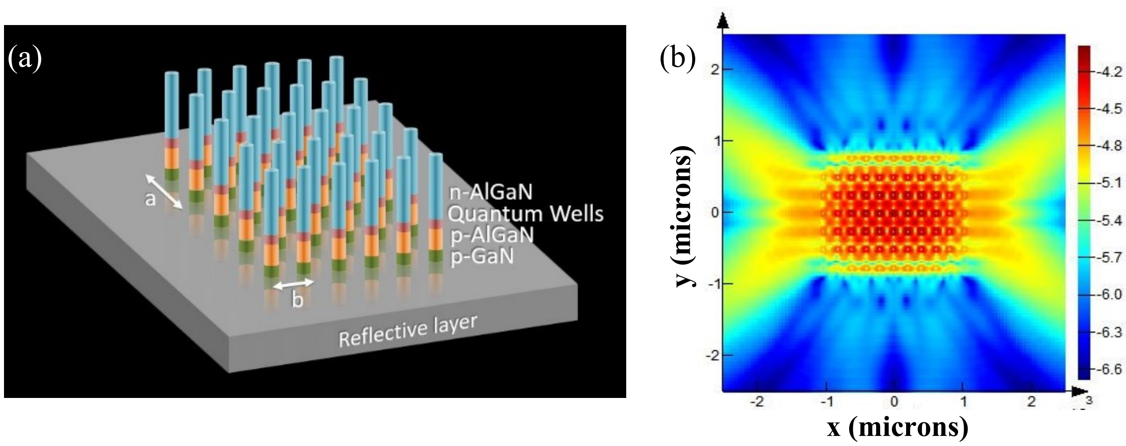

Figure 6-5. (a) The 3D schematic of the rectangular biperiodic array of nanowires, and (b) the simulated mode profiles with two different lattice constant which shows the light mostly emits in longitudinal direction.

6.6 Conclusion

In this chapter, we have studied the different regimes of light propagation in deep UV LEDs using nanowire arrays via 3D FDTD simulation. The comprehensive investigation of different nanowire array designs shows that the use of periodic nanowire arrays can lead to light extraction efficiency enhancement by ~7 times compared to conventional planar UV LEDs. The UV LEDs incorporating nanowires could help to decrease the total internal reflection caused by refractive index contrast between semiconductor and air. We have proposed the directional UV LEDs by employing biperiodic arrays which could be implemented in the photonic integrated circuits. We have further investigated photonic band edge nanowire UV LEDs with the strong gain enhancement which is required for UV edge-emitting lasers. We could extend the proposed UV LED designs into the operation wavelengths in the ranges of UV-C band (< 280 nm).

7 Achieving high efficiency deep ultraviolet LEDs by using nanowire structures

7.1 Introduction

The effect of different topologies of nanowire arrays on the light extraction efficiency of the UV LEDs has been studied in the previous chapter. We utilize the side emission properties of periodic nanowires to realize significantly enhanced extraction efficiency of UV LEDs in this chapter. As mentioned previously, due to the extremely large surface-to-volume ratios, light escapes from the nanowire structure and the total internal reflection inside the nanowire is considerably reduced. A nanowire structure can be utilized to inhibit the emission of the guided modes and redirect trapped light into radiated modes. We have comprehensively investigated the light extraction efficiency of periodic nanowire UV LEDs using three-dimensional (3D) FDTD method with a PML boundary condition. In the simulation, we have studied the dependence of light extraction efficiency on nanowire structural parameters such as the nanowire size and density and the p-GaN thickness, which play an important role on the light extraction efficiency. We have further investigated the effect of device sizes, as well as the random variation in the nanowire diameter and spacing on the light extraction efficiency. It is observed that an unprecedentedly large light extraction efficiency of up to 72% can be achieved, which is much higher than previously reported deep UV LEDs (typically <10%) [111-113]. This study therefore opens a new avenue for achieving high efficiency deep ultraviolet LEDs that were not previously possible.

7.2 Simulation model and definitions

Schematically shown in Figure 7.1(a) and (b) are the two-dimensional (2D) layer by layer structure of a nanowire UV LED and the 3D schematic of the hexagonal array of nanowires. The LED structure consists of a hexagonal array of nanowires. Each nanowire consists of 10 nm p-GaN, 100 nm p-AlGaN, 60 nm AlGaN multiple quantum well (MQW) active region, and 400 nm n-AlGaN. The underlying substrate is assumed to be a reflective layer. Using the FDTD simulation, we calculated the light extraction efficiency of nanowire UV LEDs with flip-chip structures. It is assumed the whole structure with a top surface area of 2.5×2.5 μm^2 is enclosed with perfectly matched layers to absorb outgoing waves without causing any reflection [122]. A single dipole source with Gaussian shape spectrum and TM mode (parallel to the nanowire axis) is positioned in the middle of the AlGaN MQW active region. The wavelength used for the simulation is 280 nm. The Poynting vectors used to determine the light extraction efficiency of UV LEDs are calculated on the path shown as dotted red line. Side light extraction efficiency is defined as the ratio of emitted power out from the side surfaces of the LED to the total emitted power of the device active region.

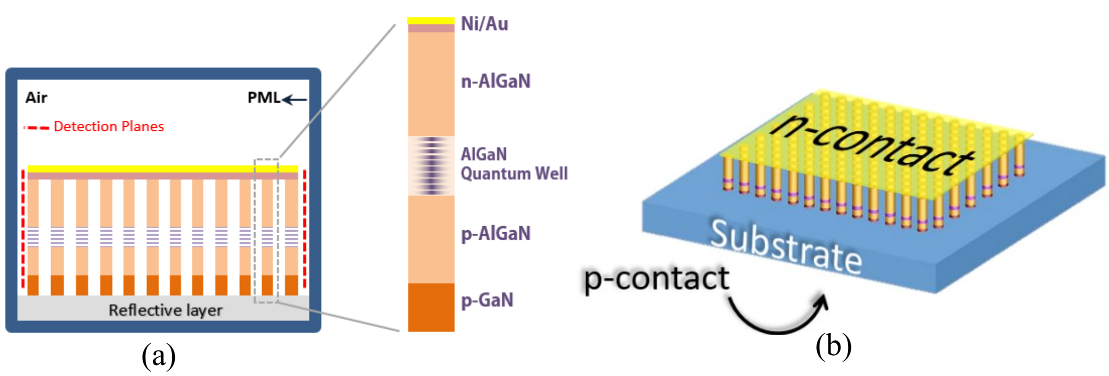

Figure 7-1. (a) The two-dimensional layer by layer schematic of the nanowire-based UV LED structure. Each nanowire consists of 10 nm p-GaN, 100 nm p-AlGaN, 60 nm AlGaN multiple quantum well active region, and 400 nm n-AlGaN. (b) The 3D schematic of the hexagonal array of nanowires.

To realize side emitting UV LEDs, the nanowires utilized in the LED structure could be grown using the MBE [36, 66, 157]. As the size of nanowires and the spacing between nanowires play an important role on the light extraction efficiency, the epitaxial growth of the nanowire arrays should be carefully controlled and engineered. The selective area growth by plasma-assisted molecular beam epitaxy may be utilized to achieve nanowire arrays with uniform size and position distribution.

The periodic array of nanowire LEDs are actually similar to the active photonic crystal structures. Though the photonic crystals are mostly utilized in photonic bandgap regions, which are sets of wavelengths prohibited from propagating through the structure, the periodic arrays of nanowire LEDs are highly desired to operate in photonic non-bandgaps region which allow light propagation through the structure to the surrounding air. The nanowire photonic crystal structures have different operation regimes including light confinement regime (nanowire lasers) and light transmission regime (nanowire LEDs), depending on the nanowire diameter and spacing. Nanowire arrays with different diameters and spacings result in varying wave vectors, and therefore different degrees of transmission at the corresponding wavelengths. Figure 7.2 (a) shows the photonic band diagram of a 2D hexagonal array of nanowires for TM polarization, which was calculated by the plane wave expansion method. The a/λ is the reduced frequency ($\omega a/2\pi c$). The three different frequency ranges were identified in the photonic band diagram shown in Figure 7.2(a). The birefringence region at the lowest frequency range below the first photonic band gap is mostly utilized in photonic crystal fibers and optical switches. The photonic band gap region with the omni-directional stop band is applied to photonic waveguides and cavities. The transmission region with higher frequency range above the photonic band gap can be used in superprisms and LEDs.

7.3 Results and discussion

7.3.1 Optimizing the spacing and diameter of nanowires

First, we focus on optimizing the spacing and the diameter of nanowires using the PSO algorithm [223, 224] to reach the maximum light extraction efficiency. The PSO as stochastic strategy has recently found different electromagnetic applications such as the filter design [225, 226] and the array antenna design [230, 231]. In this method, a population of random solutions is initialized and then search for the best solution by updating generations. To maximize light extraction efficiency, a swarm is comprised of 5 particles which represent a potential solution to light extraction efficiency. The solution for a swarm converged in 10 iterations, which means a total number of 50 simulations have been performed in the optimization process. Here, the spacing (center to center) and diameter of the nanowires are found to be 194 and 119 nm, respectively, for the maximum light extraction efficiency of 72%.

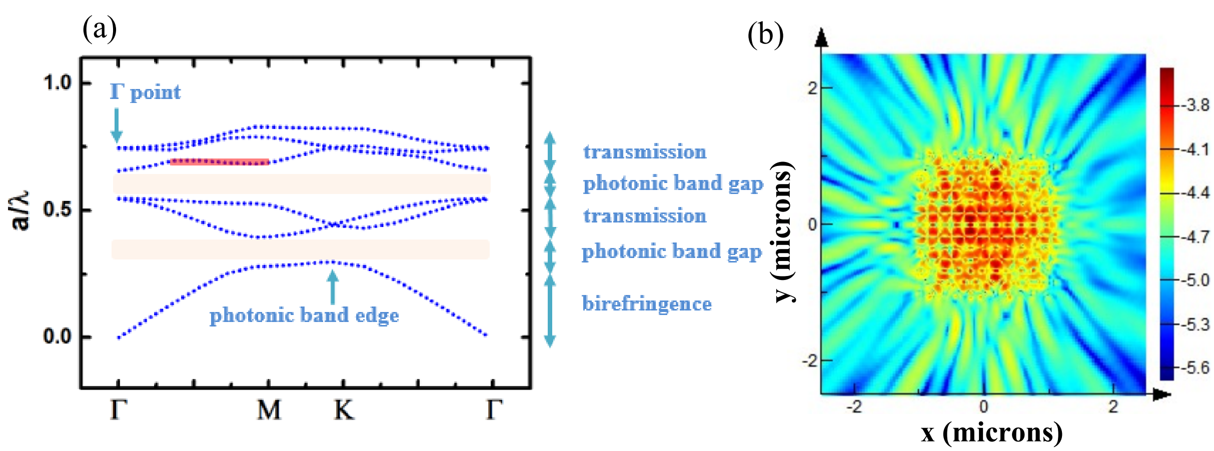

Figure 7-2. (a) Calculated photonic band structure of a 2D hexagonal array of nanowires with spacing and diameter of 194 nm and 119 nm. The flat photonic band is highlighted by red color. (b) The simulated mode profiles with the optimized spacing and diameter.

The principle behind the in-plane (i.e. lateral) light extraction from the periodic array of nanowire LEDs is directly related to the coupling of light modes through the nanowires in the photonic non-bandgap transmission region which supports the light propagation inside the structure. The flat photonic bands (highlighted by the red line in Figures 7.2(a)) exhibit a low group velocity of light and consequently strong penetration of light into the photonic crystal structure. For the nanowire spacing and diameter of 194 nm and 119 nm, the photonic band diagram showed nearly constant flat photonic band over an extended range of wave vectors which corresponds to λ = 280 nm. The optical modes related to the extended flat photonic band can be readily extracted from the UV LED structure, which is also evident from the calculations based on PSO optimization. Therefore, a careful optimization of the diameter and the spacing of nanowires could help to overcome the total internal reflection at the semiconductor and air interface, improve the escape probability of the light, and consequently increase the light extraction efficiency. Figures 7.2(b) shows simulated mode profiles with the optimized nanowire spacing and diameter, respectively. Although a single dipole source is placed at the center nanowire in the simulation field, the electric field of the flat photonic bands efficiently penetrates into and spreads across the entire periodic nanowire structure as shown in Figures 7.2(b).

7.3.2 Effect of the diameter of nanowires on the light extraction efficiency

The light extraction efficiency of nanowire deep UV LEDs with different diameters is further studied. Figure 7.3 shows the dependence of light extraction efficiency on the diameter of nanowires. Here, the spacing of nanowires and the thickness of p-GaN layer were kept at 194 and 10 nm, respectively. The light extraction efficiency was calculated as a function of the nanowire diameter from 98 to 130 nm. The corresponding light extraction efficiency varied from 8% to 72%. Since small diameter nanowires cannot support coupled modes, a significant increase in the light extraction efficiency is first observed with increasing diameter (up to ~ 119 nm). The reduction of the light extraction efficiency with further increasing nanowire diameter is due to the light confinement in each nanowire. Therefore, it is evident that there is an optimum diameter at which the light could be efficiently coupled through the nanowires for efficient lateral side emission.

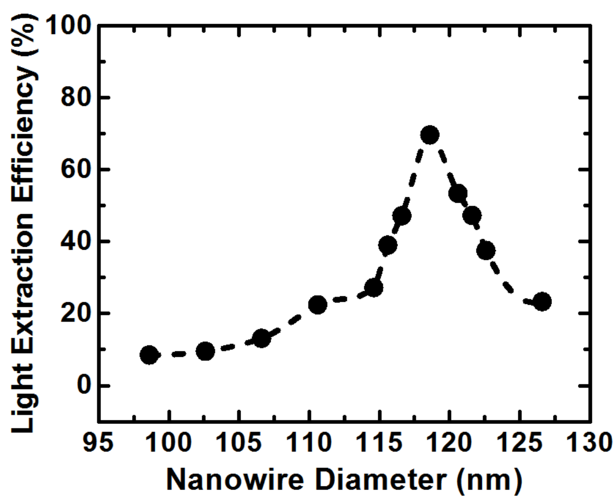

Figure 7-3. Variations of the light extraction efficiency vs. nanowire diameter.

7.3.3 Effect of the spacing of nanowires on the light extraction efficiency

Shown in Figure 7.4, the light extraction efficiency was further calculated as a function of the spacing between nanowires from 163 to 203 nm for an optimum nanowire diameter of 119 nm. The corresponding light extraction efficiency varied from 9% to 72%. For relatively small nanowire spacing, the light trapping effect plays a major role, which results in a decrease of light extraction efficiency. With increasing spacing, TM polarized light can propagate horizontally through the nanowire arrays, due to the formation of coupled modes, thereby leading to significantly enhanced light extraction efficiency. It is also seen that the light extraction efficiency remains relatively high with further increasing diameters (> 194 nm), which is partly due to the efficient light propagation through the large space amongst nanowires. Albeit the efficiency is high, a very large spacing may not be desirable, due to the reduction of the active region volume and the resulting low output power for a given device size.

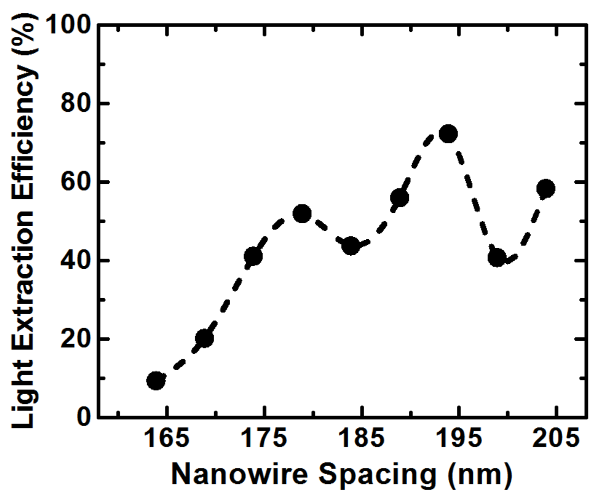

Figure 7-4. Variations of the light extraction efficiency vs. nanowire spacing.

7.3.4 Effect of the p-GaN layer thickness on the light extraction efficiency

Compared to conventional surface-emitting devices, the unique scheme of lateral side extraction of TM polarized emission can drastically reduce the light absorption of the top p-Ga(Al)N contact layer. To further elucidate the impact of the p-Ga(Al)N layer, we have studied variations of the light extraction efficiency vs. the thickness of the p-GaN layer. Shown in Figure 7.5, it is seen that the light extraction efficiency shows an overall decreasing trend with increasing GaN thickness. However, even for a GaN thickness of 50 nm, a modestly high efficiency of 37% can still be achieved. It is also noticed that the light extraction efficiency varies periodically with the thickness of p-GaN layer, which is similar to that observed in conventional planar LED structures, due to the interference of emitted light and reflected light. In this regard, it is essential to optimize the nanowire height in order to have constructive interference to achieve maximum light extraction efficiency.

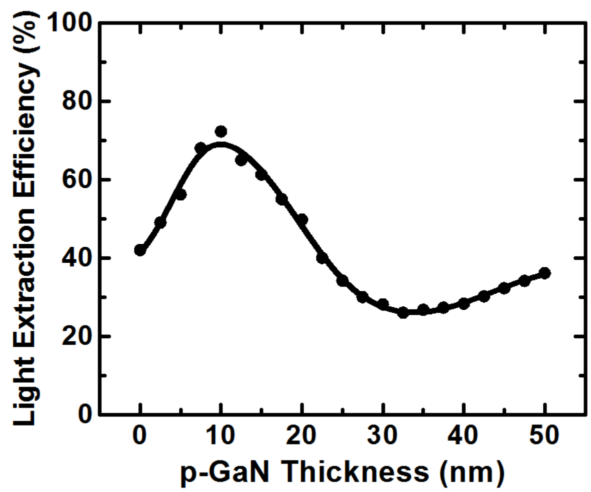

Figure 7-5. Dependence of the light extraction efficiency on the thickness of p-GaN thickness which shows the periodic dependence of light extraction efficiency on the thickness.

7.3.5 Effect of the device size on the light extraction efficiency

The light extraction efficiency also depends on the device size. In order to gain further understanding of the relation between the light extraction efficiency and the device size, we have performed simulations on devices with areal sizes in the ranges of 2.5×2.5 μm^2 to 15×15 μm^2. Illustrated in Figure 7.6, by increasing the device size from 2.5×2.5 μm2 to 15×15 μm2, the maximum achievable light extraction efficiency decreases from 72% to 54%. We thus conclude that the light extraction efficiency is less sensitive to the device size, compared to other parameters such as nanowire diameter and spacing.

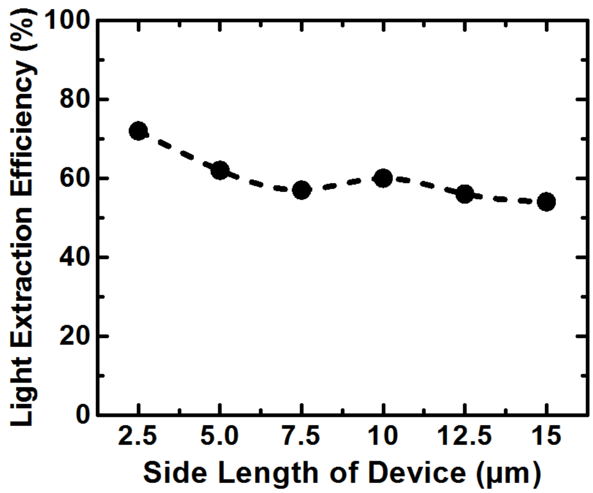

Figure 7-6. Simulated light extraction efficiency for devices with side lengths varying from 2.5 μm to 15 μm. Each device has a square dimension. In this simulation, the nanowire diameter and spacing were kept constant at 119 and 194 nm, respectively.

7.3.6 Effect of the random variation in the nanowire diameter and spacing on the light extraction efficiency

For practical applications, it is necessary to understand the dependence of the light extraction efficiency on small variations of nanowire properties due to the fabrication tolerances. The light extraction efficiency is calculated for ten different random structures. First, the spacing and diameter of the nanowires is fixed at 194 and 119 nm, respectively. Then we introduced a ±10% random variation in the spacing between nanowires. With such a random distribution, we observed that the light extraction efficiency varies from 18% to 66%. Furthermore, we also introduced ±10% random variation in the diameter of the nanowires. In this case, the light extraction efficiency varies from 17% to 62%. Figure 7.7(a) shows the light extraction efficiency derived for ten different structures with ±10% random variations in nanowire spacing and diameter.

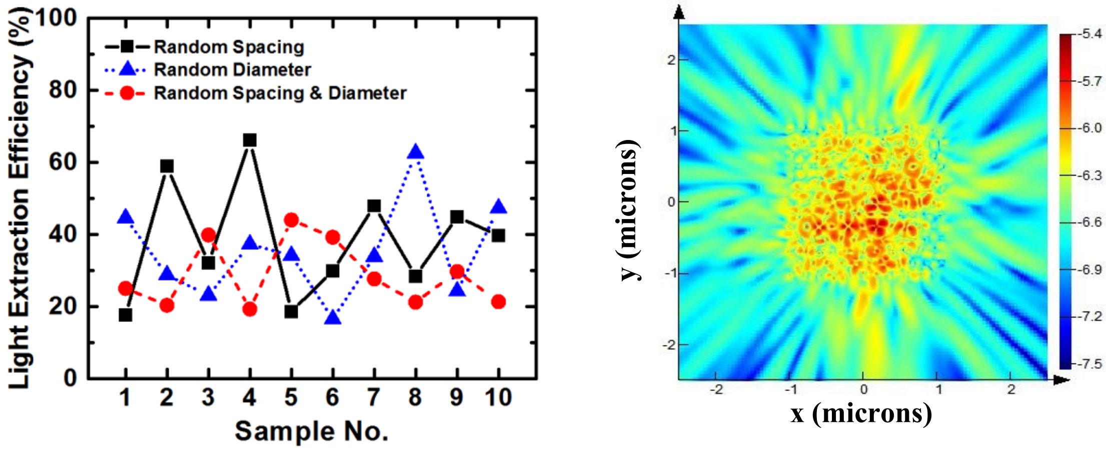

(a) (b)

Figure 7-7. (a) The light extraction efficiency for ten different structures with random nanowire spacing, random nanowire diameter, and fully random structure. (b) Simulated mode profile for the fully random structure.

We have also considered the random variations in both the spacing between nanowires and the diameter of the nanowires. The resulting light extraction efficiency varies in the range of 19% to 44%, illustrated in Figure 7.7(a). Figure 7.7(b) shows the simulated mode profiles with the random nanowire spacing and diameter. It is seen that some local cavities are formed, which confine and localize light inside the structure [232]. It is worthwhile mentioning that the light extraction efficiency of 19% is still nearly two times higher than previously reported deep UV LEDs with maximum external quantum efficiencies of <10% [111-113]. With well-controlled growth and fabrication process, it is expected that the light extraction efficiency of deep UV LEDs can become comparable to that of high efficiency visible LEDs.

7.4 Conclusion

In summary, we have studied the side emission properties of nanowire deep UV LEDs using 3D FDTD simulation. The emission of the guided modes could be inhibited and redirected into radiated modes utilizing nanowire structures. Through a comprehensive investigation of different parameters including the nanowire size and density as well as the thickness of p-GaN layer, we have shown that an unprecedentedly high light extraction efficiency of ~72% can be achieved. Although we have considered 280 nm as the operation wavelength in this study, the device design can be readily extended into the UV-C band (< 280 nm) wherein the LED emission is predominantly TM polarized.

8 Summary and future Work

8.1 Summary of the present work

The goal of this study is to enhance the external efficiency of LEDs including both the internal quantum efficiency and the light extraction efficiency. Through extensive theoretical and experimental studies, we have demonstrated unambiguously that the maximum achievable quantum efficiency of GaN based nanowire LEDs is ultimately limited by electron leakage and overflow. Detailed temperature-dependent studies further confirm that efficiency droop in nanowire LEDs becomes more severe at lower temperatures, which is directly correlated with the relatively enhanced electron overflow with decreasing temperature. We have further achieved an effective control of electron overflow in phosphor-free InGaN/GaN dot-in-a-wire white LEDs by incorporating a p-doped AlGaN electron blocking layer between the quantum dot active region and the p-GaN. The resulting nanowire LEDs exhibit remarkably stable white-light emission with virtually no efficiency droop. This work has identified and addressed one of the major obstacles of nanowire LEDs for applications in future high power phosphor-free, all-semiconductor based solid state lighting.

We have shown that self-organized InGaN/AlGaN dot-in-a-wire core-shell structures can overcome some of the critical challenges of previously reported axial nanowire LEDs, including large surface recombination and poor carrier dynamics, leading to significantly reduced carrier leakage and enhanced output power. Moreover, the p-AlGaN barrier layers can function as distributed EBLs, which is found to be highly effective in reducing electron overflow and enhancing hole transport. The dot-in-a-wire core-shell heterostructures can also emit light across the entire visible spectral range. Such unique nanowire heterostructures, with controllable carrier dynamics, will significantly advance the development of a broad range of nanowire photonic devices, including lasers, solar cells, and photodetectors.

We have developed a new approach, with the use of tunnel injection, to control electron overflow and carrier leakage in GaN-based nanowire LEDs without using any Al-containing electron blocking layer. Electron and hole injector wells are separately incorporated in the device active region to reduce electron overflow and enhance hole injection. It is further observed that the hole injector can effectively harvest electrons escaped through the near-surface region of the nanowires, leading to a highly stable, neutral white light emission.

We have shown that the light extraction efficiency of a GaN LED can be significantly enhanced by integrating with nanotube arrays. The light extraction involves two successive steps, including the coupling from the light source to the tube and the subsequent emission from the tube to the air. For the first step, a relatively large wall thickness in the bottom region of the nanotube is favorable for both TE and TM waves, and a smaller distance between the nanotube and the source offers stronger coupling. For the second step, TE waves and TM waves exhibit different behaviors, since the tube wall thickness has dramatically different effects on their respective propagation properties. In the case of nanotube arrays, the dependence of light extraction efficiency on the source position is similar to that of a single nanotube except that the extraction efficiency is also negatively affected by the light coupling from nanotubes back to the LED structure. There is an optimal separation distance of adjacent nanotubes which balances the need for minimizing this effect and the need for high surface coverage of nanotubes. It is envisioned that the use of nanotubes can offer a flexible, low cost approach for significantly enhancing the light extraction of the emerging micron- and submicron-scale LEDs for display, imaging, sensing, and communication applications.

We have studied the different regimes of light propagation in deep ultraviolet light emitting diodes using nanowire arrays using 3D FDTD simulation. The comprehensive investigation of different nanowire array topologies shows that the use of periodic nanowire arrays led to light extraction efficiency enhancement by ~7 times compared to conventional planar UV LEDs. The UV LEDs incorporating nanowires could help to decrease the total internal reflection caused by refractive index contrast between semiconductor and air. We have proposed the directional UV LEDs by employing biperiodic arrays which could be implemented in the photonic integrated circuits. We have further investigated photonic band edge nanowire UV LEDs with the strong gain enhancement which is required for UV edge-emitting lasers. We could extend the proposed UV LED designs into the operation wavelength in the ranges of UV-C band (< 280 nm).

We have presented the side emission properties of nanowire deep UV LEDs using 3D FDTD simulation. The emission of the guided modes could be inhibited and redirected into radiated modes utilizing nanowire structures. Through a comprehensive investigation of different parameters including the nanowire size and density as well as the thickness of p-GaN layer, we have shown that an unprecedentedly high light extraction efficiency of ~72% can be achieved. Although we have considered 280 nm as the operation wavelength in this study, the device design can be readily extended into the UV-C band (< 280 nm) wherein the LED emission is predominantly TM polarized.

8.2 Future work

8.2.1 High efficiency UV LEDs

Further improvement in the light extraction efficiency of nanowires LEDs in both visible and UV ranges will result in more practical and efficient light sources for different applications. UV LEDs are attractive for a wide range of applications, such as sensing, bio-medical analysis, disinfection, and water purification. UV LEDs are expected to replace conventional UV lamps because of many advantages such as wavelength selectivity, high efficiency, and compactness. One other promising candidate for such light sources is AlN, which has a direct bandgap energy of ~ 6.2 eV (~ 200 nm in wavelength) at room temperature. Progress in this field, however, has been limited by the difficulty in realizing electrically injected AlN LEDs; and to date, there are only a few reports on AlN LEDs [37-39]. The main challenges include low internal quantum efficiencies, and low light extraction efficiency [38, 40-43].

To address these challenges, besides further improving the planar AlN technology, various approaches with low dimensional structures have been explored, such as photonic crystals [74] and nanowires [75-81]. Recently, with the improved MBE growth of AlN nanowires on Si, high quality AlN nanowires were demonstrated [82], and the AlN nanowire LEDs with high internal quantum efficiency and excellent electrical performance were realized [39]. In the future work, we will address the most critical light extraction issue in AlN LEDs.

The light extraction efficiency is one of the main limiting factors of the EQE of UV LEDs which remain lower than those of visible LEDs. The low light extraction efficiency of the UV LEDs is attributed to total internal reflection from the high refractive index of the semiconductors in contrast to that of the air, and the unique optical polarization property of high Al composition AlGaN QWs. The QWs emit light with both TE) and TM polarization modes which correspond to the electric field direction perpendicular or parallel to the nanowire axis, respectively. Though TE mode emission in visible LEDs is dominant, the portion of the TM mode in AlGaN-based UV LEDs increases as the Al composition increases. As the light with TM polarization propagates mainly in the horizontal direction, the light can only propagate in-plane and cannot escape from the large area top surface, illustrated in Figure 8.1(a). This unique light polarization in AlN, therefore, makes the light extraction efficiency of conventional AlN LEDs to be only less than 1 % [55]. Here, we show that, in contrast to *c*-plane AlN LEDs wherein the emission direction is perpendicular to the *c*-axis due to the intrinsic TM polarization, the *c*-axially grown AlN nanowire LEDs show stronger emission from the top surface (see Figure 8.1(b)), i.e., along the *c*-axis, if the average nanowire diameter and spacing falls within certain range. This finding uncovers important insight of extracting TM polarized light from *c*-axially grown AlN nanowire LEDs, and provides a viable solution to realize electrically injected surface emitting deep UV light sources.

While enhanced light extraction has been predicted for nanowire structures, few studies have been paid attention to the effect of nanowire size variation on the light extraction efficiency of TM polarized light. To achieve efficient surface emission, the lateral coupling of radiation amongst nanowires should be minimized, which imposes critical requirements on the nanowire size and spacing. We consider an AlN nanowire LED structure consists of 90 nm n-AlN, 60 nm i-AlN, and 15 nm p-AlN (illustrated in the Figure 1(b)). Lumerical FDTD was utilized to explore the radiation pattern of AlN nanowire LEDs, and the PML boundary conditions was employed around the AlN nanowire LEDs. The simulation domain size is 2.5 μm × 2.5 μm. To excite the nanowires, the TM dipole source with the emission wavelength of 207 nm was employed in the center of the active region (i-AlN).

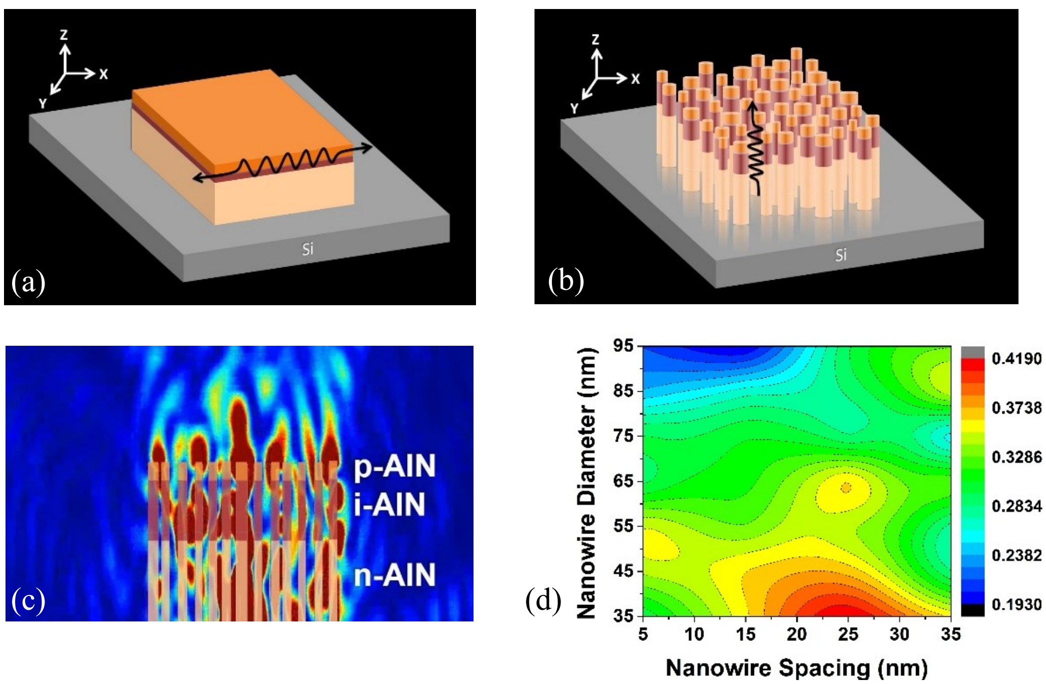

Figure 8-1. (a) The schematic of light propagation of TM polarized light in conventional c-plane AlN LEDs. (b) A schematic of the AlN nanowire LEDs with the inset showing the layer-by-layer structure. The arrows indicate the light scattering process. (c) The screen shot of light propagation of AlN nanowire LEDs with average diameter of 30 and spacing of 25 (d) The simulated light output contour plots of AlN nanowire LEDs from top.

A screen shot of light propagation with an average diameter of 30 nm and spacing of 25 nm is shown in Figure 8.1(c), and it is seen that with such nanowire geometry, light mostly comes out from the nanowire top surface.

To further provide a comprehensive understanding of light extraction from AlN nanowire structures, the contour plot formed by top light extraction efficiencies was derived. The simulation was performed on ensemble nanowires with average diameters in the range of 35 to 95 nm and average spacing in the range of 5 to 35 nm. For a given combination of nanowire diameter and spacing, five simulations were performed with a ±5 nm random variation in the nanowire diameter and spacing. As a result, each light extraction efficiency showed in the contour plot (Figure 8.1(d)) was the average of the five simulated samples. From Figure 8.1(c), it is seen that the light extraction efficiency for devices with large nanowire diameter and small nanowire spacing is more efficient from the side (top left corners in Figure 8.1(c)), which is similar to that of conventional *c*-plane planar devices. Here, the high light extraction efficiency from the side can be ascribed to mode coupling through dense large-diameter nanowires. As the spacing increases (take the spacing around 20 nm as an example in Figure 8.1(c)), light can also escape from the top surface, which can be mainly attributed to that both the coupling to and scattering from adjacent nanowires occur at the same time. These results suggest that in AlN nanowires, by optimizing the nanowire diameter and spacing, the TM polarized light can emit from the top surface of *c*-axially grown AlN nanowires. In this work, such requirements can be experimentally realized by tuning the growth parameters including substrate temperature and III/V species ratio.

8.2.2 High performance nanowire UV lasers

We will investigate the design of nanowire UV lasers utilizing the aforementioned structures in chapter 6. In the first approach, the edge emitting UV lasers consist of highly dense AlGaN nanowire arrays and SiO_x/air distributed Brag reflectors. The second approach employs a periodic nanowire arrays with and without SiOx/air distributed Brag reflectors, wherein strong light confinement occurs at the optical band edge of highly uniform AlGaN nanowire arrays, leading to significantly enhanced modal gain and greatly simplified fabrication process. The UV laser bar based on these structures are plotted in Figure 8.2. The laser bar consists of high density random or periodic nanowire arrays, and optical feedback provided by distributed Bragg reflectors in both ends, which are defined by multiple SiOx/air distributed Bragg reflectors.

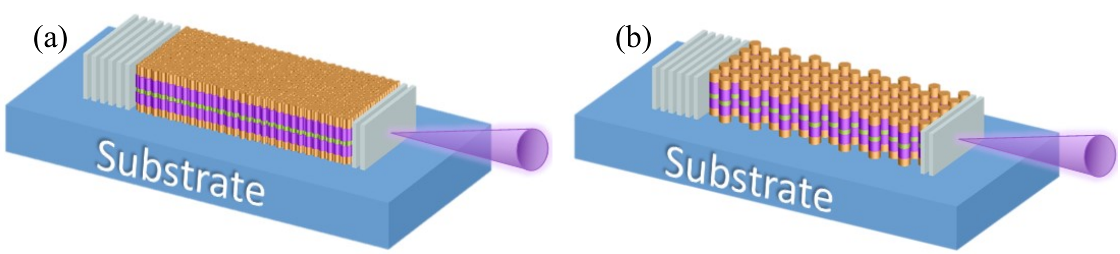

Figure 8-2. Schematic of the (a) random and (b) periodic nanowire UV laser on Si. The front and end mirrors are defined using multiple SiOx/air distributed Bragg reflectors.

The simulated mode profiles of the periodic nanowire lasers on Si with multiple SiOx/air distributed Bragg reflectors is shown in Figure 6.3. The cavity Q-factors can be further optimized for high power operations by varying the number of Bragg reflector pairs. The accurate control of the nanowire spacing and diameter is clearly required in the proposed periodic nanowire edge emitting lasers. To realize such accurate control of nanowire growth, nanopatterned substrates are necessary.

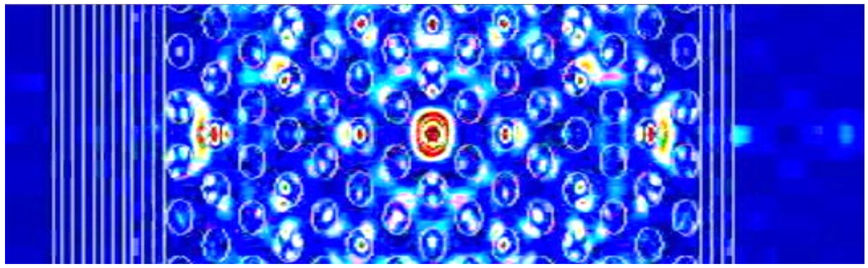

Figure 8-3. The simulated mode profiles of the periodic nanowire lasers on Si with multiple SiOx/air distributed Bragg reflectors.

8.2.3 Two-dimensional semiconductor lasers

Despite the success of planar compound semiconductor lasers over the past few decades, their applications in the emerging chip-level optical communications and flexible displays has been challenging, due to the poor performance and short lifetime when integrated onto foreign substrates [233-235]. Therefore, the search for a new class of materials which can satisfy the lasing requirements and can be grown/transferred to foreign substrates has been a major research paradigm but with limited success [236]. Here, we will investigate the use of 2D MoS_2 as a new class of materials for laser operation. The 2D MoS_2 has strong photoluminescence emission [237] and relatively high carrier mobility [238] and are therefore well suited for next generation optoelectronic devices [239-241]. Importantly, they are compatible with the existing planar technology [242] and can be readily grown on low-cost Si/SiO_2 substrates [242].

We consider the use of 4L MoS_2 as the gain medium in a vertically coupled, free-standing SiO_x microdisk and microsphere cavity, which can significantly enhance the coupling between the MoS_2 gain medium and the optical cavity modes, leading to ultralow threshold lasing under continuous wave operation at room temperature.

Schematically shown in Figure 8.4(a), MoS_2 flakes were sandwiched between a free-standing microdisk and microsphere to achieve efficient coupling with the optical modes.

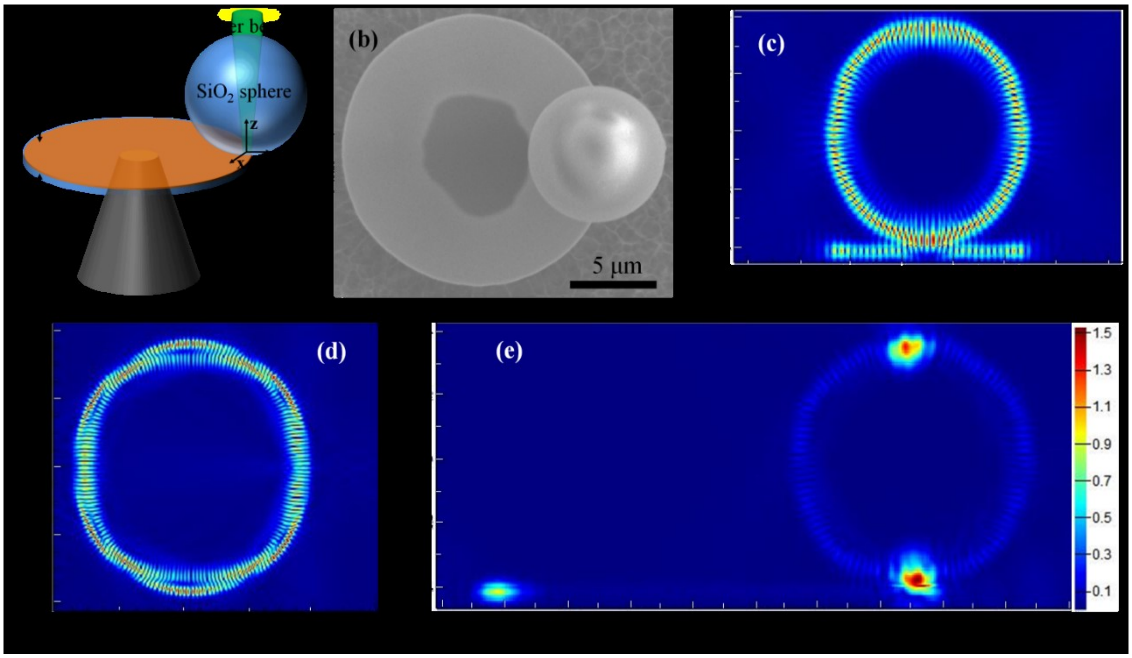

Figure 8-4. Cavity configuration and FDTD simulation. a) Schematic configuration of the coupled microsphere/microdisk optical cavity with the incorporation of 2D MoS2. b) Representative top-view SEM image of the coupled microsphere/microdisk cavity. Electric field distribution c) on the x-z plane passing through the microsphere/microdisk contact point, d) inside the microdisk on the x-y plane, and e) on the y-z plane passing through the contact point.

Shown in Figure 8.4(a), the silica microsphere has a diameter of ~ 7.7 μm. The SiO_2 microdisk diameter and thickness are ~ 15 μm and 340 nm, respectively, which is supported by a silicon post (lateral size ~ 2 to 5 μm) in the middle of the microdisk. Also shown in Figure 8.4(a) is the excitation and measurement configuration. The representative top view scanning electron microscopy image is shown in Figure 8.4(b). While the formation of whispering gallery modes (WGMs) in respective microdisk and microsphere cavities have been extensively studied and well understood, there have been no reports on the coupling between these two cavities to our knowledge. Therefore, we have first carried out detailed simulations of the WGMs and their emission characteristics in such a unique design.

In the 3D FDTD simulation, the excitation source was considered at the microsphere/microdisk contact point, i.e. the MoS_2 gain medium. A strong dependence of the cavity *Q*-factor and field distribution on the location of the microsphere on the microdisk was observed. For a microsphere sitting close to the rim of the microdisk, the simulation results confirmed the formation of coupled WGMs with large *Q*-factors. The optical modes confined in such a cavity circulate mainly along the vertical x-z equator of the microsphere and horizontal x-y equator of the microdisk, shown in Figures 8.4(c) and (d), respectively. A cross-sectional view of the electric field distribution inside the coupled cavity, on the y-z plane, indicated a highly asymmetric field distribution inside the microsphere with its maximum field overlapping with the active MoS_2, shown in Figure 8.4(e). Such a unique field distribution significantly reduces the mode volume (V_m) and increases the optical confinement factor (Γ). Considering our cavity design, i.e. microdisks with twice the diameter of the microsphere, the mode matching criterion forces the microdisk to refine its modes to match with those of the microsphere.

For a microsphere sitting at the middle of a MoS_2/SiO_2 microdisk, schematically shown in Figure 8.5(a), there is a large optical loss into the SiO_2 disk as shown in Figure 8.5(b). In this configuration, WGMs do not form inside the microdisk and there is no constructive coupling between the microsphere and the microdisk resulting in a poor *Q*-factor, unlike the case for a microsphere sitting at the rim of the disk. The maximum intensities were observed at the poles of the microsphere, shown in Figure 8.5(c), and the field distribution was similar on x-z and y-z planes.

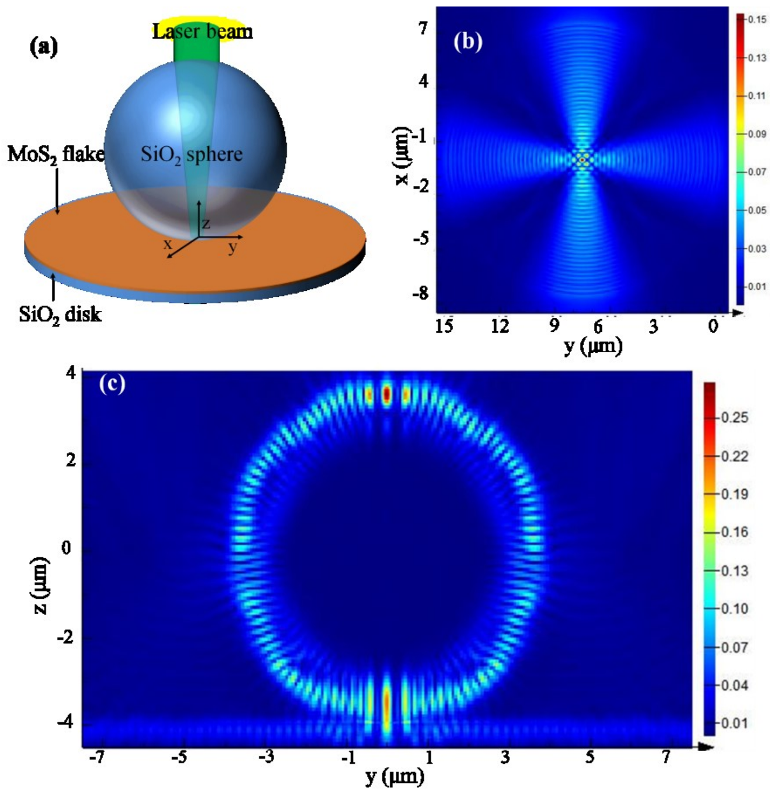

Figure 8-5. FDTD simulation of a microsphere sitting at the middle of microdisk. a) Schematic configuration of the microsphere and microdisk. Electric distribution b) inside the microdisk (on the x-y plane) and c) inside the microsphere and microdisk (on the y-z plane).

The performance of the MoS_2 microlaser will be studied by varying the pump power. Our findings, together with the proven capability of 2D MoS_2 to support high current densities, will pave the way for the realization of electrically-injected MoS_2-based lasers. This work will significantly advance the development of 2D MoS_2-based photonic devices on Si or other low cost, large area substrates for the emerging chip-level optical communications, flexible display, and lab-on-a-chip devices and systems.

List of publications

BOOK CHAPTER ►

- P. Bianucci, M.H.T. Dastjerdi, M. Djavid, and Z. Mi, "Rolled-up semiconductor tube optical cavities," In: High-Speed Photonics Interconnects, ISBN: 9781466516038, CRC press, Editor: Lukas Chrostowski, and Krzysztof Iniewski, (2012).

REFERRED JOUNRAL PUBLICATIONS ►

Current h-index according to Web of Science: 16

- M. Djavid, X. Liu, and Z. Mi, "Improvement of the light extraction efficiency of GaN-based LEDs using rolled-up nanotube arrays," Opt. Express 22, A1680-A1686 (2014).
- M. Djavid, H.P.T. Nguyen, S. Zhang, K. Cui, S. Fan, Z. Mi, "Tunnel injection InGaN/GaN dot-in-a-wire white-light-emitting diodes" Semicond. Sci. Tech., 29 (8), 085009 (2014).
- M. Djavid, and Z. Mi, "Achieving high efficiency deep ultraviolet LEDs by using nanowire structures," Appl. Phys. Lett. 108, 051102 (2016).
- O. Salehzadeh, M. Djavid, N. Tran, I. Shih, Z. Mi, "Optically pumped two-dimensional MoS2 lasers operating at room-temperature" Nano Lett. 15 (8), 5302-5306 (2015).
- S. Zhao, M. Djavid, Z. Mi, "A surface emitting, high efficiency near-vacuum ultraviolet light source with aluminum nitride nanowires monolithically grown on silicon" Nano Lett. 15 (10), 7006-7009 (2015).

- H.P.T. Nguyen, M. Djavid, S. Y. Woo, X. Liu, A. T. Connie, S. Sadaf, Q. Wang, G. A. Botton, I. Shih, and Z. Mi, "Engineering the Carrier Dynamics of InGaN Nanowire White Light-Emitting Diodes by Distributed p-AlGaN Electron Blocking Layers," Sci. Rep. 5, 7744 (2015).
- M.H.T. Dastjerdi, M. Djavid, and Z. Mi, "An electrically injected rolled-up semiconductor tube laser," Appl. Phys. Lett. 106, 021114 (2015).
- H.P.T. Nguyen, M. Djavid, K. Cui and Z. Mi, "Temperature-dependent nonradiative recombination processes in GaN-based nanowire white-light-emitting diodes on silicon," Nanotech. 23, 194012 (2012).
- M.H.T. Dastjerdi, M. Djavid, S. Arafin, X. Liu, P. Bianucci, Z. Mi, and P.J. Poole, "Optically pumped rolled-up InAs/InGaAsP quantum dash lasers at room temperature" Semicond. Sci. Tech., 28 (9), 094007 (2013).
- Y-H. Ra, R. Wang, M. Djavid and Z. Mi, "Single Nanowire Projection Displays" (submitted).
- S. Zhao, S. Y. Woo, M. Bugnet, M. Djavid, X. Liu, J. Kang, X. Kong, W. Ji, H. Guo, Z. Liu, G. A. Botton, and Z. Mi, "Molecular Beam Epitaxial Growth and Characterization of Al(Ga)N Nanowire Deep Ultraviolet Light Emitting Diodes and Lasers" Jpn. J. Appl. Phys. (submitted).
- H.P.T. Nguyen, K. Cui, S. Zhang, M. Djavid, A. Korinek, G. A. Botton, and Z. Mi, "Controlling Electron Overflow in Phosphor-Free InGaN/GaN Nanowire White Light-Emitting Diodes," Nano Lett. 12 (3), 1317–1323 (2012).

- S. M. Sadaf, Y. H. Ra, H. P. T. Nguyen, M. Djavid, Z. Mi, "Alternating-current InGaN/GaN tunnel junction nanowire white-light emitting diodes" Nano Lett. 15(10), 6696-6701 (2015).
- S. Zhao, A. Connie, M. Dastjerdi, X. Kong, Q. Wang, M. Djavid, S. Sadaf, X. Liu, I. Shih, and H. Guo, "Aluminum nitride nanowire light emitting diodes: Breaking the fundamental bottleneck of deep ultraviolet light sources," Sci. Rep. 5, 8332 (2015).
- H.P.T. Nguyen, M. Djavid, Z. Mi, "Nonradiative recombination mechanism in phosphor-free GaN-based nanowire white light emitting diodes and the effect of ammonium sulfide surface Passivation", ECS Transactions, 53 (2), 93-100 (2013).
- Z. Mi, H.P.T. Nguyen, M. Djavid, S. Zhang, A. Connie, S. Sadaf, Q. Wang, S. Zhao, I. Shih, "(Invited) High Power Phosphor-Free InGaN/GaN/AlGaN Core-Shell Nanowire White Light Emitting Diodes on Si Substrates" ECS Transactions 61 (5), 9-15 (2014)
- Z. Mi, P. Bianucci, M. H. T. Dastjerdi, S. Mukherjee, M. Djavid and P. Poole, "(Invited) Rolled-up 1.55 μm Semiconductor Quantum Dot Tube Lasers", ECS Transactions, 45 (5), 113-118 (2012).

CONFERENCE PUBLICATION ►

- M. Djavid, X. Liu, and Z. Mi, "Improvement of Light Extraction Efficiency in GaN-Based LED using GaN Microtubes", SPIE Photonic North 2013, Ottawa, Canada (2013).

- M. Djavid, and Z. Mi, “Design and Simulation of InN Nanowire Ring Resonators on a Si Platform”, SPIE Photonic North, Montreal, QC, Canada (2012).
- M. Djavid, H. P. T. Nguyen, S. Zhang, K. Cui, and Z. Mi, “Reduced Electron Overflow in InGaN/GaN Dot-in-a-Wire White-Light-Emitting Diodes by Using an Electronically Coupled Quantum Well”, SPIE Photonic North, Montreal, QC, Canada (2012).
- M.H.T Dastjerdi, M. Djavid, P Bianucci, Z Mi , “Coherent emission from electrically-injected InP/InGaAsP rolled up quantum well microtubes” Photonics Conference (IPC), 2014 IEEE, 502-503 (2014).
- H.P.T Nguyen, M. Djavid, SY Woo, X Liu, Q Wang, Z Mi, GA Botton, “High-power phosphor-free InGaN/AlGaN dot-in-a-wire core-shell white light-emitting diodes” SPIE OPTO, 938307-938307-8 (2015)
- Z. Mi, H.P.T. Nguyen, S. Zhang, K. Cui, M. Djavid, “Molecular beam epitaxial growth and characterization of InGaN/GaN dot-in-a-wire nanoscale heterostructures: Toward ultrahigh efficiency phosphor-free white light emitting diodes”, Proceedings of SPIE - The International Society for Optical Engineering, 8634, 86340B (2013).
- Z. Mi, H.P.T. Nguyen, S. Zhang, M. Djavid, “Ultrahigh-efficiency phosphor-free InGaN/GaN nanowire white light-emitting diodes on silicon”, 2012 IEEE Photonics Conference, IPC 2012, 6358676, 429-430 (2012).
- S. Fathololoumi, S. Zhao, H. P. Nguyen, M. Djavid, I. Shih, and Z. Mi, “Large Area GaN/AlN Nanowire Resonant Tunneling Devices on Silicon,” in CLEO:

Science and Innovations, OSA Technical Digest (online) (Optical Society of America, 2012), paper CTh3D.7 (2012).

- P. Bianucci, M. H. Tavakoli Dastjerdi, S. Mukherjee, M. Djavid, P. J. Poole, and Z. Mi, "An optically pumped InGaAsP/InP quantum dot rolled-up microtube laser", American Physical Society, APS March Meeting (2012).

References

1. E.F. Schubert and J.K. Kim, *Solid-state light sources getting smart.* Science, 2005. **308**(5726), p. 1274-8.
2. R. Haitz, F. Kish, J. Tsao, and J. Nelson, *The case for a national research program on semiconductor lighting.* Optoelectronics Industry Development Association, 1999.
3. D.A. Steigerwald, J.C. Bhat, D. Collins, R.M. Fletcher, M.O. Holcomb, M.J. Ludowise, P.S. Martin, and S.L. Rudaz, *Illumination with solid state lighting technology.* Selected Topics in Quantum Electronics, IEEE Journal of, 2002. **8**(2), p. 310-320.
4. S. Nakamura, *Current status of GaN-based solid-state lighting.* MRS bulletin, 2009. **34**(2), p. 101.
5. C.-C. Sun, I. Moreno, S.-H. Chung, W.-T. Chien, C.-T. Hsieh, and T.-H. Yang, *Direct LED backlight for large area LCD TVs: brightness analysis.* Proceedings of SPIE, 2007. **6669**, p. 666909.
6. A. Zukauskas, M. Shur, and R. Gaska, *Introduction to solid state lighting*. Vol. 122. 2002, John Wiley & Sons New York.
7. D.A. Kirkpatrick, *Is solid state the future of lighting?* Proceedings of SPIE, 2004. **5187**, p. 10.
8. A. Mednik, *Automotive LED lighting needs special drivers.* Power Electronics Technology Magazine, 2005.
9. N.G. Yeh, C.-H. Wu, and T.C. Cheng, *Light-emitting diodes—Their potential in biomedical applications.* Renewable and Sustainable Energy Reviews, 2010. **14**(8), p. 2161-2166.
10. M. Belz, F.A. Klein, and H. Habhegger. *UV LED fiber optic detection system for DNA and protein*. in *Biomedical Optics (BiOS)* 2007. International Society for Optics and Photonics.
11. F.R. Pereira, M. Stefani, J.A. Otoboni, E.H. Richter, G. Rossi, A.D. Mota, and L. Ventura. *UVA system for human cornea irradiation*. in *SPIE BiOS: Biomedical Optics* 2009. International Society for Optics and Photonics.

12. M. Mori, A. Hamamoto, M. Nakano, M. Akutagawa, A. Takahashi, T. Ikehara, and Y. Kinouchi. *Effects of ultraviolet LED on bacteria*. in *World Congress on Medical Physics and Biomedical Engineering 2006*. 2007. Springer.

13. J. Close, J. Ip, and K. Lam, *Water recycling with PV-powered UV-LED disinfection.* Renewable Energy, 2006. **31**(11), p. 1657-1664.

14. M. Würtele, T. Kolbe, M. Lipsz, A. Külberg, M. Weyers, M. Kneissl, and M. Jekel, *Application of GaN-based ultraviolet-C light emitting diodes–UV LEDs–for water disinfection.* Water Research, 2011. **45**(3), p. 1481-1489.

15. M. Mori, A. Hamamoto, A. Takahashi, M. Nakano, N. Wakikawa, S. Tachibana, T. Ikehara, Y. Nakaya, M. Akutagawa, and Y. Kinouchi, *Development of a new water sterilization device with a 365 nm UV-LED.* Medical & Biological Engineering & Computing, 2007. **45**(12), p. 1237-1241.

16. A. Hamamoto, M. Mori, A. Takahashi, M. Nakano, N. Wakikawa, M. Akutagawa, T. Ikehara, Y. Nakaya, and Y. Kinouchi, *New water disinfection system using UVA light‐emitting diodes.* Journal of Applied Microbiology, 2007. **103**(6), p. 2291-2298.

17. Y. Shen, G. Mueller, S. Watanabe, N. Gardner, A. Munkholm, and M. Krames, *Auger recombination in InGaN measured by photoluminescence.* Applied Physics Letters, 2007. **91**, p. 141101.

18. M. Zhang, P. Bhattacharya, J. Singh, and J. Hinckley, *Direct measurement of auger recombination in InGaN/GaN quantum wells and its impact on the efficiency of InGaN/GaN multiple quantum well light emitting diodes.* Applied Physics Letters, 2009. **95**, p. 201108.

19. M.-H. Kim, M.F. Schubert, Q. Dai, J.K. Kim, E.F. Schubert, J. Piprek, and Y. Park, *Origin of efficiency droop in GaN-based light-emitting diodes.* Applied Physics Letters, 2007. **91**, p. 183507.

20. B.-C. Lin, K.-J. Chen, C.-H. Wang, C.-H. Chiu, Y.-P. Lan, C.-C. Lin, P.-T. Lee, M.-H. Shih, Y.-K. Kuo, and H.-C. Kuo, *Hole injection and electron overflow improvement in InGaN/GaN light-emitting diodes by a tapered AlGaN electron blocking layer.* Optics Express, 2014. **22**(1), p. 463-469.

21. T. Wei, L. Zhang, X. Ji, J. Wang, Z. Huo, B. Sun, Q. Hu, X. Wei, R. Duan, and L. Zhao, *Investigation of Efficiency and Droop Behavior Comparison for InGaN/GaN Super Wide-Well Light Emitting Diodes Grown on Different Substrates.* Photonics Journal, IEEE, 2014. **6**(6), p. 1-10.
22. M. Moram, C. Ghedia, D. Rao, J. Barnard, Y. Zhang, M. Kappers, and C. Humphreys, *On the origin of threading dislocations in GaN films.* Journal of Applied Physics, 2009. **106**, p. 073513.
23. V. Narayanan, K. Lorenz, W. Kim, and S. Mahajan, *Origins of threading dislocations in GaN epitaxial layers grown on sapphire by metalorganic chemical vapor deposition.* Applied Physics Letters, 2001. **78**(11), p. 1544-1546.
24. D.S. Rao, R. Beanland, M. Kappers, D. Zhu, and C. Humphreys. *Lattice distortions in GaN thin films on (0001) sapphire*. in *Journal of Physics: Conference Series*. 2010. IOP Publishing.
25. M.Y. Ryu, P.W. Yu, E.J. Shin, J.I. Lee, S.K. Yu, E.S. Oh, Y.J. Park, H.S. Park, and T.I. Kim, *Photoluminescence study of InGaN/GaN double quantum wells with varying barrier widths.* Journal of the Korean Physical Society, 2000. **37(**4), p. 387-390.
26. S. De, A. Layek, S. Bhattacharya, D.K. Das, A. Kadir, A. Bhattacharya, S. Dhar, and A. Chowdhury, *Quantum-confined stark effect in localized luminescent centers within InGaN/GaN quantum-well based light emitting diodes.* Applied Physics Letters, 2012. **101**, p. 121919.
27. F. Bertazzi, X. Zhou, M. Goano, G. Ghione, and E. Bellotti, *Auger recombination in InGaN/GaN quantum wells: A full-Brillouin-zone study.* Applied Physics Letters, 2013. **103**, p. 081106.
28. E. Kioupakis, Q. Yan, D. Steiauf, and C.G. Van de Walle, *Temperature and carrier-density dependence of Auger and radiative recombination in nitride optoelectronic devices.* New Journal of Physics, 2013. **15**, p. 125006.
29. H.P.T. Nguyen, M. Djavid, K. Cui, and Z. Mi, *Temperature-dependent nonradiative recombination processes in GaN-based nanowire white-light-emitting diodes on silicon.* Nanotechnology, 2012. **23**(19), p. 194012.

30. Ü. Özgür, H. Liu, X. Li, X. Ni, and H. Morkoc, *GaN-based light-emitting diodes: Efficiency at high injection levels.* Proceedings of the IEEE, 2010. **98**(7), p. 1180-1196.
31. Y. Shen, G. Mueller, S. Watanabe, N. Gardner, A. Munkholm, and M. Krames, *Auger recombination in InGaN measured by photoluminescence.* Applied Physics Letters, 2007. **91**(14), p. 1101.
32. E. Kioupakis, P. Rinke, K.T. Delaney, and C.G. Van de Walle, *Indirect Auger recombination as a cause of efficiency droop in nitride light-emitting diodes.* Applied Physics Letters, 2011. **98**, p. 161107.
33. J. Iveland, L. Martinelli, J. Peretti, J.S. Speck, and C. Weisbuch, *Direct measurement of Auger electrons emitted from a semiconductor light-emitting diode under electrical injection: identification of the dominant mechanism for efficiency droop.* Physical Review Letters, 2013. **110**(17), p. 177406.
34. W. Guo, M. Zhang, P. Bhattacharya, and J. Heo, *Auger recombination in III-nitride nanowires and its effect on nanowire light-emitting diode characteristics.* Nano Letters, 2011. **11**(4), p. 1434-1438.
35. J. Xie, X. Ni, Q. Fan, R. Shimada, Ü. Özgür, and H. Morkoç, *On the efficiency droop in InGaN multiple quantum well blue light emitting diodes and its reduction with p-doped quantum well barriers.* Applied Physics Letters, 2008. **93**(12), p. 1107.
36. H.P.T. Nguyen, K. Cui, S. Zhang, M. Djavid, A. Korinek, G.A. Botton, and Z. Mi, *Controlling electron overflow in phosphor-free InGaN/GaN nanowire white light-emitting diodes.* Nano Letters, 2012. **12**(3), p. 1317-1323.
37. Y. Taniyasu and M. Kasu, *Surface 210 nm light emission from an AlN p–n junction light-emitting diode enhanced by A-plane growth orientation.* Applied Physics Letters, 2010. **96**, p. 221110.
38. Y. Taniyasu, M. Kasu, and T. Makimoto, *An aluminium nitride light-emitting diode with a wavelength of 210 nanometres.* Nature, 2006. **441**(7091), p. 325-8.
39. S. Zhao, A.T. Connie, M.H. Dastjerdi, X.H. Kong, Q. Wang, M. Djavid, S. Sadaf, X.D. Liu, I. Shih, H. Guo, and Z. Mi, *Aluminum nitride nanowire light*

emitting diodes: Breaking the fundamental bottleneck of deep ultraviolet light sources. Scientific Reports, 2015. **5**, p. 8332.

40. A. Bhattacharyya, T.D. Moustakas, L. Zhou, D.J. Smith, and W. Hug, *Deep ultraviolet emitting AlGaN quantum wells with high internal quantum efficiency.* Applied Physics Letters, 2009. **94**, p. 181907.

41. A. Khan, K. Balakrishnan, and T. Katona, *Ultraviolet light-emitting diodes based on group three nitrides.* Nature Photonics, 2008. **2**, p. 77.

42. M.S. Shur and R. Gaska, *Deep-Ultraviolet Light-Emitting Diodes.* IEEE Transcations on Electron Devices, 2010. **57**, p. 12.

43. H. Hirayama, N. Noguchi, S. Fujikawa, J. Norimatsu, N. Kamata, T. Takano, K. Tsubaki, C.W. Litton, J.-I. Chyi, Y. Nanishi, J. Piprek, and E. Yoon, *222-282 nm AlGaN and InAlGaN based deep-UV LEDs fabricated on high-quality AlN template.* Proceeding of SPIE, 2009. **7216**, p. 721621:1-14.

44. H. Hirayama, N. Noguchi, S. Fujikawa, J. Norimatsu, N. Kamata, T. Takano, and K. Tsubaki. *222-282 nm AlGaN and InAlGaN based deep-UV LEDs fabricated on high-quality AlN template*. in *SPIE OPTO: Integrated Optoelectronic Devices*. 2009. International Society for Optics and Photonics.

45. M. Martens, F. Mehnke, C. Kuhn, C. Reich, V. Kueller, A. Knauer, C. Netzel, C. Hartmann, J. Wollweber, and J. Rass, *Performance Characteristics of UV-C AlGaN-Based Lasers Grown on Sapphire and Bulk AlN Substrates.* Photonics Technology Letters, IEEE, 2014. **26**(4), p. 342-345.

46. Y. Taniyasu, M. Kasu, and T. Makimoto, *Electrical conduction properties of n-type Si-doped AlN with high electron mobility (> 100 cm2 V-1 s-1).* Applied Physics Letters, 2004. **85**, p. 4672.

47. A. Bhattacharyya, T. Moustakas, L. Zhou, D.J. Smith, and W. Hug, *Deep ultraviolet emitting AlGaN quantum wells with high internal quantum efficiency.* Applied Physics Letters, 2009. **94**, p. 181907.

48. C. Himwas, M.d. Hertog, F. Donatini, L.S. Dang, L. Rapenne, E. Sarigiannidou, R. Songmuang, and E. Monroy, *AlGaN/AlN quantum dots for UV light emitters.* Physica Status Solidi (c), 2013. **10**(3), p. 285-288.

49. T. Nishida, T. Ban, H. Saito, and T. Makimoto. *High current injection to a UV-LED grown on a bulk AlN substrate*. in *MRS Proceedings*. 2003. Cambridge Univ Press.

50. L. Wang, L. Wang, F. Ren, W. Zhao, J.X. Wang, J.N. Hu, C. Zhang, Z.B. Hao, and Y. Luo, *GaN grown on AIN/sapphire templates.* Acta Physica Sinica, 2010. **59**(11), p. 8021-8025.

51. S. Li-Wen, Q. Zhi-Xin, F. Hao, Z. Yan-Zhao, L. Tao, X. Zheng-Yu, Y. Zhi-Jian, S. Bo, Z. Guo-Yi, and L. Shu-Ping, *AlGaN-based deep-ultraviolet light emitting diodes fabricated on AlN/sapphire template.* Chinese Physics Letters, 2009. **26**(11), p. 117801.

52. M.L. Nakarmi, N. Nepal, J.Y. Lin, and H.X. Jiang, *Photoluminescence studies of impurity transitions in Mg-doped AlGaN alloys.* Applied Physics Letters, 2009. **94**, p. 091903.

53. H. Jiang and J. Lin, *Hexagonal boron nitride for deep ultraviolet photonic devices.* Semiconductor Science and Technology, 2014. **29**(8), p. 084003.

54. W. Sun, M. Shatalov, J. Deng, X. Hu, J. Yang, A. Lunev, Y. Bilenko, M. Shur, and R. Gaska, *Efficiency droop in 245–247 nm AlGaN light-emitting diodes with continuous wave 2 mW output power.* Applied Physics Letters, 2010. **96**, p. 061102.

55. Y. Taniyasu, M. Kasu, and T. Makimoto, *An aluminium nitride light-emitting diode with a wavelength of 210 nanometres.* Nature, 2006. **441**(7091), p. 325-328.

56. F. Qian, S. Gradecak, Y. Li, C.-Y. Wen, and C.M. Lieber, *Core/multishell nanowire heterostructures as multicolor, high-efficiency light-emitting diodes.* Nano Letters, 2005. **5**(11), p. 2287-2291.

57. J. Zhu, L. Wang, S. Zhang, H. Wang, D. Zhao, J. Zhu, Z. Liu, D. Jiang, and H. Yang, *The fabrication of GaN-based nanopillar light-emitting diodes.* Journal of Applied Physics, 2010. **108**, p. 074302.

58. C. Chiu, T.-C. Lu, H. Huang, C. Lai, C. Kao, J. Chu, C. Yu, H.-C. Kuo, S. Wang, and C. Lin, *Fabrication of InGaN/GaN nanorod light-emitting diodes with self-assembled Ni metal islands.* Nanotechnology, 2007. **18**(44), p. 445201.

59. H.P.T. Nguyen, S. Zhang, A.T. Connie, M.G. Kibria, Q. Wang, I. Shih, and Z. Mi, *Breaking the Carrier Injection Bottleneck of Phosphor-Free Nanowire White Light-Emitting Diodes.* Nano Letters, 2013. **13**(11), p. 5437-5442.
60. H.P.T. Nguyen, M. Djavid, S.Y. Woo, X. Liu, A.T. Connie, S. Sadaf, Q. Wang, G.A. Botton, I. Shih, and Z. Mi, *Engineering the Carrier dynamics of ingan nanowire white light-emitting diodes by distributed p-AlGaN electron blocking layers.* Scientific Reports, 2015. **5**, p. 7744.
61. H.P. Nguyen, S. Zhang, K. Cui, X. Han, S. Fathololoumi, M. Couillard, G.A. Botton, and Z. Mi, *p-Type modulation doped InGaN/GaN dot-in-a-wire white-light-emitting diodes monolithically grown on Si(111).* Nano Letters, 2011. **11**(5), p. 1919-1924.
62. H.-S. Chen, D.-M. Yeh, Y.-C. Lu, C.-Y. Chen, C.-F. Huang, T.-Y. Tang, C. Yang, C.-S. Wu, and C.-D. Chen, *Strain relaxation and quantum confinement in InGaN/GaN nanoposts.* Nanotechnology, 2006. **17**(5), p. 1454.
63. P.T.N. Hieu, K. Cui, S.F. Zhang, S. Fathololoumi, and Z.T. Mi, *Full-color InGaN/GaN dot-in-a-wire light emitting diodes on silicon.* Nanotechnology, 2011. **22**(44), p. 445202.
64. Y.-L. Chang, J. Wang, F. Li, and Z. Mi, *High efficiency green, yellow, and amber emission from InGaN/GaN dot-in-a-wire heterostructures on Si (111).* Applied Physics Letters, 2010. **96**, p. 013106.
65. W. Guo, M. Zhang, A. Banerjee, and P. Bhattacharya, *Catalyst-Free InGaN/GaN Nanowire Light Emitting Diodes Grown on (001) Silicon by Molecular Beam Epitaxy.* Nano Letters, 2010. **10**(9), p. 3355-3359.
66. H.P.T. Nguyen, S. Zhang, K. Cui, X. Han, S. Fathololoumi, M. Couillard, G. Botton, and Z. Mi, *P-type modulation doped InGaN/GaN dot-in-a-wire white-light-emitting diodes monolithically grown on Si (111).* Nano Letters, 2011. **11**(5), p. 1919-1924.
67. A. Kikuchi, M. Kawai, M. Tada, and K. Kishino, *InGaN/GaN multiple quantum disk nanocolumn light-emitting diodes grown on (111) Si substrate.* Japanese Journal of Applied Physics, 2004. **43**(12A), p. L1524.

68. S.D. Hersee, X. Sun, and X. Wang, *The controlled growth of GaN nanowires.* Nano Letters, 2006. **6**(8), p. 1808-1811.
69. K. Kishino, H. Sekiguchi, and A. Kikuchi, *Improved Ti-mask selective-area growth (SAG) by rf-plasma-assisted molecular beam epitaxy demonstrating extremely uniform GaN nanocolumn arrays.* Journal of Crystal Growth, 2009. **311**(7), p. 2063-2068.
70. Y.J. Hong, C.H. Lee, A. Yoon, M. Kim, H.K. Seong, H.J. Chung, C. Sone, Y.J. Park, and G.C. Yi, *Visible-Color-Tunable Light-Emitting Diodes.* Advanced Materials, 2011. **23**(29), p. 3284-3288.
71. H.-W. Lin, Y.-J. Lu, H.-Y. Chen, H.-M. Lee, and S. Gwo, *InGaN/GaN nanorod array white light-emitting diode.* Applied Physics Letters, 2010. **97**, p. 073101.
72. H.P. Nguyen, K. Cui, S. Zhang, M. Djavid, A. Korinek, G.A. Botton, and Z. Mi, *Controlling electron overflow in phosphor-free InGaN/GaN nanowire white light-emitting diodes.* Nano Letters, 2012. **12**(3), p. 1317-1323.
73. L.-Y.C. C-H. Chang, L-C. Huang, Y-T. Wang, T-C. Lu, and J. J. Huang, *Effects of Strains and Defects on the Internal Quantum Efficiency of InGaN/GaN Nanorod Light Emitting Diodes.* IEEE Journal of. Quantum Electronics, 2012. **48**(4), p. 6.
74. N. Nepal, J. Shakya, M.L. Nakarmi, J.Y. Lin, and H.X. Jiang, *Deep ultraviolet photoluminescence studies of AlN photonic crystals.* Applied Physics Letters, 2006. **88**, p. 133113.
75. J. Ristic, M.A. Sanchez-Garcia, E. Calleja, J. Sanchez-Paramo, J.M. Calleja, U. Jahn, and K.H. Ploog, *AlGaN Nanocolumns Grown by Molecular Beam Epitaxy: Optical and Structural Characterization.* Physica Status Solidi (a), 2002. 192**(1)**, p. 60-66.
76. J. Su, M. Gherasimova, G. Cui, H. Tsukamoto, J. Han, T. Onuma, M. Kurimoto, S.F. Chichibu, C. Broadbridge, Y. He, and A.V. Nurmikko, *Growth of AlGaN nanowires by metalorganic chemical vapor deposition.* Applied Physics Letters, 2005. **87**, p. 183108.

77. K.A. Bertness, A. Roshko, N.A. Sanford, J.M. Barker, and A.V. Davydov, *Spontaneously grown GaN and AlGaN nanowires.* Journal of Crystal Growth, 2006. **287**(2), p. 522-527.
78. H. Sekiguchi, K. Kishino, and A. Kikuchi, *GaN/AlGaN nanocolumn ultraviolet light-emitting diodes grown on n-(111) Si by RF-plasma-assisted molecular beam epitaxy.* Electronics Letters, 2008. **44**(2), p. 151.
79. S.D. Carnevale, T.F. Kent, P.J. Phillips, M.J. Mills, S. Rajan, and R.C. Myers, *Polarization-induced pn diodes in wide-band-gap nanowires with ultraviolet electroluminescence.* Nano Letters, 2012. **12**(2), p. 915-20.
80. Q. Wang, H.P.T. Nguyen, K. Cui, and Z. Mi, *High efficiency ultraviolet emission from AlxGa1−xN core-shell nanowire heterostructures grown on Si (111) by molecular beam epitaxy.* Applied Physics Letters, 2012. **101**, p. 043115.
81. A. Pierret, C. Bougerol, S. Murcia-Mascaros, A. Cros, H. Renevier, B. Gayral, and B. Daudin, *Growth, structural and optical properties of AlGaN nanowires in the whole composition range.* Nanotechnology, 2013. **24**(11), p. 115704.
82. Q. Wang, S. Zhao, A.T. Connie, I. Shih, Z. Mi, T. Gonzalez, M.P. Andrews, X.Z. Du, J.Y. Lin, and H.X. Jiang, *Optical properties of strain-free AlN nanowires grown by molecular beam epitaxy on Si substrates.* Applied Physics Letters, 2014. **104**, p. 223107.
83. S.E. Brinkley, C.L. Keraly, J. Sonoda, C. Weisbuch, J.S. Speck, S. Nakamura, and S.P. DenBaars, *Chip shaping for light extraction enhancement of bulk C-plane light-emitting diodes.* Applied Physics Express, 2012. **5**(3), p. 2104.
84. H.-W. Huang, C. Kao, J. Chu, H. Kuo, S. Wang, and C. Yu, *Improvement of InGaN-GaN light-emitting diode performance with a nano-roughened p-GaN surface.* Photonics Technology Letters, IEEE, 2005. **17**(5), p. 983-985.
85. Y.-C. Lee, C.-H. Ni, and C.-Y. Chen, *Enhancing light extraction mechanisms of GaN-based light-emitting diodes through the integration of imprinting microstructures, patterned sapphire substrates, and surface roughness.* Optics Express, 2010. **18**(S4), p. 489-498.

86. C. Huh, K.-S. Lee, E.-J. Kang, and S.-J. Park, *Improved light-output and electrical performance of InGaN-based light-emitting diode by microroughening of the p-GaN surface.* Journal of Applied Physics, 2003. **93**(11), p. 9383-9385.
87. S.-H. Huang, R.-H. Horng, K.-S. Wen, Y.-F. Lin, K.-W. Yen, and D.-S. Wuu, *Improved light extraction of nitride-based flip-chip light-emitting diodes via sapphire shaping and texturing.* Photonics Technology Letters, IEEE, 2006. **18**(24), p. 2623-2625.
88. D.-H. Kim, C.-O. Cho, Y.-G. Roh, H. Jeon, Y.S. Park, J. Cho, J.S. Im, C. Sone, Y. Park, and W.J. Choi, *Enhanced light extraction from GaN-based light-emitting diodes with holographically generated two-dimensional photonic crystal patterns.* Applied Physics Letters, 2005. **87**, p. 203508.
89. H.K. Cho, J. Jang, J.-H. Choi, J. Choi, J. Kim, J.S. Lee, B. Lee, Y.H. Choe, K.-D. Lee, and S.H. Kim, *Light extraction enhancement from nano-imprinted photonic crystal GaN-based blue light-emitting diodes.* Optics Express, 2006. **14**(19), p. 8654-8660.
90. J.K. Kim, A.N. Noemaun, F.W. Mont, D. Meyaard, E.F. Schubert, D.J. Poxson, H. Kim, C. Sone, and Y. Park, *Elimination of total internal reflection in GaInN light-emitting diodes by graded-refractive-index micropillars.* Applied Physics Letters, 2008. **93**, p. 221111.
91. K. Okamoto, I. Niki, A. Shvartser, Y. Narukawa, T. Mukai, and A. Scherer, *Surface-plasmon-enhanced light emitters based on InGaN quantum wells.* Nature Materials, 2004. **3**(9), p. 601-605.
92. E.E. Loebner, *The future of electroluminescent solids in display application.* Proceedings of IEEE, 1973. **61**(7), p. 25.
93. W.N. Carr and G.E. Pittman, *ONE-WATT GaAs p-n JUNCTION INFRARED SOURCE.* Applied Physics Letters, 1963. **3**(10), p. 173.
94. A.R. Franklin and R. Newman, *Shaped Electroluminescent GaAs Diodes.* Journal of Applied Physics, 1964. **35**(4), p. 1153.
95. J. Van Campenhout, P. Rojo-Romeo, P. Regreny, P. Seasal, D. Van Thourhout, S. Verstuyft, L. Di Cioccio, J.M. Fedeli, C. Lagahe, and R. Baets, *Electrically*

pumped InP-based microdisk lasers integrated with a nanophotonic silicon-on-insulator waveguide circuit. Optics Express, 2007. **15**, p. 6744.

96. D. Liang, M. Fiorentino, T. Okumura, H.H. Chang, D.T. Spencer, Y.H. Kuo, A.W. Fang, D. Dai, R.G. Beausoleil, and J.E. Bowers, *Electricaly-pumped compact hybrid silicon microring lasers for optical interconnects.* Optics Express, 2009. **17**, p. 20355.
97. S. Reitzenstein, A. Bazhenov, A. Gorbunov, C. Hofmann, S. Munch, A. Loffler, M. Kamp, J.P. Reithmaier, V.D. Kulakovskii, and A. Forchel, *Lasing in high-Q quantum-dot micropillar cavities.* Applied Physics Letters, 2006. **89**, p. 051107.
98. M. Loncar, T. Yoshie, A. Scherer, P. Gogna, and Y. Qiu, *Low-threshold photonic crystal laser.* Applied Physics Letters, 2002. **81**, p. 2680.
99. X. Li, *Strain induced semiconductor nanotubes: from formation process to device applications.* J.ournal of Physics D: Applied Physics, 2008. **41**, p. 193001.
100. C. Strelow, H. Rehberg, C.M. Schultz, H. Welsch, C. Heyn, D. Heitmann, and T. Kipp, *Optical microcavities formed by semiconductors using a bottlelike geometry.* Physical Review Letters, 2008. **101**, p. 127403.
101. F. Li, Z. Mi, and S. Vicknesh, *Coherent emission from ultrathin-walled spiral InGaAs/InAs quantum dot microtubes.* Optics Letters, 2009. **34**, p. 2915.
102. C. Strelow, H. Rehberg, C.M. Schultz, H. Welsch, C. Heyn, D. Heitmann, and T. Kipp, *Spatial emission characteristics of a semiconductor microtube ring resonator.* Physica E, 2008. **40**, p. 1836.
103. M. Hosoda and T. Shigaki, *Degeneracy breaking of optical resonance modes in rolled-up spiral microtubes.* Applied Physics Letters, 2007. **90**, p. 181107.
104. Z. Tian, F. Li, Z. Mi, and D.V. Plant, *Controlled transfer of single rolled-up InGaAs-GaAs quantum-dot microtube ring resonators using optical fiber abrupt tapers.* IEEE Photonics Technology Letters, 2010. **22**, p. 311.
105. V.Y. Prinz, V. Seleznev, A. Gutakovsky, A. Chehovskiy, V. Preobrazhenskii, M. Putyato, and T. Gavrilova, *Free-standing and overgrown InGaAs/GaAs nanotubes, nanohelices and their arrays.* Physica E: Low-dimensional Systems and Nanostructures, 2000. **6**(1), p. 828-831.

106. M.H.T. Dastjerdi, M. Djavid, S. Arafin, X. Liu, P. Bianucci, Z. Mi, and P. Poole, *Optically pumped rolled-up InAs/InGaAsP quantum dash lasers at room temperature.* Semiconductor Science and Technology, 2013. **28**(9), p. 094007.

107. P. Bianucci, S. Mukherjee, M.H.T. Dastjerdi, P.J. Poole, and Z. Mi, *Self-organized InAs/InGaAsP quantum dot tube lasers.* Applied Physics Letters, 2012. **101**, p. 031104.

108. T. Kolbe, A. Knauer, C. Chua, Z. Yang, S. Einfeldt, P. Vogt, N.M. Johnson, M. Weyers, and M. Kneissl, *Optical polarization characteristics of ultraviolet (In)(Al) GaN multiple quantum well light emitting diodes.* Applied Physics Letters, 2010. **97**, p. 171105.

109. J. Shakya, K. Knabe, K. Kim, J. Li, J. Lin, and H. Jiang, *Polarization of III-nitride blue and ultraviolet light-emitting diodes.* Applied Physics Letters, 2005. **86**(9), p. 091107.

110. J. Li, K. Nam, M. Nakarmi, J. Lin, H. Jiang, P. Carrier, and S.-H. Wei, *Band structure and fundamental optical transitions in wurtzite AlN.* Applied Physics Letters, 2003. **83**(25), p. 5163-5165.

111. P. Dong, J. Yan, J. Wang, Y. Zhang, C. Geng, T. Wei, P. Cong, Y. Zhang, J. Zeng, and Y. Tian, *282-nm AlGaN-based deep ultraviolet light-emitting diodes with improved performance on nano-patterned sapphire substrates.* Applied Physics Letters 2013. **102**, p. 241113.

112. M. Shatalov, W. Sun, A. Lunev, X. Hu, A. Dobrinsky, Y. Bilenko, J. Yang, M. Shur, R. Gaska, and C. Moe, *AlGaN deep-ultraviolet light-emitting diodes with external quantum efficiency above 10%.* Applied Physics Express, 2012. **5**(8), p. 082101.

113. H.-Y. Ryu, I.-G. Choi, H.-S. Choi, and J.-I. Shim, *Investigation of light extraction efficiency in AlGaN deep-ultraviolet light-emitting diodes.* Applied Physics Express, 2013. **6**(6), p. 062101.

114. A. Taflove and M.E. Brodwin, *Numerical solution of steady-state electromagnetic scattering problems using the time-dependent Maxwell's equations.* Microwave Theory and Techniques, IEEE Transactions on, 1975. **23**(8), p. 623-630.

115. K.S. Yee, *Numerical solution of initial boundary value problems involving Maxwell's equations in isotropic media.* IEEE Transactions Antennas and Propagation, 1966. **14**(3), p. 302-307.

116. J.-P. Berenger, *A perfectly matched layer for the absorption of electromagnetic waves.* Journal of Computational Physics, 1994. **114**(2), p. 185-200.

117. F. Monifi, M. Djavid, A. Ghaffari, and M. Abrishamian, *A new bandstop filter based on photonic crystals.* Proceedings of PIER, Cambridge, USA, 2008, p. 674-677.

118. J. Niegemann, W. Pernice, and K. Busch, *Simulation of optical resonators using DGTD and FDTD.* Journal of Optics A: Pure and Applied Optics, 2009. **11**(11), p. 114015.

119. Y. Yi, P. Bermel, K. Wada, X. Duan, J. Joannopoulos, and L. Kimerling, *Tunable multichannel optical filter based on silicon photonic band gap materials actuation.* Applied Physics Letters, 2002. **81**(22), p. 4112-4114.

120. P. Zhu, G. Liu, J. Zhang, and N. Tansu, *FDTD analysis on extraction efficiency of GaN light-emitting diodes with microsphere arrays.* Journal of Display Technology, 2013. **9**(5), p. 317-323.

121. D.H. Long, I.-K. Hwang, and S.-W. Ryu, *Design optimization of photonic crystal structure for improved light extraction of GaN LED.* Selected Topics in Quantum Electronics, IEEE Journal of, 2009. **15**(4), p. 1257-1263.

122. J.-P. Bérenger, *Perfectly matched layer (PML) for computational electromagnetics.* Synthesis Lectures on Computational Electromagnetics, 2007. **2**(1), p. 1-117.

123. Q. Dai, Q. Shan, J. Wang, S. Chhajed, J. Cho, E.F. Schubert, M.H. Crawford, D.D. Koleske, M.-H. Kim, and Y. Park, *Carrier recombination mechanisms and efficiency droop in GaInN/GaN light-emitting diodes.* Applied Physics Letters, 2010. **97**, p. 133507.

124. H.-Y. Ryu, H.-S. Kim, and J.-I. Shim, *Rate equation analysis of efficiency droop in InGaN light-emitting diodes.* Applied Physics Letters, 2009. **95**, p. 081114.

125. Q. Dai, Q. Shan, J. Wang, S. Chhajed, J. Cho, E.F. Schubert, M.H. Crawford, D.D. Koleske, M.-H. Kim, and Y. Park, *Carrier recombination mechanisms and*

efficiency droop in GaInN/GaN light-emitting diodes. Applied Physics Letters, 2010. **97**, p. 133507.

126. G.-B. Lin, D. Meyaard, J. Cho, E.F. Schubert, H. Shim, and C. Sone, *Analytic model for the efficiency droop in semiconductors with asymmetric carrier-transport properties based on drift-induced reduction of injection efficiency.* Applied Physics Letters, 2012. **100**, p. 161106.
127. H.-Y. Ryu, H.-S. Kim, and J.-I. Shim, *Rate equation analysis of efficiency droop in InGaN light-emitting diodes.* Applied Physics Letters, 2009. **95**(8), p. 081114.
128. Q. Dai, Q.F. Shan, J. Wang, S. Chhajed, J. Cho, E.F. Schubert, M.H. Crawford, D.D. Koleske, M.H. Kim, and Y. Park, *Carrier recombination mechanisms and efficiency droop in GaInN/GaN light-emitting diodes.* Applied Physics Letters, 2010. **97**, p. 133507.
129. M.H. Kim, M.F. Schubert, Q. Dai, J.K. Kim, E.F. Schubert, J. Piprek, and Y. Park, *Origin of efficiency droop in GaN-based light-emitting diodes.* Applied Physics Letters, 2007. **91**, p. 183507.
130. D.S. Meyaard, Q. Shan, Q. Dai, J. Cho, E.F. Schubert, M.-H. Kim, and C. Sone, *On the temperature dependence of electron leakage from the active region of GaInN/GaN light-emitting diodes.* Applied Physics Letters, 2011. **99**, p. 041112.
131. C. Kölper, M. Sabathil, F. Römer, M. Mandl, M. Strassburg, and B. Witzigmann, *Core–shell InGaN nanorod light emitting diodes: Electronic and optical device properties.* Physica Status Solidi (a), 2012. **209**(11), p. 2304-2312.
132. W. Guo, A. Banerjee, P. Bhattacharya, and B.S. Ooi, *InGaN/GaN disk-in-nanowire white light emitting diodes on (001) silicon.* Applied Physics Letters, 2011. **98**, p. 193102.
133. H.P.T. Nguyen, S. Zhang, K. Cui, X. Han, S. Fathololoumi, M. Couillard, G.A. Botton, and Z. Mi, *p-Type Modulation Doped InGaN/GaN Dot-in-a-Wire White-Light-Emitting Diodes Monolithically Grown on Si(111).* Nano Letters, 2011. **11**(5), p. 1919-1924.

134. D.S. Meyaard, Q. Shan, Q. Dai, J. Cho, E.F. Schubert, M.-H. Kim, and C. Sone, *On the temperature dependence of electron leakage from the active region of GaInN/GaN light-emitting diodes*. Applied Physics Letters, 2011, **99**, p. 041112.
135. M. Zhang, P. Bhattacharya, J. Singh, and J. Hinckley, *Direct measurement of auger recombination in In(0.1)Ga(0.9)N/GaN quantum wells and its impact on the efficiency of In(0.1)Ga(0.9)N/GaN multiple quantum well light emitting diodes.* Applied Physics Letters, 2009. **95**, p. 201108.
136. M. Meneghini, N. Trivellin, G. Meneghesso, E. Zanoni, U. Zehnder, and B. Hahn, *A combined electro-optical method for the determination of the recombination parameters in InGaN-based light-emitting diodes.* Journal of Applied Physics, 2009. **106**, p. 114508.
137. S. Chevtchenko, X. Ni, Q. Fan, A.A. Baski, and H. Morkoc, *Surface band bending of a-plane GaN studied by scanning Kelvin probe microscopy.* Applied Physics Letters, 2006. **88**(12), p. 122104.
138. U. Ozgur, X. Ni, X. Li, J. Lee, S. Liu, S. Okur, V. Avrutin, A. Matulionis, and H. Morkoc, *Ballistic transport in InGaN-based LEDs: impact on efficiency.* Semiconductor Science and Technology, 2011. **26**(1), p. 014022.
139. P. Bhattacharya and Z. Mi, *Quantum-dot optoelectronic devices.* Proceedings of the IEEE, 2007. **95**(9), p. 1723-1740.
140. D.S. Meyaard, G.-B. Lin, Q. Shan, J. Cho, E. Fred Schubert, H. Shim, M.-H. Kim, and C. Sone, *Asymmetry of carrier transport leading to efficiency droop in GaInN based light-emitting diodes.* Applied Physics Letters, 2011. **99**, p. 251115.
141. J. Piprek and S. Li, *Electron leakage effects on GaN-based light-emitting diodes.* Optical and Quantum Electronics, 2010. **42**(2), p. 89-95.
142. A. Kikuchi, M. Kawai, M. Tada, and K. Kishino, *InGaN/GaN multiple quantum disk nanocolumn light-emitting diodes grown on (111)Si substrate.* Japanese Journal of Applied Physics Part 2-Letters & Express Letters, 2004. **43**(12A), p. L1524-L1526.

143. H. Sekiguchi, K. Kishino, and A. Kikuchi, *Emission color control from blue to red with nanocolumn diameter of InGaN/GaN nanocolumn arrays grown on same substrate.* Applied Physics Letters, 2010. **96**, p. 231104.

144. F. Qian, S. Gradecak, Y. Li, C. Wen, and C. Lieber, *Core/multishell nanowire heterostructures as multicolor, high-efficiency light-emitting diodes.* Nano Letters, 2005. **5**(11), p. 2287-2291.

145. C.C. Hong, H. Ann, C.Y. Wu, and S. Gwo, *Strong green photoluminescence from InxGa1-xN/GaN nanorod arrays.* Optics Express, 2009. **17**(20), p. 17227-17233.

146. Y.L. Chang, J.L. Wang, F. Li, and Z. Mi, *High efficiency green, yellow, and amber emission from InGaN/GaN dot-in-a-wire heterostructures on Si(111).* Applied Physics Letters, 2010. **96**, p. 013106.

147. P.T. Barletta, E.A. Berkman, B.F. Moody, N.A. El-Masry, A.M. Emara, M.J. Reed, and S.M. Bedair, *Development of green, yellow, and amber light emitting diodes using InGaN multiple quantum well structures.* Applied Physics Letters, 2007. **90**, p. 151109.

148. B. Damilano, N. Grandjean, J. Massies, L. Siozade, and J. Leymarie, *InGaN/GaN quantum wells grown by molecular-beam epitaxy emitting from blue to red at 300 K.* Applied Physics Letters, 2000. **77**(9), p. 1268-1270.

149. H. Masui, J. Sonoda, N. Pfaff, I. Koslow, S. Nakamura, and S.P. DenBaars, *Quantum-confined Stark effect on photoluminescence and electroluminescence characteristics of InGaN-based light-emitting diodes.* Journal of Physics D-Applied Physics, 2008. **41**, p. 165105.

150. F. Qian, Y. Li, S. Gradečak, D. Wang, C.J. Barrelet, and C.M. Lieber, *Gallium Nitride-Based Nanowire Radial Heterostructures for Nanophotonics.* Nano Letters, 2004. **4**(10), p. 1975-1979.

151. T. Kuykendall, P. Ulrich, S. Aloni, and P. Yang, *Complete composition tunability of InGaN nanowires using a combinatorial approach.* Nature Materials, 2007. **6**(12), p. 951-956.

152. R.C. Tu, C.J. Tun, S.M. Pan, C.C. Chuo, J.K. Sheu, C.E. Tsai, T.C. Wang, and G.C. Chi, *Improvement of near-ultraviolet InGaN-GaN light-emitting diodes*

with an AlGaN electron-blocking layer grown at low temperature. IEEE Photonics Technology Letters, 2003. **15**(10), p. 1342-1344.

153. Y.K. Kuo and Y.A. Chang, *Effects of electronic current overflow and inhomogeneous carrier distribution on InGaN quantum-well laser performance.* IEEE Journal of Quantum Electronics, 2004. **40**(5), p. 437-444.

154. Q. Dai, Q.F. Shan, J. Wang, S. Chhajed, J. Cho, E.F. Schubert, M.H. Crawford, D.D. Koleske, M.H. Kim, and Y. Park, *Carrier recombination mechanisms and efficiency droop in GaInN/GaN light-emitting diodes.* Applied Physics Letters, 2010. **97**, p. 133507.

155. Y.-J. Lin, W.-X. Lin, C.-T. Lee, and F.-T. Chien, *Changes in optical and electrical properties and surface recombination velocity of n-type GaN due to (NH4)2Sx treatment.* Solid State Communications, 2006. **137**(5), p. 257-259.

156. M. Boroditsky, I. Gontijo, M. Jackson, R. Vrijen, E. Yablonovitch, T. Krauss, C.-C. Cheng, A. Scherer, R. Bhat, and M. Krames, *Surface recombination measurements on III--V candidate materials for nanostructure light-emitting diodes.* Journal of Applied Physics, 2000. **87**(7), p. 3497-3504.

157. H.P.T. Nguyen, K. Cui, S. Zhang, S. Fathololoumi, and Z. Mi, *Full-color InGaN/GaN dot-in-a-wire light emitting diodes on silicon.* Nanotechnology, 2011. **22**(44), p. 445202.

158. S.C. Ling, T.C. Lu, S.P. Chang, J.R. Chen, H.C. Kuo, and S.C. Wang, *Low efficiency droop in blue-green m-plane InGaN/GaN light emitting diodes.* Applied Physics Letters, 2010. **96**, p. 231101.

159. H.J. Chung, R.J. Choi, M.H. Kim, J.W. Han, Y.M. Park, Y.S. Kim, H.S. Paek, C.S. Sone, Y.J. Park, J.K. Kim, and E.F. Schubert, *Improved performance of GaN-based blue light emitting diodes with InGaN/GaN multilayer barriers*. Applied Physics Letters, 2009. **95**, p. 241109.

160. A. Laubsch, M. Sabathil, J. Baur, M. Peter, and B. Hahn, *High-Power and High-Efficiency InGaN-Based Light Emitters.* IEEE Transactions on Electron Devices, 2010. **57**(1), p. 79-87.

161. M. Zhang, P. Bhattacharya, J. Singh, and J. Hinckley, *Direct measurement of auger recombination in In(0.1)Ga(0.9)N/GaN quantum wells and its impact on*

the efficiency of In(0.1)Ga(0.9)N/GaN multiple quantum well light emitting diodes. Applied Physics Letters, 2009. **95**, p. 201108

162. J.Q. Xie, X.F. Ni, Q. Fan, R. Shimada, U. Ozgur, and H. Morkoc, *On the efficiency droop in InGaN multiple quantum well blue light emitting diodes and its reduction with p-doped quantum well barriers.* Applied Physics Letters, 2008. **93**, p. 121107

163. S. Fernández-Garrido, X. Kong, T. Gotschke, R. Calarco, L. Geelhaar, A. Trampert, and O. Brandt, *Spontaneous Nucleation and Growth of GaN Nanowires: The Fundamental Role of Crystal Polarity.* Nano Letters, 2012. **12**(12), p. 6119-6125.

164. K. Hestroffer, C. Leclere, C. Bougerol, H. Renevier, and B. Daudin, *Polarity of GaN nanowires grown by plasma-assisted molecular beam epitaxy on Si(111).* Physical Review B, 2011. **84**(24), p. 245302.

165. Z. Shaofei, A.T. Connie, D.A. Laleyan, N. Hieu Pham Trung, W. Qi, S. Jun, S. Ishiang, and M. Zetian, *On the Carrier Injection Efficiency and Thermal Property of InGaN/GaN Axial Nanowire Light Emitting Diodes.* Quantum Electronics, IEEE Journal of, 2014. **50**(6), p. 483-490.

166. Ü. Özgür, X. Ni, X. Li, J. Lee, S. Liu, S. Okur, V. Avrutin, A. Matulionis, and H. Morkoç, *Ballistic transport in InGaN-based LEDs: impact on efficiency.* Semiconductor Science and Technology, 2011. **26**(1), p. 014022.

167. H.P.T. Nguyen, K. Cui, S. Zhang, M. Djavid, A. Korinek, G.A. Botton, and Z. Mi, *Controlling Electron Overflow in Phosphor-Free InGaN/GaN Nanowire White Light-Emitting Diodes.* Nano Letters, 2012. **12**(3), p. 1317–1323.

168. S.-H. Han, D.-Y. Lee, S.-J. Lee, C.-Y. Cho, M.-K. Kwon, S.P. Lee, D.Y. Noh, D.-J. Kim, Y.C. Kim, and S.-J. Park, *Effect of electron blocking layer on efficiency droop in InGaN/GaN multiple quantum well light-emitting diodes.* Applied Physics Letters, 2009. **94**, p. 231123.

169. S. Singh, D. Robidas, N. Rohila, S. Pal, and C. Dhanavantri, *Effect of electron blocking layer on efficiency droop in blue InGaN/GaN based light-emitting diodes.* Optoelectronics and Advanced Materials-Rapid Communications, 2010. **4**(8), p. 1106-1110.

170. C.S. Xia, Z.M.S. Li, W. Lu, Z.H. Zhang, Y. Sheng, W.D. Hu, and L.W. Cheng, *Efficiency enhancement of blue InGaN/GaN light-emitting diodes with an AlGaN-GaN-AlGaN electron blocking layer.* Journal of Applied Physics, 2012. **111**, p. 094503.

171. C.H. Wang, C.C. Ke, C.Y. Lee, S.P. Chang, W.T. Chang, J.C. Li, Z.Y. Li, H.C. Yang, H.C. Kuo, T.C. Lu, and S.C. Wang, *Hole injection and efficiency droop improvement in InGaN/GaN light-emitting diodes by band-engineered electron blocking layer.* Applied Physics Letters, 2010. **97**, p. 261103.

172. J. Verma, P.K. Kandaswamy, V. Protasenko, A. Verma, H. Grace Xing, and D. Jena, *Tunnel-injection GaN quantum dot ultraviolet light-emitting diodes.* Applied Physics Letters, 2013. **102**, p. 041103.

173. F. Akyol, D. Nath, S. Krishnamoorthy, P. Park, and S. Rajan, *Suppression of electron overflow and efficiency droop in N-polar GaN green light emitting diodes.* Applied Physics Letters, 2012. **100**, p. 111118.

174. Ü. Özgür, X. Ni, X. Li, J. Lee, S. Liu, S. Okur, V. Avrutin, A. Matulionis, and H. Morkoc, *Ballistic transport in InGaN-based LEDs: impact on efficiency.* Semiconductor Science and Technology, 2011. **26**(1), p. 014022.

175. X. Ni, X. Li, J. Lee, S. Liu, V. Avrutin, U. Ozgur, H. Morkoç, A. Matulionis, T. Paskova, and G. Mulholland, *InGaN staircase electron injector for reduction of electron overflow in InGaN light emitting diodes.* Applied Physics Letters, 2010. **97**, p. 031110.

176. U. Ozgur, H. Liu, X. Li, X. Ni, and H. Morkoç, *GaN-based light-emitting diodes: Efficiency at high injection levels.* Proceedings of the IEEE, 2010. **98**(7), p. 1180-1196.

177. M.-H. Kim, M.F. Schubert, Q. Dai, J.K. Kim, E.F. Schubert, J. Piprek, and Y. Park, *Origin of efficiency droop in GaN-based light-emitting diodes.* Applied Physics Letters, 2007. **91**, p. 183507.

178. J. Xie, X. Ni, Q. Fan, R. Shimada, U. Ozgur, and H. Morkoç, *On the efficiency droop in InGaN multiple quantum well blue light emitting diodes and its reduction with p-doped quantum well barriers.* Applied Physics Letters, 2008. **93**, p. 121107.

179. S.-H. Han, D.-Y. Lee, S.-J. Lee, C.-Y. Cho, M.-K. Kwon, S. Lee, D. Noh, D.-J. Kim, Y.C. Kim, and S.-J. Park, *Effect of electron blocking layer on efficiency droop in InGaN/GaN multiple quantum well light-emitting diodes.* Applied Physics Letters, 2009. **94**, p. 231123.

180. C. Wang, C. Ke, C. Lee, S. Chang, W. Chang, J. Li, Z. Li, H. Yang, H. Kuo, and T. Lu, *Hole injection and efficiency droop improvement in InGaN/GaN light-emitting diodes by band-engineered electron blocking layer.* Applied Physics Letters, 2010. **97**, p. 261103.

181. R.-C. Tu, C.-J. Tun, S.-M. Pan, C.-C. Chuo, J. Sheu, C.-E. Tsai, T.-C. Wang, and G.-C. Chi, *Improvement of near-ultraviolet InGaN-GaN light-emitting diodes with an AlGaN electron-blocking layer grown at low temperature.* Photonics Technology Letters, 2003. **15**(10), p. 1342-1344.

182. S. Chichibu, A. Abare, M. Mack, M. Minsky, T. Deguchi, D. Cohen, P. Kozodoy, S. Fleischer, S. Keller, and J. Speck, *Optical properties of InGaN quantum wells.* Materials Science and Engineering B 1999. **59**(1), p. 298-306.

183. J. Verma, P.K. Kandaswamy, V. Protasenko, A. Verma, H. Grace Xing, and D. Jena, *Tunnel-injection GaN quantum dot ultraviolet light-emitting diodes.* Applied Physics Letters, 2013. **102**, p. 041103.

184. N. Bochkareva, V. Voronenkov, R. Gorbunov, P. Latyshev, Y.S. Lelikov, Y.T. Rebane, A. Tsyuk, and Y.G. Shreter, *Tunnel injection and power efficiency of InGaN/GaN light-emitting diodes.* Semiconductors, 2013. **47**(1), p. 127-134.

185. P. Bhattacharya, M. Zhang, and J. Hinckley, *Tunnel injection In0. 25Ga0. 75N/GaN quantum dot light-emitting diodes.* Applied Physics Letters, 2010. **97**, p. 251107.

186. T. Lu, S. Li, C. Liu, K. Zhang, Y. Xu, J. Tong, L. Wu, H. Wang, X. Yang, and Y. Yin, *Advantages of GaN based light-emitting diodes with a p-InGaN hole reservoir layer.* Applied Physics Letters, 2012. **100**, p. 141106.

187. J.H. Son and J.-L. Lee, *Strain engineering for the solution of efficiency droop in InGaN/GaN light-emitting diodes.* Optics Express, 2010. **18**(6), p. 5466-5471.

188. Q. Li and G.T. Wang, *Strain influenced indium composition distribution in GaN/InGaN core-shell nanowires.* Applied Physics Letters, 2010. **97**, p. 181107.

189. H. Sekiguchi, K. Kishino, and A. Kikuchi, *Emission color control from blue to red with nanocolumn diameter of InGaN/GaN nanocolumn arrays grown on same substrate.* Applied Physics Letters, 2010. **96**, p. 231104.

190. M. Djavid, H. Nguyen, S. Zhang, K. Cui, S. Fan, and Z. Mi, *Tunnel injection InGaN/GaN dot-in-a-wire white-light-emitting diodes.* Semiconductor Science and Technology, 2014. **29**(8), p. 085009.

191. D.S. Meyaard, G.-B. Lin, Q. Shan, J. Cho, E.F. Schubert, H. Shim, M.-H. Kim, and C. Sone, *Asymmetry of carrier transport leading to efficiency droop in GaInN based light-emitting diodes.* Applied Physics Letters, 2011. **99**, p. 251115.

192. H.-Y. Ryu, J.-I. Shim, C.-H. Kim, J.H. Choi, H.M. Jung, M.-S. Noh, J.-M. Lee, and E.-S. Nam, *Efficiency and electron leakage characteristics in GaN-based light-emitting diodes without AlGaN electron-blocking-layer structures.* Photonics Technology Letters, IEEE, 2011. **23**(24), p. 1866-1868.

193. H. Masui, J. Sonoda, N. Pfaff, I. Koslow, S. Nakamura, and S.P. DenBaars, *Quantum-confined Stark effect on photoluminescence and electroluminescence characteristics of InGaN-based light-emitting diodes.* Journal of Physics D: Applied Physics, 2008. **41**(16), p. 165105.

194. F. Ponce and D. Bour, *Nitride-based semiconductors for blue and green light-emitting devices.* Nature, 1997. **386**(6623), p. 351-359.

195. C. Strelow, C. Schultz, H. Rehberg, H. Welsch, C. Heyn, D. Heitmann, and T. Kipp, *Three dimensionally confined optical modes in quantum-well microtube ring resonators.* Physical Review B, 2007. **76**(4), p. 045303.

196. Y. Mei, D.J. Thurmer, C. Deneke, S. Kiravittaya, Y.-F. Chen, A. Dadgar, F. Bertram, B. Bastek, A. Krost, J.r. Christen, T. Reindl, M. Stoffel, E. Coric, and O.G. Schmidt, *Fabrication, self-assembly, and properties of ultrathin AlN/GaN porous crystalline nanomembranes: tubes, spirals, and curved sheets.* Acs Nano, 2009. **3**(7), p. 1663-1668.

197. X. Li, *Strain induced semiconductor nanotubes: from formation process to device applications.* Journal of Physics D: Applied Physics, 2008. **41**(19), p. 193001.

198. A. Vorob'ev, P. Vaccaro, K. Kubota, T. Aida, T. Tokuda, T. Hayashi, Y. Sakano, J. Ohta, and M. Nunoshita, *SiGe/Si microtubes fabricated on a silicon-on-insulator substrate.* Journal of Physics D: Applied Physics, 2003. **36**(17), p. L67.

199. Y. Sun, J. Hu, Z. Chen, Y. Bando, and D. Golberg, *Prospective important semiconducting nanotubes: synthesis, properties and applications.* Journal of Materials Chemistry, 2009. **19**(41), p. 7592-7605.

200. S. Vicknesh, F. Li, and Z. Mi, *Optical microcavities on Si formed by self-assembled InGaAs/GaAs quantum dot microtubes.* Applied Physics Letters, 2009. **94**, p. 081101.

201. Z. Tian, F. Li, Z. Mi, and D.V. Plant, *Controlled transfer of single rolled-up InGaAs–GaAs quantum-dot microtube ring resonators using optical fiber abrupt tapers.* Photonics Technology Letters, IEEE, 2010. **22**(5), p. 311-313.

202. I.S. Chun and X. Li, *Controlled assembly and dispersion of strain-induced InGaAs/GaAs nanotubes.* Nanotechnology, IEEE Transactions on, 2008. **7**(4), p. 493-495.

203. C. Strelow, C. Schultz, H. Rehberg, M. Sauer, H. Welsch, A. Stemmann, C. Heyn, D. Heitmann, and T. Kipp, *Light confinement and mode splitting in rolled-up semiconductor microtube bottle resonators.* Physical Review B, 2012. **85**(15), p. 155329.

204. T. Kipp, C. Strelow, and D. Heitmann, *Light confinement in microtubes*, in *Quantum Materials, Lateral Semiconductor Nanostructures, Hybrid Systems and Nanocrystals*. 2010, Springer. p. 165-182.

205. J.P.A. Bastos and N. Sadowski, *Electromagnetic modeling by finite element methods*. 2003, CRC press.

206. M. Djavid, X. Liu, and Z. Mi, *Improvement of the light extraction efficiency of GaN-based LEDs using rolled-up nanotube arrays.* Optics Express, 2014. **22**(S7), p. A1680-A1686.

207. F. Krumeich, M. Wark, L. Ren, H.J. Muhr, and R. Nesper, *Electron microscopy characterization of silicon dioxide nanotubes.* Zeitschrift für anorganische und allgemeine Chemie, 2004. **630**(7), p. 1054-1058.

208. M. Steinhart, J. Wendorff, A. Greiner, R. Wehrspohn, K. Nielsch, J. Schilling, J. Choi, and U. Gösele, *Polymer nanotubes by wetting of ordered porous templates.* Science, 2002. **296**(5575), p. 1997-1997.

209. H.-W. Huang, J. Chu, C. Kao, T. Hseuh, T. Lu, H. Kuo, S. Wang, and C. Yu, *Enhanced light output of an InGaN/GaN light emitting diode with a nano-roughened p-GaN surface.* Nanotechnology, 2005. **16**(9), p. 1844.

210. E. Ejder, *Refractive index of GaN.* Physica Status Solidi (a), 1971. **6**(2), p. 445-448.

211. H.H. Li, *Refractive index of silicon and germanium and its wavelength and temperature derivatives.* Journal of Physical and Chemical Reference Data, 1980. **9**(3), p. 561-658.

212. S.J. Lee, *Analysis of light-emitting diodes by Monte Carlo photon simulation.* Applied Optics, 2001. **40**(9), p. 1427-1437.

213. C.W. Yeh and F.I. Shimabukuro, *Planar Dielectric Waveguides*, in *The essence of dielectric waveguides*. 2008, Springer. p. 99-135.

214. M. Hosoda and T. Shigaki, *Degeneracy breaking of optical resonance modes in rolled-up spiral microtubes.* Applied Physics Letters, 2007. **90**, p. 181107.

215. P. Zhao and H. Zhao, *Analysis of light extraction efficiency enhancement for thin-film-flip-chip InGaN quantum wells light-emitting diodes with GaN micro-domes.* Optics Express, 2012. **20**(105), p. 765-776.

216. S. Zhao, A. Connie, M. Dastjerdi, X. Kong, Q. Wang, M. Djavid, S. Sadaf, X. Liu, I. Shih, and H. Guo, *Aluminum nitride nanowire light emitting diodes: Breaking the fundamental bottleneck of deep ultraviolet light sources.* Scientific Reports, 2015. **5**, p. 83332.

217. M.-T. Chen, M.-P. Lu, Y.-J. Wu, J. Song, C.-Y. Lee, M.-Y. Lu, Y.-C. Chang, L.-J. Chou, Z.L. Wang, and L.-J. Chen, *Near UV LEDs made with in situ doped pn homojunction ZnO nanowire arrays.* Nano Letters, 2010. **10**(11), p. 4387-4393.

218. C. Lee, B. Cheng, Y. Lee, H. Kuo, T. Lu, and S. Wang, *Output Power Enhancement of Vertical-Injection Ultraviolet Light-Emitting Diodes by GaN-*

Free and Surface Roughness Structures. Electrochemical and Solid-State Letters, 2009. **12**(2), p. 44-46.

219. M. Yamada, T. Mitani, Y. Narukawa, S. Shioji, I. Niki, S. Sonobe, K. Deguchi, M. Sano, and T. Mukai, *InGaN-based near-ultraviolet and blue-light-emitting diodes with high external quantum efficiency using a patterned sapphire substrate and a mesh electrode.* Japanese Journal of Applied Physics, 2002. **41**(12B), p. 1431.
220. Y. Lee, T. Hsu, H. Kuo, S. Wang, Y. Yang, S. Yen, Y. Chu, Y. Shen, M. Hsieh, and M. Jou, *Improvement in light-output efficiency of near-ultraviolet InGaN–GaN LEDs fabricated on stripe patterned sapphire substrates.* Materials Science and Engineering: B, 2005. **122**(3), p. 184-187.
221. M. Djavid, X. Liu, and Z. Mi, *Improvement of the light extraction efficiency of GaN-based LEDs using rolled-up nanotube arrays.* Optics Express, 2014. **22**(107), p. 1680-1686.
222. J. Shakya, K. Kim, J. Lin, and H. Jiang, *Enhanced light extraction in III-nitride ultraviolet photonic crystal light-emitting diodes.* Applied physics letters, 2004. **85**, p. 142-144.
223. R. Eberhart, P. Simpson, and R. Dobbins, *Computational intelligence PC tools*. 1996, Academic Press Professional, Inc.
224. R.C. Eberhart and J. Kennedy. *A new optimizer using particle swarm theory*. in *Proceedings of the sixth international symposium on micro machine and human science*. 1995. New York, NY.
225. M. Shokooh-Saremi and R. Magnusson, *Particle swarm optimization and its application to the design of diffraction grating filters.* Optics Letters, 2007. **32**(8), p. 894-896.
226. M. Djavid, S. Mirtaheri, and M. Abrishamian, *Photonic crystal notch-filter design using particle swarm optimization theory and finite-difference time-domain analysis.* Journal of the Optical Society of America B: Optical Physics 2009. **26**(4), p. 849-853.

227. S.-P. Chang, K.-P. Sou, C.-H. Chen, Y.-J. Cheng, J.-K. Huang, C.-H. Lin, H.-C. Kuo, C.-Y. Chang, and W.-F. Hsieh, *Lasing action in gallium nitride quasicrystal nanorod arrays.* Optics Express, 2012. **20**(11), p. 12457-12462.

228. T. Kouno, K. Kishino, K. Yamano, and A. Kikuchi, *Two-dimensional light confinement in periodic InGaN/GaN nanocolumn arrays and optically pumped blue stimulated emission.* Optics Express, 2009. **17**(22), p. 20440-20447.

229. R. Merlin and S. Young, *Photonic crystals as topological high-Q resonators.* Optics Express, 2014. **22**(15), p. 18579-18587.

230. M.S.Y. Najjar and N.D.M. Khodier, *Design of non–uniform circular antenna arrays using particle swarm optimization.* Journal of Electrical Engineering, 2008. **59**(4), p. 216-220.

231. N. Jin and Y. Rahmat-Samii, *Advances in particle swarm optimization for antenna designs: Real-number, binary, single-objective and multiobjective implementations.* Antennas and Propagation, IEEE Transactions on, 2007. **55**(3), p. 556-567.

232. K. Li, X. Liu, Q. Wang, S. Zhao, and Z. Mi, *Ultralow-threshold electrically injected AlGaN nanowire ultraviolet lasers on Si operating at low temperature.* Nature Nanotechnology, 2015. **10**, p. 140–144.

233. D. Liang and J.E. Bowers, *Recent progress in lasers on silicon.* Nature Photonics, 2010. **4**(8), p. 511-517.

234. M. Howlader, T. Watanabe, and T. Suga, *Investigation of the bonding strength and interface current of p-Si/n-GaAs wafers bonded by surface activated bonding at room temperature.* Journal of Vacuum Science & Technology B: Microelectronics and Nanometer Structures, 2001. **19**(6), p. 2114-2118.

235. Y. Zhou, Z. Zhu, D. Crouse, and Y. Lo, *Electrical properties of wafer-bonded GaAs/Si heterojunctions.* Applied Physics Letters, 1998. **73**(16), p. 2337-2339.

236. K. Tanabe, K. Watanabe, and Y. Arakawa, *III-V/Si hybrid photonic devices by direct fusion bonding.* Scientific Reports, 2012. **2**, p. 349.

237. A. Splendiani, L. Sun, Y. Zhang, T. Li, J. Kim, C.-Y. Chim, G. Galli, and F. Wang, *Emerging photoluminescence in monolayer MoS2.* Nano Letters, 2010. **10**(4), p. 1271-1275.

238. W. Bao, X. Cai, D. Kim, K. Sridhara, and M.S. Fuhrer, *High mobility ambipolar MoS2 field-effect transistors: Substrate and dielectric effects.* Applied Physics Letters, 2013. **102**, p. 042104.

239. J.S. Ross, P. Klement, A.M. Jones, N.J. Ghimire, J. Yan, D. Mandrus, T. Taniguchi, K. Watanabe, K. Kitamura, and W. Yao, *Electrically tunable excitonic light-emitting diodes based on monolayer WSe2 pn junctions.* Nature Nanotechnology, 2014. **9**(4), p. 268-272.

240. O. Lopez-Sanchez, D. Lembke, M. Kayci, A. Radenovic, and A. Kis, *Ultrasensitive photodetectors based on monolayer MoS2.* Nature Nanotechnology, 2013. **8**(7), p. 497-501.

241. K. Roy, M. Padmanabhan, S. Goswami, T.P. Sai, G. Ramalingam, S. Raghavan, and A. Ghosh, *Graphene-MoS2 hybrid structures for multifunctional photoresponsive memory devices.* Nature Nanotechnology, 2013. **8**(11), p. 826-830.

242. Y. Huang, J. Wu, X. Xu, Y. Ho, G. Ni, Q. Zou, G.K.W. Koon, W. Zhao, A.C. Neto, and G. Eda, *An innovative way of etching MoS2: Characterization and mechanistic investigation.* Nano Research, 2013. **6**(3), p. 200-207.